The Pennsylvania State University

The Graduate School

College of Earth and Mineral Sciences

THERMODYNAMICS OF MICROEMULSION SYSTEMS: PARTITIONING RELATIONSHIPS, PHASE BEHAVIOR AND INTERFACIAL TENSIONS

A Dissertation in

Energy and Mineral Engineering

by

Victor A. Torrealba

Submitted in Partial Fulfillment

of the Requirements

for the Degree of

Doctor of Philosophy

December 2017

The dissertation of Victor A. Torrealba was reviewed and approved* by the following:

Russell T. Johns

Professor of Petroleum and Natural Gas Engineering
Program Chair for Petroleum and Natural Gas Engineering
John and Willie Leone Family Department of Energy and Mineral Engineering
Dissertation Advisor
Chair of Committee

Hamid Emami-Meybodi

Assistant Professor of Petroleum and Natural Gas Engineering
John and Willie Leone Family Department of Energy and Mineral Engineering

Zuleima T. Karpyn

Professor of Petroleum and Natural Gas Engineering
Quentin E. and Louise L. Wood Faculty Fellow in Petroleum and Natural Gas Engineering
John and Willie Leone Family Department of Energy and Mineral Engineering

Themistoklis Matsoukas

Professor of Chemical Engineering
Department of Chemical Engineering

Luis F. Ayala

Professor of Petroleum and Natural Gas Engineering
Associate Department Head for Graduate Education

*Signatures are on file in the Graduate School

Abstract

Surfactant-based enhanced oil recovery is a promising technique in the petroleum industry due to surfactant's ability to mobilize previously trapped oil by reducing capillary forces at the pore-scale. However, the field-scale implementation of these techniques has been challenging by the high cost of chemicals, which makes the margin of error for the deployment of such methods increasingly narrow. Some commonly recognized issues are surfactant adsorption, surfactant partitioning to the excess phases, surfactant thermal and physical degradation, and scale-representative microemulsion phase behavior.

In this dissertation, we present a novel microemulsion phase behavior model accounting for changing micellar curvature conditions under the assumption of a general prolate spheroid geometry. This approach is shown to be consistent with the definition of the three-phase solubilization ratios obtained by combining our previously developed interfacial tension model with Huh's correlation. This model removes key assumptions in recent microemulsion phase behavior model of Khorsandi and Johns (2016), such as symmetric phase behavior in the Type III region, constant characteristic length- the Type III, constant spherical geometry of micelles, and finite critical characteristic length-scale. Finally, the model is coupled with Huh's correlation to present a coupled approach that allows for the accurate capturing of both phase behavior and interfacial tensions.

For the case considered, the curvature model provided excellent results compared to experimental data. The results of the coupled approach are compared with results consisting of only phase behavior tuning, where the interfacial tensions are described using Huh's correlation and the standard scaling constant. For the case considered, the curvature model yielded excellent capturing of both phase behavior and interfacial tension data, whereas the alternative approach of just tuning phase behavior yielded unsatisfactory values of interfacial tensions, with discrepancies of over an order of magnitude.

Then, we introduce a consistent and robust model that predicts interfacial tensions for all microemulsion Winsor types and overall compositions. The model incorporates film bending arguments and Huh's equation, and is coupled to phase behavior so that simultaneous tuning of both IFT and phase behavior is possible. The oil-water interfacial tension and characteristic length are shown to be related to each other through the hydrophilic-lipophilic deviation (*HLD*). The phase behavior is tied to the micelle curvatures, without the need for using net average curvature (NAC).

The interfacial tension model is tied to solubilization ratios in order to introduce a coupled interfacial tension-phase behavior model for all phase environments. The approach predicts two- and three-phase interfacial tensions and phase behavior (i.e. tie lines and tie triangles) for changes in composition and *HLD* input parameters, such as temperature, pressure, surfactant structure parameters, and oil equivalent alkane carbon number. Comparisons to experimental data show excellent fits and predictive capability.

Further, we introduce a new empirical phase behavior model based on chemical potentials and HLD. The model is able to describe physical two-phase regions, and is shown to represent accurately experimental data at fixed composition and changing HLD (e.g. a salinity scan) as well as variable composition data at fixed HLD. Further, the model is extended to account for surfactant partitioning into the excess phases. The model is benchmarked against experimental data (considering both pure alkane and crude oil cases), showing excellent fits for a wide variety of experiments, and is compared to the HLD-*NAC* EoS model for reference.

In this research, we allow for surfactant partitioning into both the water and oil excess phases using a simple approach, and then relate the relevant surfactant partitioning coefficients to the HLD state function so that all independent *K*-values are predicted for all Winsor environments. Surfactant screening based on EO and PO groups is also considered based on estimated K-values. Key dimensionless groups as a function of activity coefficients are identified, which allow for a simplified description of the surfactant partition coefficients. As an example, the surfactant partition coefficients are combined with the CP equation-of-state model to describe and predict the phase behavior when the excess phases are not pure.

One common theme in all contributions in this dissertation is the emphasis on having improved predictive capabilities. For every contribution, we propose a way forward for how to determine model parameters using a single or reduced number of experiments, and then predict for conditions outside the range of

experimental observation. This is of great importance for petroleum engineering applications.

Table of Contents

List of Figures

List of Tables

List of Symbols

English letters

A_{CI}	Interaction between the adsorbed surfactant and component I
A_S	Interface surface area, Å^2
c	Principal curvature, $1/\text{Å}$
c	Constant related to the phase behavior in the Type II region
c_γ	Constant related to the oil-water interfacial tension, mN/m
C_{ij}	Volumetric concentration of component i in phase j
C_K^X	K-th empirical parameter in the $HLD - NAC$ model for the Type II(X) region
CSE	Salinity of the aqueous phase, wt%
G	Dimensionless group related to the Type II solubilization ratio development in the CP model
H	Mean curvature, $1/\text{Å}$
$\langle H \rangle$	Mean curvature, $1/\text{Å}$
$\mathcal{H}$	Hydrophilic-Lipophilic Deviation or HLD
I	I-ratio
K_i	Two-phase CP model parameter for component i
K_{jk}^i	Concentration ratio of component i between phases j and k
L	Surfactant length, Å
n	Number of formulation variables
P	Pressure, bar
r_i	Micellar radius with component i internal, Å
R	Interaction energy ratio, J
R	Gas constant, $J/(Kmol)$
T	Temperature, K
V	Volume, cc
V_i	Volume of component i in the system, cc
V_{ij}	Volume of component i in phase j, cc
X	Formulation variable X

Greek letters

γ_{jk}	Interfacial tension between phases j and k, mN/m
γ_{ij}	Activity coefficient for component i in phase j
κ	Bending modulus, Nm
$\bar{\kappa}$	Saddle-splay modulus, Nm
μ_{ij}	Chemical potential of component i in phase j
ξ	Characteristic length scale, Å
ξ_i	Characteristic length scale for component i in the

	microemulsion, Å
ξ^X	Characteristic or correlation length scale in Type X environment, Å
ξ_D^X	Dimensionless characteristic or correlation length scale in Type X environment
σ_i	Solubilization ratio of component i in the microemulsion
σ_{ij}	Solubilization ratio of component i in phase j
σ_{im}^o	Ratio of total concentration of component i in the system to the total concentration of surfactant
Ω	CP model Type III phase behavior parameter under symmetric conditions
Ω	Scaling constant in Huh's correlation, mN/m
Ω_{jk}^i	Activity group for component i between phases j and k
Ω_i^X	Experimental constant related to the solubilization of component i in the microemulsion phase in the Type X environment

Superscripts

cp	Critical point
i	ith component
max	Maximum value
min	Minimum value
o	Oil component
s	Surfactant component
w	Water component
°	Standard state
$*$	Optimum condition
$+$	Type II+ microemulsion environment
$-$	Type II- microemulsion environment
3p	Three-phase

Subscripts

C	Surfactant adsorbed at the interface
D	Microemulsion phase
i	ith component
i	ith formulation variable
j	jth phase
I	Ith component
k	kth phase
k	kth formulation variable
l	Compositionally dependent lower limit
L	Minimum lower limit
m	Microemulsion phase
n	Normalized
o	Oil component or phase

O	Oil dimensionless group related to the Type II solubilization ratio development in the CP model
p	Pseudo-surfactant component
ref	Reference state
s	Surfactant component
u	Compositionally dependent upper limit
U	Maximum upper limit
w	Water component or phase
W	Water dimensionless group related to the Type II solubilization ratio development in the CP model
1	First principal curvature
2	Second principal curvature

Abbreviations

ACL	Alcohol Chain Length
C8B	Octylbenzene
EACN	Equivalent Alkane Carbon Number
EO	Ethylene Oxide
FA	Fatty Acids
HCL	Hydrophilic Chain Length
HLB	Hydrophilic-Lipophilic Balance
HLD	Hydrophilic-Lipophilic Deviation
LCL	Lipophilic Chain Length
NAC	Net-Average Curvature
NAPL	Non-Aqueous Phase Liquids
O	Oil phase or component
OPE	Octylphenoxyethanol
PIT	Phase Inversion Temperature
PO	Polypropylene Oxide
S	Surfactant component
SAD	Surfactant Affinity Difference
SDS	Sodium Dodecyl Sulfate
Surfactant	Surface active agent
W	Water phase or component

Acknowledgements

I would like to acknowledge Dr. Russell T. Johns for being a fantastic doctoral advisor. He offered an incredibly challenging but equally rewarding research environment. Specially, I would like to thank him for giving me the opportunity to pursue different ideas, while helping me develop them to the best of my abilities.

I am extremely grateful to both Drs. Zuleima Karpyn and Luis Ayala for being great inspirational figures, and being my mentors for all my time at Penn State. They have had an unbelievable impact in my development as a Petroleum Engineer.

I am grateful to Dr. Hamid Emami-Meybodi for being my part of my committee and providing valuable feedback during my research. I am also very grateful to Dr. Themis Matsoukas, whom I met during a class he taught me on Statistical Thermodynamics. In this class, he completely demystified a number of aspects of Classical Thermodynamics, which inspired many elements of this dissertation. I also thank him for being part of my committee.

I would like to thank Drs. Hussein Hoteit and Adwait Chawathe for providing extremely enjoyable summer internship experiences, and for offering me a different view on how to develop and apply technology in the industrial sense. I would like to single out Soumyadeep Ghosh who taught me the value of bridging ideas to come up with something new. I based a lot of this research on that philosophy. I deeply enjoyed many fruitful discussions with my research

group and department mates, including Pooya Khodaparast, Daulet Magzymov, Liwei Li, Saeid Khorsandi, Bahareh Nojabaei, Miral Tawfik, Prakash Purswani, Eunnam Ahn, Zhenke Xi, Michael Cronin, and Devesh Kumar.

I gratefully acknowledge the financial support from the member companies of the Enhanced Oil Recovery Joint Industry Project at Penn State.

Dedication

To my baby Adam, my wife Lucy, and my parents Lilia and Victor.

Part I

Introductory Remarks

Chapter 1

Introduction

Surfactants (short for surface active agents) are components that have affinity to two inherently dissimilar components. They have a wide range of applications in pharmaceutical, cosmetics, detergents, biotechnology, among many other industries. Of special interest for this dissertation is the application of surfactants for enhanced oil recovery in subsurface applications, where small concentrations of surfactants are sufficient to reduce interfacial tensions between oil and water to levels low enough to induce oil ganglia mobilization at the pore scale. The relevant physics of surfactant-oil-water systems is overly complex, and requires careful examination. In this chapter, we will focus on understanding surfactant interactions, and how that relates to both microemulsion phase behavior and interfacial tensions. Further, we will examine the impact of different parameters on the surfactant interaction to both oil and water, and how that translates into microemulsion phase behavior changes.

The length of surfactant molecules can be estimated using simple intermolecular distance considerations (Tanford, 1972), ranging from 10-100 Å (i.e. 1-10 nm). Microemulsions can be considered as small-scale versions of emulsions (i.e. droplet type dispersions either of oil-in-water (o/w) or of water-in-oil (w/o), with a size range in the order of 10-100 nm in drop diameter (Eastoe,

2003). Pore-throat sizes have an average diameter that is generally greater than 2 μm in conventional reservoir rocks, range from about 0.03-2 μm in tight-gas sandstones, and range from 0.005-0.1 μm in shales (Nelson, 2009). For most conventional reservoir rocks, micelles are about an order of magnitude smaller than pore throats, which ensures micellar flow through the porous medium.

1.1 Interfacial fundamentals

For efficient mobilization of oil from the pores of subsurface reservoirs, the interfacial tension between the brine and oil must be in the order of 10^{-3}mN/m. This situation only occurs when the interaction energy across the interface is quite high, which is equivalent to saying the nature of the material on both sides of the interface must be quite similar (Rosen and Kunjappu, 2012). Given that both oil and water are very different, this condition of having a similar nature on both sides of the interface can only occur when each side has similar concentration of oil, water and surfactant.

Figure 1-1 shows a good illustration for understanding the impact of changing interfacial interaction on both interfacial tensions and the accompanying phase behavior. When the surfactant is primarily affine to the aqueous components, we can expect a large interfacial tension between oil and water. This happens because the system consists of an oil excess phase and a water-rich microemulsion, where small quantities of oil are solubilized in nearly spherical micellar domains; in this instance, both sides of the interface are still dissimilar. On the other end of the spectrum, for a surfactant that is mainly affine

to the oleic components, the interfacial tension between oil and water is still large. The reason is similar to that described above, since the system consists of a water excess phase and an oil-rich microemulsion, which contains small quantities of water in nearly spherical micellar domains. The desirable condition occurs when the surfactant has approximately equal affinity to both oil and water. For this scenario, the system consists of three phases: both excess oil and water phases, as well as a microemulsion phase with comparable volume of solubilized oil and water. This microemulsion is arranged in such a way that the oil and water are present in nearly bicontinuous domains; hence, the composition on both sides of the interface is quite comparable, which results in ultra-low interfacial tensions.

1.2 Microemulsion fundamentals

Microemulsions are macroscopically homogeneous mixtures of surfactant, oil and water, which at the microscopic level are comprised of separated domains of oil and water with surfactant films or monolayers at the interface. The typical length scale of these domains is on the order of nanometers. A key characteristic of microemulsions is that they are thermodynamically stable with a very high degree of dynamics with regard to the internal structure (Kronberg et al., 2014). Though microemulsions can form in the presence of only surfactant, oil and water, they are commonly designed with a second amphiphile known as a cosurfactant; this cosurfactant can be either a different surfactant molecule or a medium-chain alcohol. The benefit of adding a cosurfactant is that the

amphiphilic monolayer will become less rigid, hence decreasing the risk of forming liquid crystals or lamellar phases.

The typical phase behavior of surfactant-oil-brine systems can be expressed in a ternary diagram, as shown by Figure 1-2. This figure shows an overall concentration corresponding to low surfactant concentration, and comparable amounts of oil and water (as shown by the small circle close to the W-O axis). For a highly hydrophilic surfactant, the water is completely solubilized in the microemulsion phase (as a continuous phase) while the oil is partially solubilized in near spherical domains; the remaining oil is in the excess oil phase that coexists with the microemulsion in equilibrium. This environment is depicted on the left of Figure 1-2, and is known as Winsor I or Type II- (the minus sign comes from the slope of the tie-lines in the two-phase region). Alternatively, for a highly lipophilic surfactant, the oil is completely solubilized in the microemulsion phase (as a continuous phase) while the water is partially solubilized in near spherical domains; the remaining water is in the excess water phase coexisting with the microemulsion phase. This condition is shown to the right of Figure 1-2, and is known as Winsor II or Type II+ (the plus sign denotes the positive slope of the tie-lines in the two-phase region). Finally, for comparable affinity to both oil and water, the oil and water are partially solubilized in the microemulsion phase arranged in bicontinuous domains, coexisting with both excess oil and water phases. This environment is shown in the center of Figure 1-2, and is known as Winsor III or Type III. Note that there are regions of two-phase coexistence on each side of the tie-triangle.

1.3 Impact of formulation variables on microemulsion phase behavior

An important question related to microemulsion phase behavior is how to change formulation variables (either surfactant internal or surfactant external) to induce changes in phase behavior in order to achieve desirable conditions (i.e. Type III phase behavior and ultralow interfacial tensions).

Surfactant internal parameters are structural parameters related to the surfactant (i.e. changing the surfactant molecule) such as the lipophilic chain length (e.g. number of PO groups, hydrocarbon chain length, degree of branching) and the hydrophilic chain length (e.g. number of EO groups). Figures 1-3 and 1-4 show relevant schematics indicating how these characteristics may change the surfactant structure at the interface, and hence changing its relative affinity to either component. Cosurfactant type and content can be considered as a surfactant internal parameter, since it will change the effective structure of the equivalent pseudo-surfactant component that will be used in the three-pseudo-component approximation of the system.

Surfactant external parameters are parameters that impact the condition of the system. Some examples are salt content of the water phase (changing the water or brine pseudo-component), equivalent alkane carbon number of the oil component (a measure of the oil composition depicting the change in the oil pseudo-component), temperature, and pressure.

The impact of the surfactant internal parameters on phase behavior is straightforward based on the description presented above: increasing the

lipophilic chain length increases the lipophilicity of the surfactant, while increasing the hydrophilic chain length increases the hydrophilicity of the surfactant. The impact of cosurfactant is a function of its corresponding affinity to both oil and water.

The impact of the surfactant external parameters is less intuitive. An increase in salinity tends to increase lipophilicity of the surfactant molecule for ionic surfactants, presumably due to the increased repulsion of the surfactant head to the ions present in the water phase. An increase in equivalent alkane carbon number (EACN) causes an increase in the hydrophilicity of the surfactant molecule, since the oil becomes more dissimilar to the lipophilic chain of the surfactant molecule. An increase in pressure tends to increase the hydrophilicity of the surfactant molecule, presumably due to the increased compressibility of the oil phase compared to the water phase that is nearly incompressible. For nonionic surfactants, an increase in temperature causes an increase in the lipophilicity of the surfactant molecule, whereas for ionic surfactants the effect of temperature is reversed. Table 1-1 summarizes the effect of different formulation parameters on microemulsion phase behavior.

1.4 Measures of surfactant affinity

In the last 60 years, a number of measures have been introduced to combine the effect of different formulation variables on surfactant affinity. These include the hydrophilic-lipophilic balance (HLB), the phase-inversion temperature (PIT), the cohesive energy ratio, and the interaction energy ratio (Salager et al., 2005). The

interaction energy ratio (R) was introduced by Winsor (1954), and it offers an insightful understanding of how changing interactions impact phase behavior at the interface level. The R ratio can be defined using the following equation,

$$R = \frac{A_{CO}}{A_{CW}}, \qquad (1-1)$$

where A_{CI} is the interaction between the surfactant adsorbed at the interface and component I per unit area of interface. Figure 1-5 presents a clear illustration of this interaction forces by looking at a surfactant monolayer at the interface between oil and water domains. From Equation 1-1, an R value of 1 is equivalent to a condition of equal interaction between the surfactant and both oil and water components. This condition would correspond to a Type III or Winsor III environment. When physicochemical formulation variables change, at least one of the interactions will change. For instance, if salinity in the system is reduced, then A_{CW} will increase, and the R value will be less than one, which corresponds to a Type II- or Winsor I environment. Alternatively, if salinity increases, then A_{CW} will decrease, making the R value to be greater than one, corresponding to a Type II+ or Winsor II environment. An illustrative diagram is presented in Figure 1-6, showing the ternary diagram representation for each affinity case, as well as the corresponding test tube observation.

1.5 Research goals

The objectives of this dissertation are to:

- Develop a curvature-based microemulsion phase behavior model, which can be coupled to interfacial tension.
- Model how microscopic structures in microemulsion systems can be tied to surfactant affinity, and key microemulsion parameters such as interfacial tension and phase behavior.
- Develop a microemulsion phase behavior model based on chemical potential empirical observations that can be directly tied to the thermodynamic definition of HLD.
- Capture surfactant affinity to both oil and water components in the context of surfactant partitioning through the HLD concept for a wide range of formulation variables.
- Capture the surfactant partitioning phenomena to the excess phases, and tie this behavior with a microemulsion phase behavior model.

1.6 Organization of the Dissertation

This dissertation presents a thermodynamic treatment of key properties in microemulsion systems. In Chapter 2, we present a literature review for all relevant aspects of this dissertation. In Chapter 3, we present a curvature-based microemulsion phase behavior model that considers the definition of principal curvatures. This model is coupled with interfacial tensions, and a tuning approach is presented that considers both phase behavior and interfacial tensions.

In Chapter 4, we present a model for the oil-water interfacial tension as a function of surfactant affinity in the three-phase region, as captured by the HLD, which relies on film bending energy arguments and empirical relationships for the microscopic curvatures. Following a similar approach, we present a model for the characteristic length scale. After an appropriate normalization, the interfacial tension is related to the characteristic length scale using a simple expression. Further, we introduce models for the oil-microemulsion and microemulsion-water interfacial tensions using phase transition boundary condition arguments, which are extended to account for compositional changes. These interfacial tension models are tied to solubilization ratios in order to introduce a coupled interfacial tension-phase behavior model for all phase environments.

In Chapter 5, we develop a new empirical phase behavior model based on chemical potentials and HLD. Further, the model is extended to account for surfactant partitioning into the excess phases. The model is compared to the $HLD - NAC$ EoS model for reference.

In Chapter 6, we allow for surfactant partitioning into both the water and oil excess phases, and then relate the relevant surfactant partitioning coefficients to the HLD state function so that all independent *K*-values of the three-phase region can be predicted. Surfactant screening based on EO and PO groups is also considered based on estimated K-values. Key dimensionless groups are identified, which allow for a simplified description of the surfactant partition coefficients. These groups are tied to phase behavior parameters. The surfactant

partition coefficients are combined with a phase behavior model to describe and predict the phase behavior when the excess phases are not pure.

Finally, in Chapter 7, we conclude by summarizing the key contributions from this dissertation, including main results and suggestions for future research.

Table 1-1. Impact of formulation variables on surfactant affinity and microemulsion phase behavior.

Increasing variable		Increased affinity	Phase behavior impact
Lipophilic chain length		Lipophilicity	Towards Type II+
Hydrophilic chain length		Hydrophilicity	Towards Type II-
Salinity		Lipophilicity	Towards Type II+
EACN		Hydrophilicity	Towards Type II-
Temperature	Nonionic	Lipophilicity	Towards Type II+
	Ionic	Hydrophilicity	Towards Type II-
Pressure		Hydrophilicity	Towards Type II-

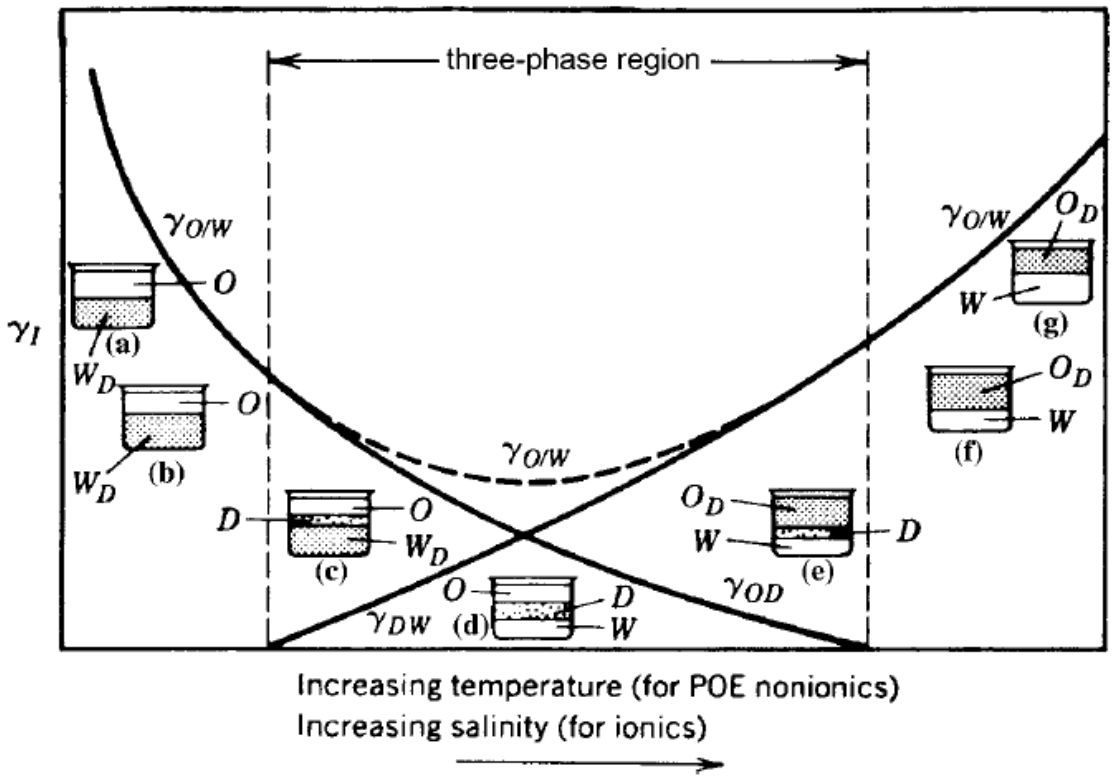

Figure 1-1. Impact of changing formulation variables on the microemulsion phase behavior, and relevant interfacial tensions. Rosen and Kunjappu (2012).

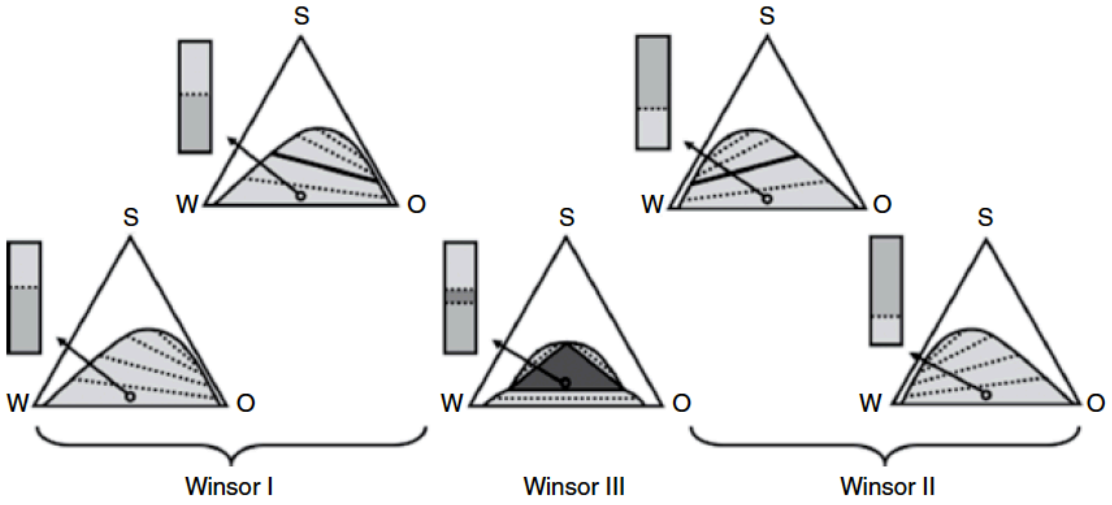

Figure 1-2. Schematic of different microemulsion environments for surfactant-oil-water systems. Kronberg et al. (2014).

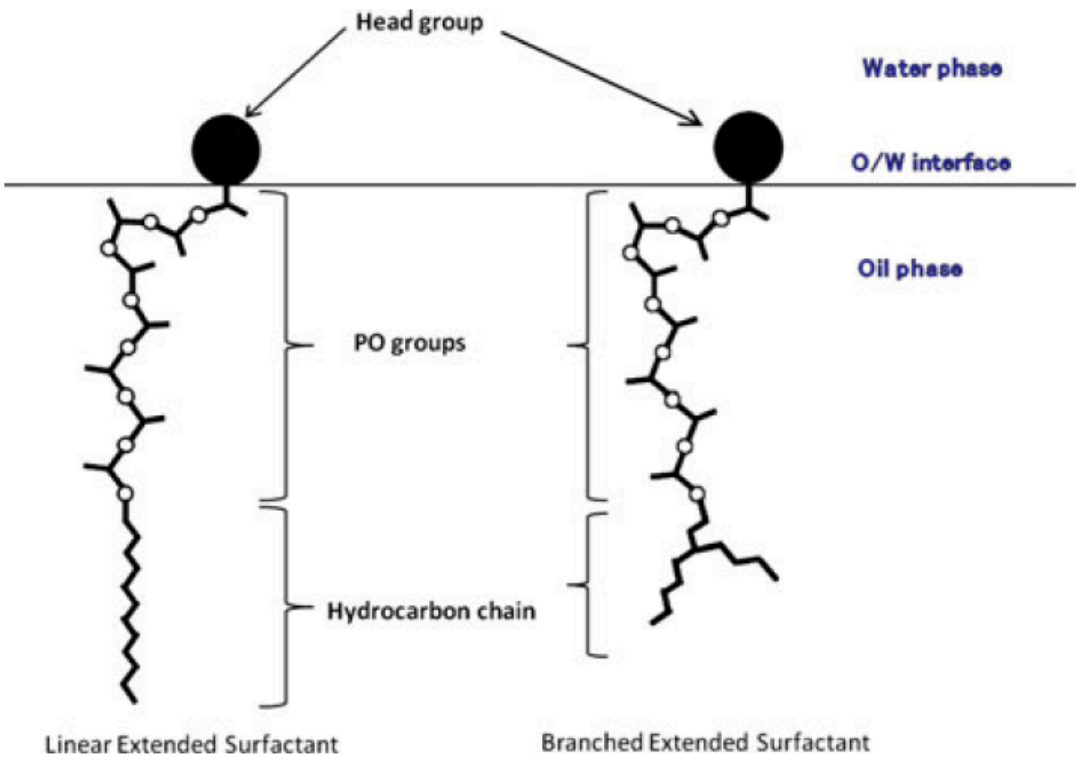

Figure 1-3. Schematic of extended surfactant molecule configuration, emphasizing different elements of the lipophilic chain of the surfactant. Phan et al. (2011).

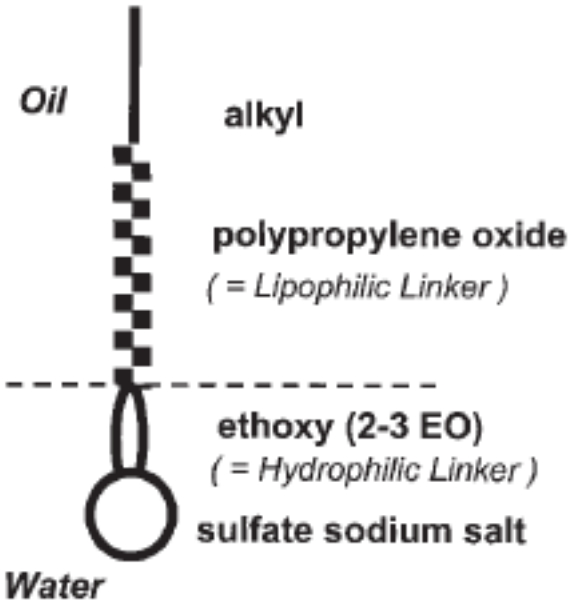

Figure 1-4. Schematic of extended surfactant molecule configuration, emphasizing different elements of the lipophilic and hydrophilic chains of the surfactant. Salager et al. (2005).

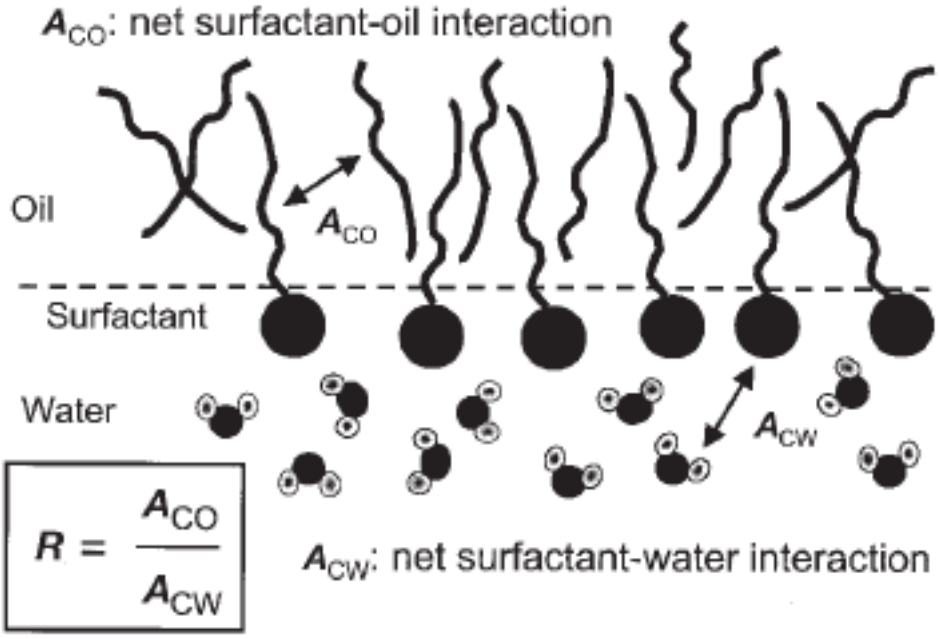

Figure 1-5. Interfacial picture of a surfactant-oil-water system, highlighting the relevant interactions needed to define Winsor's interaction energy ratio (R). Salager et al. (2005).

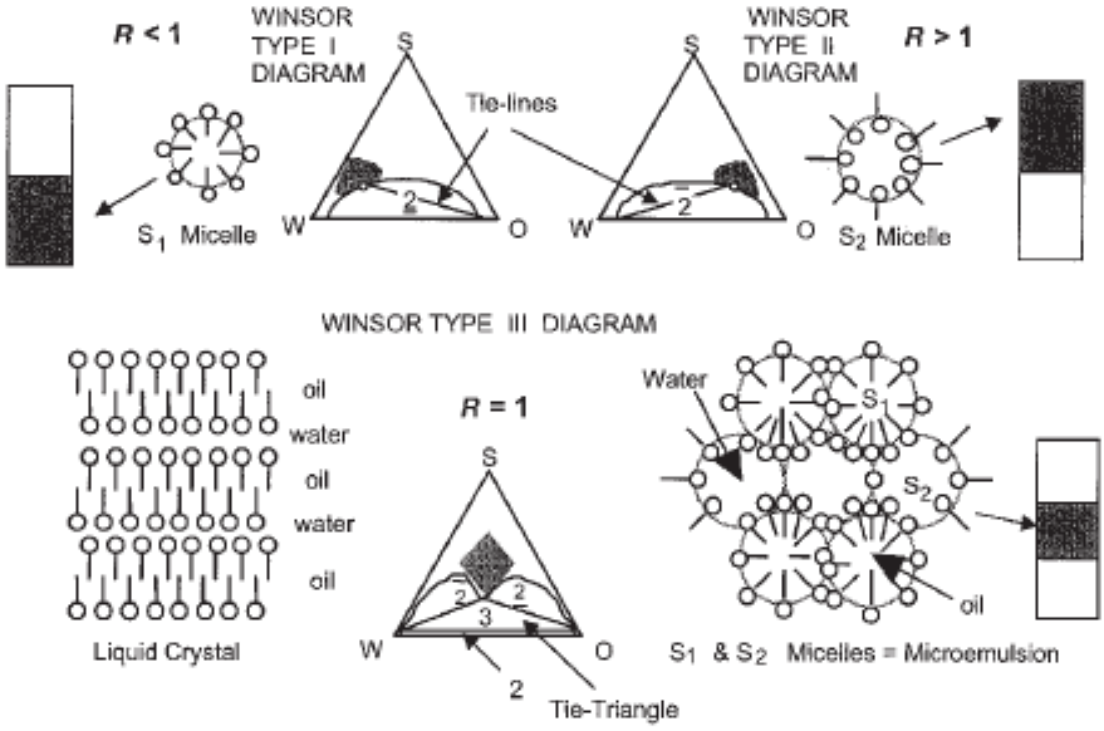

Figure 1-6. Schematic of the different type of phase behavior as a function of the interaction energy ratio (R) as defined by Winsor. Salager et al. (2005).

Chapter 2

Literature Review

The interaction of surfactant, oleic and aqueous compounds has been studied for decades due to its relevance for a wide range of industrial processes, including aquifer remediation and enhanced oil recovery. Under appropriate conditions, this interaction will result in the formation of a microemulsion phase. Microemulsions are complex phases consisting of oil and water domains, separated by a surfactant monolayer (Safran et al., 1986). Depending on the surfactant affinity for the oleic and aqueous compounds, the monolayer curvature changes determining what component is preferentially solubilized. Microemulsion phase behavior, in this context, describes the microemulsion composition (i.e. fraction of different components) as a function of surfactant affinity.

For most common applications, the microemulsion system can be in one of four environments, depending on the surfactant affinity state and overall composition. For a sufficiently large hydrophilic character, the system exhibits a microemulsion that is rich in the water component and an excess oil phase. In this case, known as a Type II- environment, the surfactant monolayer bends towards the oil domains, which by convention is characterized with a positive average curvature (Strey, 1994). Alternatively, for a sufficiently large lipophilic character, the system exhibits a microemulsion that is rich in the oil component and an excess water phase. In this case, known as a Type II+ environment, the

surfactant monolayer bends towards the water domains, hence a negative average curvature. For a balanced affinity state, the system exhibits a microemulsion with comparable proportions of oil and water components, and both excess oil and water phases. This case is known as a Type III environment, and the surfactant monolayer is approximately flat or bicontinuous, corresponding to a vanishing curvature. The final environment of interest, known as the Type IV environment, occurs for sufficiently large surfactant concentrations or near critical points, where the system exhibits only a single microemulsion phase. This occurs due to the abundance of surfactant molecules compared to the other components, which allows for a complete solubilization of the oil and water components into the microemulsion phase. Other exotic microemulsion environments, such as regions of liquid crystals, are beyond the scope of this study. Due to the importance of representatively capturing the surfactant affinity to both the oil and water, we will cover some fundamental aspects in the following section.

2.1 Surfactant interaction fundamentals

Surfactants are amphiphilic compounds that are characterized by having in the same molecule two groups that significantly differ in their solubility. For example, the hydrophilic group is water soluble, whereas the lipophilic group is hydrocarbon soluble (Winsor, 1968). The aggregate interaction of the surfactant molecule can be divided into electrostatic and electrokinetic interactions. Electrostatic interactions arise from the charges on ions and from an uneven

distribution of charge in certain electrically neutral molecules. On the other side, electrokinetic interactions occur between electrically nonpolar molecules, which attract one another due to the movements of electrons within the molecules (Winsor, 1968).

Changes in surfactant formulation variables (e.g. salinity, temperature, oil composition) have been widely documented to change the affinity of the surfactant molecule, and hence impact the microemulsion phase behavior (Wade et al., 1978, Chan and Shah, 1979, Salager et al., 2000). Salager et al. (2000) introduced the hydrophilic-lipophilic deviation (HLD), which is the dimensionless free energy of transfer of a surfactant molecule from the oil phase to the water phase. This measure can be directly defined to the surfactant concentration in both oil and water excess phases, as shown in Equation 2-1.

$$HLD - HLD_{ref} = \frac{\mu^{\circ}_{so} - \mu^{\circ}_{sw}}{RT} = ln\left(\frac{K^{s}_{wo}}{K^{s}_{wo_{ref}}}\right), \qquad (2-1)$$

where μ°_{sj} is the reference chemical potential of the surfactant in phase *j*, K^{s}_{jk} is the ratio of the surfactant concentrations between phases *j* and *k*. Assuming $K^{s}_{wo_{ref}} = 1$ for $HLD_{ref} = 0$ significantly simplifies Equation 2-1. Positive values of HLD signify an increased lipophilicity, whereas negative values of HLD correspond to an increased hydrophilicity. The HLD has been widely used as measure of surfactant affinity (Acosta et al. 2003, Ghosh and Johns, 2016A).

Figure 2-1 shows a tent diagram showing how different phase behavior environments can be obtained for varying HLD conditions.

2.2 Surfactant partitioning

For surfactant-oil-brine systems, surfactants have simultaneous affinity to both oil and brine components, due to their amphiphilic nature. This is the reason behind the existence of a microemulsion phase, which contains large proportions of two immiscible fluids (i.e. oil and brine) that are bridged by the surfactant molecules. However, the presence of surfactants in the excess phases is typically ignored due to limited modeling capabilities of the coupling between surfactant partitioning and microemulsion phase behavior, even though there has been extensive experimental data suggesting surfactant's dynamic partitioning as formulation parameters are changed**.**

Numerous experiments have been done to measure surfactant partitioning coefficients, but these results have not been used meaningfully yet in any equation-of-state methodology. For example, the surfactant partitioning coefficients of p,t-octylphenoxyethanols (OPE) between water and isooctane at 25°C were determined by Crook et al. (1965). They found that surfactant partitioning between the oil and water excess phases increased by four orders of magnitude when the ethylene oxide (EO) chain length was increased from 1 to 10, showing that the length of the EO chain is a measure of the hydrophilicity of the surfactant. Wade et al. (1978) studied the surfactant partition coefficient for TRS 10-80 (a petroleum sulfonate) for changing oil equivalent alkane carbon

number (*EACN*). An increasing EACN corresponds to increasing the hydrophilicity of the surfactant-oil-brine system. Further, they showed that optimum conditions occur when the change in chemical potential of the surfactant in the brine equals that of the oil.

Koukounis et al. (1979) studied the problem of selective surfactant partitioning for both anioninc and nonionic mixtures. They found that binary and ternary mixtures of anionic mixtures exhibited little fractionation, and there was very little partitioning into the oleic phase. Alternatively, they found that polydispersed nonionic systems showed selective fractionation, and in general that nonionic systems partition preferentially into the oil phase.

Chan and Shah (1979) stated that for low surfactant concentration systems the transition from a surfactant-rich lower to upper phase occurs when the partition coefficient is unity. Further, they mentioned the same behavior is characteristic of high surfactant concentration systems, and studied the partition coefficient of petroleum sulfonates as brine salinity and equivalent alkane carbon number changed.

Brooks and Richmond (1994) studied nonionic surfactant partitioning as a function of EO chain length and temperature in the context of defining a transitional inversion. Salager et al. (1995) studied ethoxylated nonylphenol surfactants and their partitioning behavior for changes in salinity, alcohol content, and EO chain length. Ysambertt et al. (1997) extended this work by investigating the effect of benzene content on the partitioning as the EO chain length was changed. Butler and Hayes (1998) also examined partitioning of ethoxylated

dodecyl alcohol surfactants in the aqueous phase and nonaqueous phase liquids (NAPL) as EO chain length was varied.

Additional experiments were done by Ravera et al. (2000) on surfactant partitioning as the hydrophobic and hydrophilic chain lengths, and temperature were increased. Salager et al. (2000) discussed the partitioning behavior of ethoxylated alkyl phenol surfactants, naming the EO chain length, alkyl chain length, and surfactant branching as key controlling parameters. More importantly, they identified that there exists a linear relationship of the log of the surfactant partitioning between excess phases with the hydrophilic-lipophilic difference (HLD). This fact suggests that all formulation variables that impact microemulsion phase behavior are likely to affect the partitioning of surfactants. Further, they presented partitioning experimental data as the EO chain length changed at different temperatures. Marquez et al. (2002) extended this work by studying the partitioning in the context of surfactant branching as the EO chain length was increased, and for oils with different *EACN*. Ben Ghoulam et al. (2002) examined the partitioning of poly(oxyethylene glycol n-dodecyl ether) between water and isooctane, for different temperatures as the EO chain length was changed.

Marquez et al. (2003) presented data on polyethoxylated nonylphenol surfactants, emphasizing the role of this type of surfactant in the Venezuelan production of over 100,000 bbl/D of bitumen in water emulsions. They also compared those results to the partitioning of polyethoxylated alcohol surfactants.

Surfactant partitioning between an aqueous phase and a NAPL using surfactants with various hydrophilic and hydrophobic chain lengths was

examined by Cheng et al. (2005). Graciaa et al. (2006) studied the surfactant partitioning as a function of the EO chain length, and changing different formulation variables (e.g. *EACN*, salinity, surfactant branching, alcohol content). They then measured partitioning as a function of the EO chain length as the octylbenzene content in the oil phase was changed.

Bravo et al. (2008) measured the partitioning of a surfactant-oil-water system, where the surfactant was taken to be a fatty acid. The fatty acid carbon number was varied, and different alcohols were added in equal proportions. Marquez et al. (2012) also studied fatty acid surfactant systems, in addition to ethoxylated surfactants. They explored fatty acid partitioning as different electrolytes and the fatty acid carbon number was changed. For ethoxylated surfactants surfactant partitioning with changing EO chain length for different alcohol concentrations, salt concentrations, and alkyl chain lengths was considered.

Finally, Salager et al. (2013A) examined surfactant partitioning for a very pure alkylbenzene sulfonate as function of salinity, and a technical grade alkylbenze as a function of *EACN* for different surfactant concentrations. Troncoso and Acosta (2015) studied the partitioning of alkyl and alkylphenol ethoxylate surfactants with changing EO chain length.

2.3 Phase behavior modeling of surfactant-oil-brine systems

There are a variety of microemulsion phase behavior models reported in the literature, with different levels of theoretical basis and practicality. Robbins (1977)

presented a model that predicts the oil and water solubilization ratios as a function of the ratio of surfactant head to chain volume, which was tied to different degrees of surfactant affinity. Talmon and Prager (1977, 1978) presented their widely known qualitative model, based on statistical mechanical concepts aimed at generating random two-fluid geometries. Pope and Nelson (1978) extended the empirical Hand model (Hand, 1929), to represent the binodal and distribution curves as a function of composition and salinity. Rossen et al. (1982) presented microemulsion phase behavior modeling by means of representative free-energy functions including the linearly screened Flory-Huggins and the exponentially screened Flory-Huggins equations.

In 1982, De Gennes and Taupin proposed a model for the formation of microemulsions in surfactant-oil-water systems, extending the earlier work of Schulman and Montagne (1961) by considering the entropy of a fluctuating interface. Jouffroy et al. (1982) built on the Talmon and Prager model discussed above, identifying that the characteristic size of the random fluid geometries is the persistence length (i.e. ξ) and removing other assumptions related to the interfacial curvature.

Fredenslund et al. (1975) introduced the UNIFAC model as a group-contribution method to predict the activity coefficients in nonelectrolyte liquid mixtures. In a multicomponent mixture, the activity coefficient of component i in phase j has a combinatorial and a residual contribution. The combinatorial contribution reflects entropic effects, and depends on the size and shape of the molecule for component i, while the residual contribution is controlled by the

interaction of different components (Chen et al., 1993). Cheng et al. (2005) used the UNIFAC method to predict the partitioning of nonionic surfactant between octanol and water phases. Troncoso and Acosta (2015) also used the UNIFAC method to predict the partition of alkyl and alkylphenol ethoxylate surfactants between the excess phases. Kahl et al. (1997) used the UNIQUAC method to capture qualitative trends in the phase behavior for ternary and quaternary microemulsion systems. Because of the complexities of these approaches in capturing activity coefficients, we are motivated to find an empirical approach to understand the behavior of relevant activity coefficients that arise in a chemical potential description of the oil and water solubilities in the microemulsion phase for changing surfactant affinity conditions.

Salager et al. (2013B; 2014) introduced the notion of the performance index as a measure of formulation quality, which is defined as the co-logarithm of optimum interfacial tension. They presented the performance index as a function of the optimum solubilization through Chun Huh's correlation (Huh, 1979; Huh, 1983). The performance index was shown to be a linear function of formulation variables, and was used to describe the phase behavior away from experimental conditions. Similarly, the optimum solubilization ratio has been correlated to different formulation variables (Ghosh and Johns, 2016a; Khorsandi and Johns, 2016).

Acosta et al. (2003) introduced a microemulsion phase behavior model based on particular definitions of a net and the average curvatures. The average curvature in the HLD-NAC model is a quantity defined as the average of the oil

curvature and the water curvature. Under the assumption of spherical micelles, the model allows to estimate oil and water solubilization ratios for different HLD conditions. However, the model assumes there exist both oil and water spherical micelles across all microemulsion environments. For example, in a Type II- environment, the model assumes the continuous water component can be approximated by spherical micelles.

Many contributions have relied on the HLD-NAC model to study the phase behavior of oil-water-surfactant systems for a wide variety of cases (Acosta, 2008; Acosta et al., 2012; Kiran and Acosta, 2015; Ghosh and Johns, 2016b; Jin et al., 2017). However, Khorsandi and Johns (2016) noted the original HLD-NAC equations yielded unphysical results in both Type II- and Type II+ environments as shown in Figure 2-2. Further, they presented an algorithm that allows to compute physical results in both Type II- and Type II+ environments by modeling the correlation length at the critical points in the two-phase lobes as shown in Figure 2-3. Nouraei and Acosta (2017) improved upon the original HLD-NAC equations to present an alternative approach that allows for a physical computation of two-phase lobes.

2.4 Microemulsion phase behavior and interfacial bending

A microemulsion is a mixture of oil, water and surfactant, which is in thermodynamic equilibrium (Chandra and Safran, 1991). Though macroscopically homogeneous, water and oil domains can be observed at the microscopic level. These domains are separated by surfactant monolayers,

which can preferentially bend towards either domain depending on the relative affinity of the surfactant to the oil and water.

Both experimental and theoretical studies have found that the shapes of these oil and water domains can change depending on the surfactant affinity. For example, when the surfactant affinity for the water is significantly greater than that of the oil (i.e. Type II-), the water domains are completely connected and the oil domains are approximately spherical. Alternatively, when the surfactant affinity for the oil surpasses that of the water, the oil domains are connected and the water domains are approximately spherical (i.e. Type II+). For comparable surfactant interaction between the oil and water, the resulting morphology is approximately bicontinuous (i.e. Type III). Finally, as the surfactant affinity transitions from the Type II- or Type II+ to the Type III environment, the morphology of the domains changes from spherical to bicontinuous by going through a cylindrical domain (Chandra and Safran, 1991, Strey, 1994). Strey (1994) presented a schematic of how the mean, principal, and Gaussian curvatures change for a temperature scan, which is shown in Figure 2-4.

2.4.1 Interfacial tension

The interfacial tension is the force that holds the surface between two phases together. For the case of surfactant-oil-water interaction, three interfacial tensions are of interest, namely γ_{ow}, γ_{om} and γ_{mw}. In the absence of surfactant, γ_{ow} is typically around 50mN/m, denoting the dissimilarity between the oil and water components. By the introduction of surfactants, surface forces are reduced by

the role of the surfactant component as a bridge at the interface. It is of interest whenever the affinity of the surfactant to both the oil and water is equivalent (i.e. $HLD = 0$ or optimum condition), since the interfacial tension between the oil and water phases can reach ultra-low values, which is typically below 10^{-3}mN/m (Huh, 1979).

The interfacial tension can be thermodynamically defined as the change in free energy upon an infinitesimal increase of the contact area between the two phases of interest. Strey (1994) developed an equation for the interfacial tension considering the free energy per unit area associated with curvature deformations as presented by Helfrich (1973) in his treatment of lipid bilayers. The resulting expression is,

$$\gamma_{ow} = 2H^2(\kappa + \overline{\kappa}) - \overline{\kappa}c_1c_2, \qquad (2-2)$$

where H is the mean curvature, which is defined as $H = (c_1 + c_2)/2$, c_1 and c_2 are the principal curvatures, and κ and $\overline{\kappa}$ are the bending and saddle-splay moduli, respectively (both κ and $\overline{\kappa}$ have dimensions of energy). These moduli, which control the shape of the interfacial layer, can be estimated from experimental methods (Lee et al., 2001), molecular dynamics simulations (May et al., 2007), or analytical techniques (Kheyfets et al., 2016). Figure 2-5 shows how the mean curvature changes for a temperature scan, and Figure 2-6 shows the interfacial tension data corresponding to the same microemulsion system.

Pouchelon et al. (1980) studied the relevant interfacial tensions for the brine-toluene-SDS-butanol quaternary mixture as a function of salinity. Salinity changes the affinity of the surfactant at the interface between the aqueous and organic domains. They found how γ_{om} decreases with increasing salinity, until the organic and microemulsion phase are fully miscible (i.e. $\gamma_{om} = 0$). Alternatively, γ_{mw} increases from zero (i.e. the aqueous and microemulsion phases are fully miscible) with increasing salinity. Consequently, γ_{ow} decreases with salinity until reaching a minimum value at optimum salinity (i.e. $HLD = 0$), and thereafter increasing with salinity. Kunieda and Shinoda (1982) studied the behavior of γ_{ow}, γ_{om}, and γ_{mw} as a function of temperature for a surfactant-oil-brine system finding a similar behavior as the one described above for salinity changes.

Recently, Salager et al. (2016) studied the change in optimum oil-water interfacial tension (γ_{ow}^{min}) as a function of various formulation variables. Their approach is equivalent to noting that the log of (γ_{ow}^{min}) is a state function of the relevant formulation variables. Therefore,

$$log\left(\frac{\gamma_{ow}^{min}}{\gamma_{ow,ref}^{min}}\right) = \sum_{i=1}^{N}\left(\frac{\partial log\left(\gamma_{ow}^{min}\right)}{\partial X_i^*}\right)_{X_k^* \neq X_i^*}\left(X_i^* - X_{i,ref}^*\right), \qquad (2-3)$$

where X_i^* is formulation variable i at optimum condition and the partial derivatives of $log\left(\gamma_{ow}^{min}\right)$ were assumed constant based on experimental observations.

Huh (1979, 1983) developed a theoretical and highly practical result to couple relevant interfacial tensions with their corresponding solubilization ratios,

$$\gamma_{om} = \frac{\Omega}{{\sigma_o}^2}$$

$$\gamma_{mw} = \frac{\Omega}{{\sigma_w}^2}, \qquad (2-4)$$

where Ω is a scaling constant (typically 0.3 mN/m), $\sigma_i \equiv C_{im}/C_{sm}$ is the solubilization ratio of component i and C_{ij} is the concentration of component i in phase j. Recently, Ghosh and Johns (2016A) showed that Eq. 2-4 can be obtained from the HLD-NAC model, finding $\Omega = E_r/(36\pi I^2 L^2)$, where E_r is the interfacial rigidity (dimension of energy), I is the dimensionless I-ratio parameter defined as $I = V_s/A_s L$, V_s is the total surfactant volume, A_s is the interfacial surface area, and L is the thickness of the interface (approximate tail-length of surfactant).

Most interfacial tension models in the literature for microemulsion systems are defined to be functions of a single formulation variable (typically temperature or salinity), and they do not explicitly consider the effect of variable overall composition. For example, Bellocq et al. (1982) presented a free energy-based model to capture the dependence of interfacial tensions with composition changes. Their model was extended to account for density differences between the phases for a microemulsion system. Cazabat et al. (1982) used a scaling law model to describe the dependence of interfacial tension with changes in density

differences between the phases. Further, they estimated the characteristic length corresponding to the relevant interfacial tensions (i.e. γ_{om} or γ_{mw}).

Borkovec (1989) presented a model for spherical micelles, which allows for a description of the distribution of aggregate sizes and interfacial tensions. Aveyard et al. (1990) scaled interfacial tension and characteristic length for spherical micelles to estimate changes in interfacial tension with temperature. Their scaling is based on prior knowledge of both the characteristic length and the bending modulus.

Leitao et al. (1996) extended the ideas of Strey (1994) to develop a model for γ_{ow} by substituting the correlations for mean and principal curvatures as a function of temperature into Eq. 2-2. They were able to scale the IFTs of different systems onto a single curve by considering a reduced temperature definition.

Wennerstrom et al. (2006) presented models for γ_{om} for a Type II- environment and γ_{mw} for a Type II+ environment, both as a function of temperature by considering the contribution of curvature energy and entropy of mixing. Further, they presented a model for γ_{ow} in Type III as a function of temperature, showing symmetry around the optimum.

Given that γ_{ow}, γ_{om}, and γ_{mw} appear to have similar behavior as different formulation variables (e.g. salinity, temperature), we are motivated to find a model to correlate each of these interfacial tensions with HLD.

2.4.2 Characteristic length scale

The quality of a microemulsion system can be assessed by the capacity to solubilize oil and water components for a given surfactant concentration. This quality is directly related to the correlation length of a microemulsion (ξ), which is inversely related to the amount of surface per unit volume (S/V) as has been shown for various bicontinuous models (Debye et al., 1957; Talmon and Prager, 1978; De Gennes and Taupin, 1982). For spherical micelles, the correlation length can be taken as the inverse of the mean curvature (Strey, 1994). Therefore, $\xi = r$ for spherical micelles, with r being the radius of the sphere. For tertiary oil recovery applications, it is common for the microemulsion to transition between a Type II- environment (corresponding to $H > 0$) to a Type II+ environment (corresponding to $H < 0$). Therefore, we will have a vanishing H in the bicontinuous regime (i.e. at optimum condition, or $\mathcal{H} = 0$), but experimentally it is known that ξ does not diverge at optimum and instead it attains a maximum value (Strey, 1994; Strey, 1996). Strey (1994, 1996) showed the following definition for the correlation length is consistent across all phase environments,

$$\xi = \left(\frac{2}{c_1^2 + c_2^2}\right)^{0.5}. \qquad (2-5)$$

The correlation length has been experimentally studied in the literature as a function of relevant formulation variables. Guest et al. (1985) studied the characteristic length scale as a function of salinity for a surfactant-oil-brine system. The behavior of ξ is complementary to that of γ_{ow}, increasing with

salinity until reaching a maximum value at optimum salinity, and thereafter decreasing with salinity. Strey (1994) studied the correlation length for an oil-water-$C_{12}E_5$ system as a function of temperature. Sottmann et al. (1997) studied the correlation length for an oil-water-C_jE_k system as a function of the carbon number of the alkyl chain (j) and the surfactant headgroup size (k). Berghaus et al. (2016) studied the correlation length for an oil-water-$C_{10}E_4$ system as a function of pressure.

Following a similar argument as the one presented for interfacial tensions, we are motivated to find a model to characterize the characteristic length scale as a function of HLD in order to account for changes in multiple formulation variables.

2.5 Research problems and solutions

In this section, we identify gaps in the literature and describe how we address such gaps in the upcoming chapters of this dissertation.

2.5.1 Problem 1: rigorous description of curvatures in phase behavior modeling

The HLD-NAC model from its origins replaces the definition of principal curvatures used to estimate the correlation length by what are called the oil and water curvatures. To understand the significance of this, let us consider a sufficiently hydrophilic state where we have a Type II- microemulsion. This state consists of oil internal micelles, which for simplicity we assume to be perfectly

spherical. For a given oil internal micelle, the principal curvatures are equal. The water component is present in the microemulsion phase as the continuous domain. Nevertheless, the HLD-NAC approximates this continuous domain as *spheres*. Needless to say, using this approach would yield a definition of the microemulsion correlation length that has no mechanistic connection to the correlation length that can be measured from scattering experiments (even though in the two-phase regions they have the same qualitative trend). Further, the three-phase correlation length as defined by the HLD-NAC model is constant (e.g. Figure 2-8), whereas experiments show this correlation length to be increasing in the three-phase region, reaching a maximum at optimum condition (e.g. Figure 2-7). Finally, the HLD-NAC extension of Khorsandi and Johns (2016) presents an interpolation function that allows for construction of physical two-phase regions (previously, all HLD-NAC contributions were not able to construct physical two-phase regions). However, their interpolation function relies on a definition of a correlation length at the critical point that is finite (this is key in their development). As well-known scaling from the physics literature suggests (De Gennes and Taupin, 1982) considering a finite correlation length at the critical point is equivalent to saying the interfacial tension at the critical point does not vanish (in other words, phases do not become fully miscible).

In Chapter 3, we develop a microemulsion phase behavior model that is defined based on the principal curvatures of micelles. In this approach, the correlation length has a mechanistic connection to the size of micelles in the system, with a physical behavior in the three-phase region (i.e. non-constant

behavior reaching a maximum at optimum). Furthermore, the model has a physical definition of the correlation length at the critical point, diverging to infinity, which translates into vanishing interfacial tensions.

One important potential of this novel model is its future extension to couple phase behavior with microemulsion viscosity, where micellar shapes are known to be an important factor determining the complex viscosity behavior of surfactant-oil-brine systems (Kaur et al., 2012).

2.5.2 Problem 2: robust interfacial tension modeling

All interfacial tension models in the literature for microemulsion systems are defined to be functions of a single formulation variable (typically temperature), and they do not explicitly consider the effect of variable overall composition.

In Chapter 4 we present a consistent interfacial tension model for all relevant interfacial tensions in microemulsion systems (i.e. oil-microemulsion, microemulsion-water, and oil-water). These interfacial tensions are made functions of both HLD (simultaneously accounting for changes in multiple formulation variables) and overall composition. Further, this model is coupled with Huh's equation that allows for phase behavior estimations.

2.5.3 Problem 3: flexible phase behavior modeling

Recent contributions to the petroleum engineering literature have relied on the HLD-NAC model to describe microemulsion phase behavior. However, the HLD-NAC model in its most current form (Khorsandi and Johns, 2016) has a number

of assumptions and limitations including symmetric phase behavior in the three-phase region and the inability to independently tune all model parameters at a fixed HLD condition.

In Chapter 5 we develop a microemulsion phase behavior model based on chemical potentials that is accurate in both tuning and prediction of phase behavior data, and removes the assumptions described above of the model by Khorsandi and Johns (2016).

2.5.4 Problem 4: surfactant partitioning

Most phase behavior models assume pure excess phases (i.e. the surfactant component is only present in the microemulsion phase).

In Chapter 6 we develop a surfactant partitioning model based on chemical potentials that is coupled with a phase behavior model, allowing the surfactant component to partition to both oil and water excess phases.

2.6 Summary

In this chapter, a literature was presented covering relevant aspects of surfactant-oil-brine interactions that are used in subsequent chapters in this dissertation.

The state-of-the-art was reviewed as it relates to surfactant affinity quantification, and explaining in great detail the hydrophilic-lipophilic deviation (HLD) measure. From its thermodynamic definition, the HLD measure is tied to the surfactant partitioning between the oil and water phases.

Then, a review was presented for surfactant partitioning behavior for a wide variety of surfactant type and for a wide variety of formulation variables, including both surfactant internal and external parameters (as defined in Chapter 1).

Next, microemulsion phase behavior models were reviewed, showing models with varying degrees of rigor and practicality. A special emphasis was placed on HLD-NAC approaches, which have been of increasing interest in the petroleum engineering literature in recent years.

Then, a review was presented describing a number of aspects related to the microstructure of microemulsion systems, as they relate to both interfacial tension and characteristic length scale. Also described were the experimental behavior for both interfacial tension and characteristic length scale, and relevant models.

Finally, the interaction of alcohols in microemulsion systems was reviewed, describing a number of experimental results, and discussing a variety of modeling approaches.

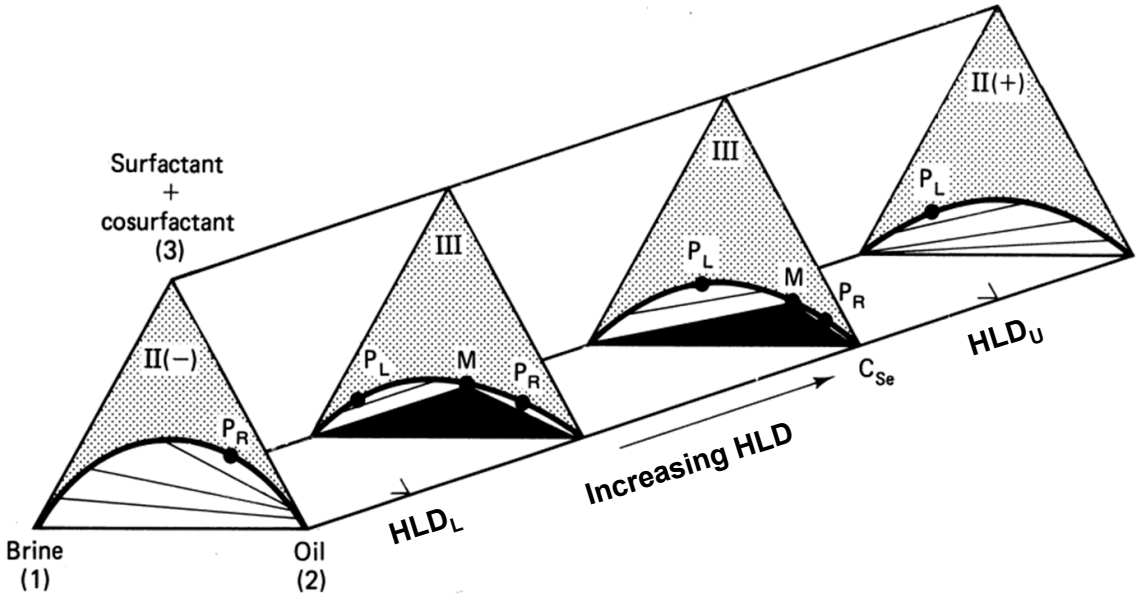

Figure 2-1. Tent diagram showing the different type of phase behavior as a function of the hydrophilic-lipophilic deviation (HLD) as defined by Salager et al. (2000) for changes in a single formulation variable (e.g. salinity). Modified from Lake et al. (2014).

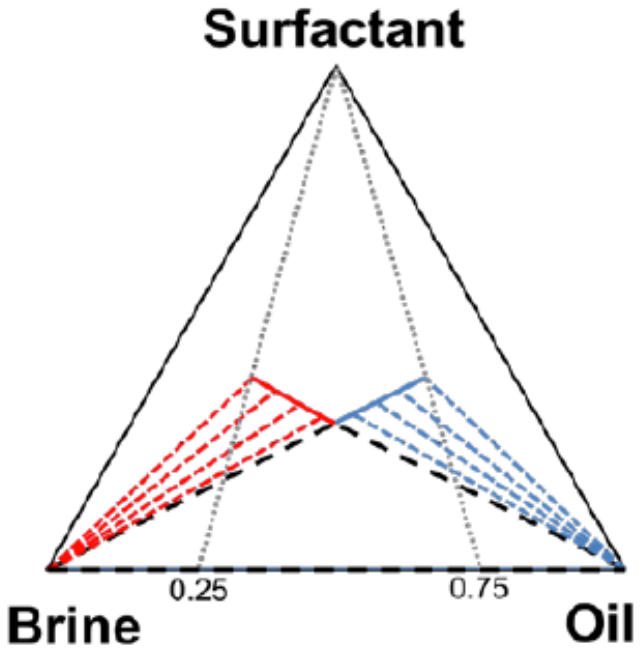

Figure 2-2. Ternary diagrams showing unphysical two-phase regions obtained from the original description of the $HLD - NAC$ model based on catastrophe theory. Khorsandi and Johns (2016).

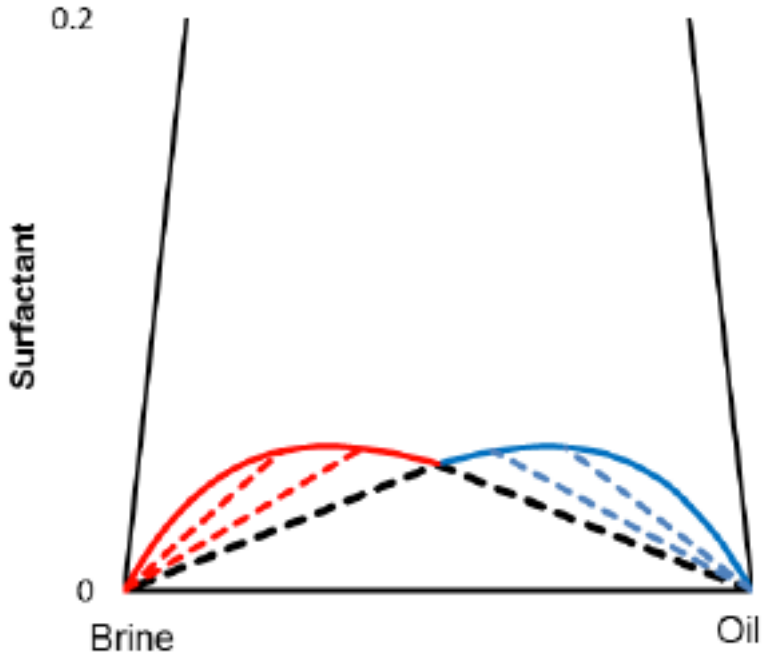

Figure 2-3 Ternary diagrams showing the extension of the $HLD - NAC$ model to obtain physical two-phase regions obtained from the robust algorithm presented by Khorsandi and Johns (2016).

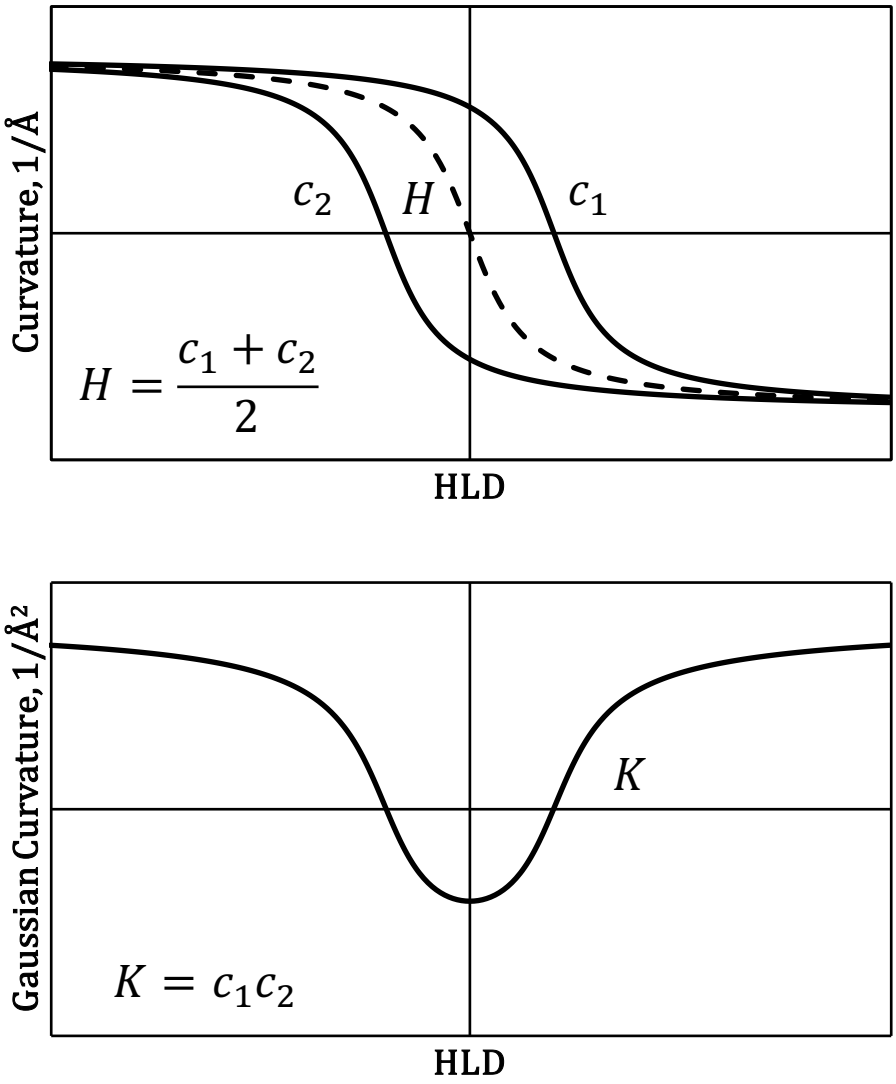

Figure 2-4. Schematic showing the general trend of the microscopic mean curvature and principal curvatures (top), and Gaussian curvature (bottom) of a microemulsion system for an HLD scan. Modified from Strey (1994).

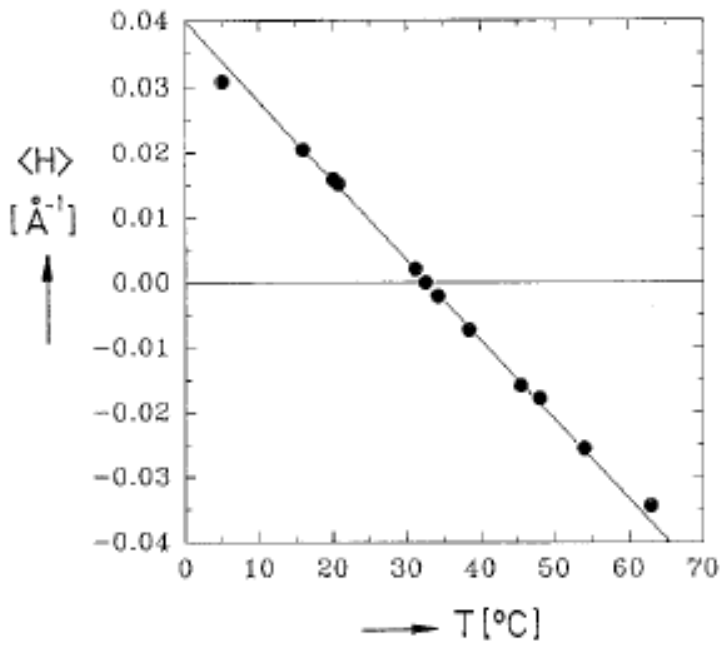

Figure 2-5. Experimental data for the mean curvature for a temperature scan obtained using both small-angle neutron scattering (SANS) and freeze-fracture electron microscopy (FFEM). Strey (1994).

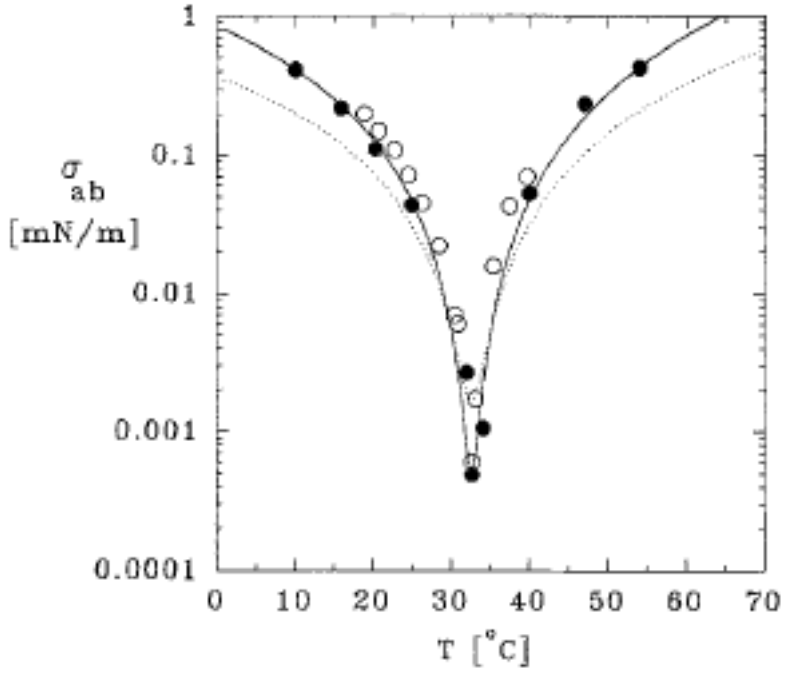

Figure 2-6. Interfacial tension data for a temperature scan obtained using both spinning drop and laser light scattering. Strey (1994).

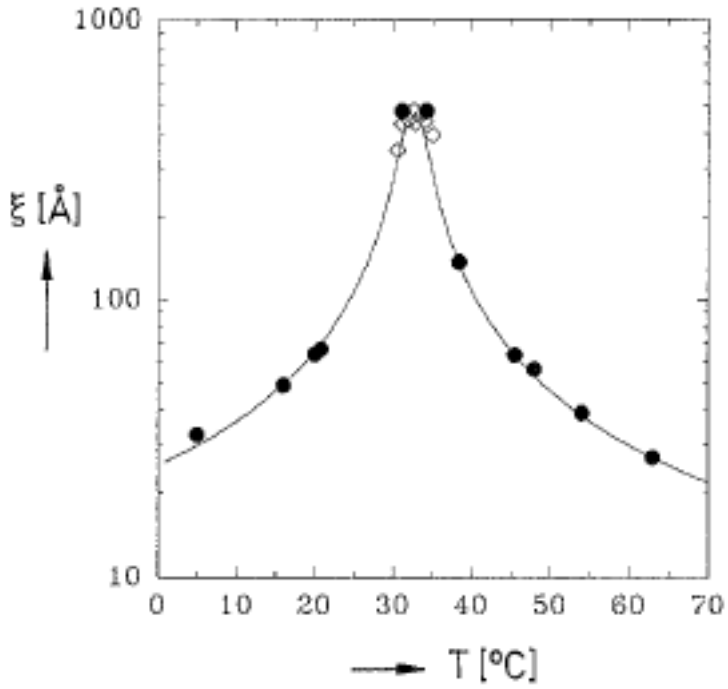

Figure 2-7. Experimental data for the characteristic length for a temperature scan. Strey (1994).

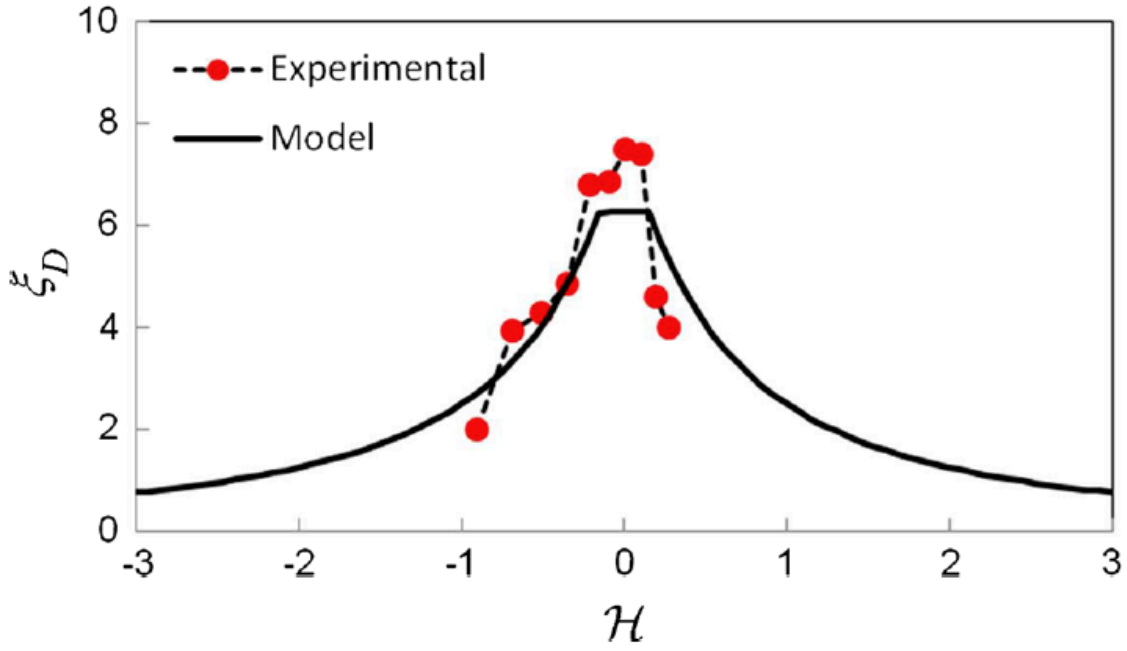

Figure 2-8. Model and experimental results for the dimensionless correlation length as defined by the $HLD - NAC$ model. Khorsandi and Johns (2016).

Part II

Curvature-Based Methods

Chapter 3

Curvature-Based Equation-of-State for Microemulsion Phase Behavior and Interfacial Tensions

In this chapter, we present a physical equation-of-state using a proper definition of principal curvatures. This improved model removes assumptions and limitations of the previous flash (Khorsandi and Johns, 2016) such as assuming spherical micelles, symmetric phase behavior, constant correlation length in the three-phase region, two-phase tuning parameter that can only be defined under variable HLD conditions; all of these assumptions and limitations were identified by Torrealba and Johns (2017B). Another limitation of the previous flash is the assumption of a non-diverging correlation length at the critical point. Using well-known scaling (De Gennes and Taupin, 1982), this corresponds to a critical point with non-vanishing interfacial tensions. Our model allows for a diverging correlation length at the critical point. Furthermore, we allow for a variable micellar curvature under the assumption of a general prolate spheroid micellar geometry. The resulting equations in the three-phase region (where bicontinuity is assumed) are consistent with Eq. 4-16, which are derived using an IFT approach where principal curvatures are also considered. The curvature model is combined with Huh's equation to capture interfacial tensions. This improved curvature approach is shown to accurately capture both phase behavior and interfacial tension data using this framework. Further, it is shown that using the common approach of assuming a fixed value of $\Omega = 0.3$ mN/m in Huh's equation

yields unacceptably large errors in interfacial tensions. Finally, compositional ternary experimental data is tuned using this novel approach.

3.1. Methodology

For a Type II- environment, we can consider micelles to be prolate spheroids such as the one depicted in Figure 3-1, where $r_b \geq r_a$. Assuming the thickness of the surfactant interfacial film is negligible compared to the solubilized volume, the oil volume inside the micelle is given by,

$$V_{om} = \frac{4\pi}{3} r_a^2 r_b. \qquad (3-1)$$

Similarly, the surfactant interfacial area (A_s) is,

$$A_s = 2\pi r_a^2 \left(1 + \frac{r_b}{r_a t} \sin^{-1} t\right), \qquad (3-2)$$

where $t^2 = 1 - r_a^2/r_b^2$. Therefore, we can define a domain size corresponding to these micelles as,

$$\xi^{II-} = \frac{V_{om}}{A_s}. \qquad (3-3)$$

Since we are accounting for the deviation from spherical micelles, the volume of surfactant in the micelle can be expressed by $V_{sm} = A_s L$, which allows us to rewrite Eq. 3-3,

$$\xi^{II-} = \sigma_o L, \tag{3-4}$$

or in dimensionless form for both Type II- and Type II+,

$$\begin{aligned} \xi_D^{II-} &= \sigma_o \\ \xi_D^{II+} &= \sigma_w. \end{aligned} \tag{3-5}$$

In the Type III environment, we consider bicontinuous micelles (Scriven, 1976). For the oil domains, we can assume the same volume and area terms defined in Eqs. 3-1 and 3-2 in the limit where $r_\infty \to \infty$. For this limit, the area term in Eq. 3-2 reduces to $A_S^\infty = \pi^2 r_o r_\infty$. Similar to Eq. 3-5, we can write the dimensionless correlation length for the oil domains in the Type III region as follows,

$$\xi_{Do}^{III} = \frac{4r_o}{3\pi L} = \sigma_o^{III}. \tag{3-6}$$

For the water domains, the corresponding expression is,

$$\xi_{Dw}^{III} = \frac{4r_w}{3\pi L} = \sigma_w^{III}. \tag{3-7}$$

The principal curvatures corresponding to the invariant point (i.e. three-phase composition) are considered to have the following form (Strey, 1994; Torrealba and Johns, 2017),

$$\begin{aligned} c_1^{III} &= c_c(\mathcal{H} - \mathcal{H}_L) \\ c_2^{III} &= c_c(\mathcal{H} - \mathcal{H}_U). \end{aligned} \tag{3-8}$$

These curvatures can be inferred from scattering experiments (Strey, 1994). The corresponding radii are calculated by,

$$\begin{aligned} r_w = r_1 &= \left|\frac{1}{c_1^{III}}\right| \\ r_o = r_2 &= \left|\frac{1}{c_2^{III}}\right|. \end{aligned} \tag{3-9}$$

Combining Eqs. 3-6—3-9, and considering $c_c < 0$ (Strey, 1994), we obtain the following equations for the oil and water solubilization ratios in the Type III region,

$$\begin{aligned} \sigma_o^{III} &= \frac{4}{3\pi L c_c(\mathcal{H} - \mathcal{H}_U)} \\ \sigma_w^{III} &= \frac{4}{3\pi L c_c(\mathcal{H}_L - \mathcal{H})}. \end{aligned} \tag{3-10}$$

Equation 3-10 can be simplified by noting that $\sigma_o^{III} = \sigma_w^{III} = \sigma^*$ at $\mathcal{H} = 0$, which interestingly results in the same Eq. 4-16. This emphasizes the consistency of the approach presented in this chapter with that shown in Chapter 4 using interfacial tensions. For asymmetric phase behavior in the Type III region (i.e. $\mathcal{H}_U \neq -\mathcal{H}_L$), we can define $L_o = -4/(3\pi c_c \mathcal{H}_U \sigma^*)$ and $L_w = 4/(3\pi c_c \mathcal{H}_L \sigma^*)$.

Let us define c_i^{cp-} and c_i^{cp+} as the i-th principal curvatures corresponding to the Type II- and Type II+ critical points, respectively. Based on the definition of $\mathcal{H}_L$ and $\mathcal{H}_U$, we can say,

$$\begin{aligned} c_i^{cp-} &= \{c_i^{III} \quad \mathcal{H} = \mathcal{H}_U \quad i = 1,2 \\ c_i^{cp+} &= \{c_i^{III} \quad \mathcal{H} = \mathcal{H}_L \quad i = 1,2 \end{aligned} \tag{3-11}$$

A zeroth-order approximation would be to assume a constant value of the critical point principal curvatures based on Eq. 3-11. In this chapter, we improve this approximation by considering a limiting value for c_i^{cp-} and c_i^{cp+} as $\mathcal{H}$ approaches $-\infty$ and ∞, respectively, as shown below,

$$\begin{aligned} c_i^{cp-} &= \left\{c_{i,\infty}^{cp-} \quad \mathcal{H} = -\infty \quad i = 1,2 \right. \\ c_i^{cp+} &= \left\{c_{i,\infty}^{cp+} \quad \mathcal{H} = \infty \quad i = 1,2 \right. \end{aligned} \tag{3-12}$$

For $-\infty < \mathcal{H} \leq \mathcal{H}_U$, we can estimate c_i^{cp-} using the following simple interpolation function,

$$c_i^{cp-} = c_{i,\infty}^{cp-} + A_{c_i}^{cp-} b_{H-} \quad i = 1,2 \qquad (3-13)$$

where $b_{H-} = 1/(1 + \mathcal{H}_U - \mathcal{H})$ is the interpolation variable, and $A_{c_i}^{cp-}$ is a constant defined by evaluating Eq. 3-13 at $\mathcal{H}_U$ based on Eq. 3-11. Similarly, for $\mathcal{H}_L \leq \mathcal{H} < \infty$, we can estimate c_i^{cp+} by,

$$c_i^{cp+} = c_{i,\infty}^{cp+} + A_{c_i}^{cp+} b_{H+} \quad i = 1,2 \qquad (3-14)$$

where $b_{H+} = 1/(1 + \mathcal{H} - \mathcal{H}_L)$ in the interpolation variable, and $A_{c_i}^{cp+}$ is a constant defined by evaluating Eq. 3-14 at $\mathcal{H}_L$ based on Eq. 3-11.

In Appendix 3-A, we make a similar argument to define the tie-lines corresponding to the Type II- and Type II+ critical points. Further, in Appendix 3-B we present a robust interpolation procedure to define the principal curvatures corresponding to given tie-line in composition-space, based on the bounding principal curvatures from both invariant and critical points, which is illustrated in Figure 3-2.

Finally, the interfacial tensions for all phase environments can be defined by using Huh's equation (Huh, 1979; Huh, 1983) shown in Eq. 2-4.

3.2. Results

In this section, we explore different properties of the new curvature model for an example case. Next, we compare the quantitative performance of curvature

model against phase behavior and interfacial tension experimental data for an $\mathcal{H}$-scan. Finally, we compare the curvature model against compositional data for a fixed $\mathcal{H}$, where all Winsor regions are present.

3.2.1. Model properties

To evaluate some curvature model properties, we consider Example 1 with model parameters listed in Table 3-1. For this set of model parameters, we study a hypothetical $\mathcal{H}$-scan with an overall composition given by $C_s = 0.02$ and a water-oil-ratio of 1. Figure 3-3 (left) shows the principal curvatures for a typical $\mathcal{H}$ range of interest. Near $\mathcal{H} = 0$, the system is in a Type III region, and the principal curvatures are calculated using the invariant point principal curvatures defined in Eq. 3-8. Figure 3-3 (center) shows the corresponding characteristic length-scale using the definition of Strey (1994) presented in Eq. 2-5. In this curvature model, the characteristic length-scale is non-constant in the three-phase region, reaching a maximum value at optimum, which is consistent with scattering experiment results of microemulsion systems. Figure 3-3 (right) shows the oil and water solubilization results based on the curvature model using Eqs. 3-1—3-5 and 3-10.

Figure 3-4 (top, left) shows the principal curvatures, same as in Fig. 3-3 (left), for an extended $\mathcal{H}$ range. For sufficiently negative and positive $\mathcal{H}$ values, both principal curvatures approach each other corresponding to oil internal near-spherical micelles (for $\mathcal{H} < 0$) and water internal near-spherical micelles (for $\mathcal{H} > 0$). As we approach $\mathcal{H} = 0$, these micelles start transitioning towards a cylindrical

micellar geometry (when one of the principal curvatures goes to zero), followed by a bicontinuous micellar arrangement (when the principal curvatures differ in sign). Figure 3-4 (top, right) shows all principal curvatures relevant in the interpolation process described in Appendix 3-B. The principal curvatures corresponding to the overall composition under consideration is bounded by those corresponding to the invariant and critical points. Figure 3-4 (bottom, left) presents a closer look into the curvatures for $\mathcal{H} < 0$ and Figure 3-4 (bottom, right) for $\mathcal{H} > 0$.

Figure 3-5 shows first (top) second (bottom) principal curvatures, same as in Fig. 3-4 (top, right) for $\mathcal{H} < \mathcal{H}_U$ (left) and $\mathcal{H} > \mathcal{H}_L$ (right) using a narrow range in $\mathcal{H}$. For Type II- environment, the microemulsion consists of oil micelles. By convention, we consider oil micelles to have positive curvature, and water micelles to have negative curvature. If the principal curvatures for an oil micelle are less than zero, the assumed value is zero. Alternatively, if they are greater than zero for a water micelle, the assumed value is zero. This is consistent with the assumption for the Type III region, where the principal curvatures differ in sign (one corresponding to oil and the other to water domains), therefore r_b was taken to be r_∞. From Fig. 3-5 (left) we see both $c_i^{cp-} \leq 0$, which means that as we approach the Type II- critical point in composition space, the principal curvatures will approach zero. From Eq. 2-5, the critical characteristic length-scale will diverge, which is physical result (De Gennes and Taupin, 1982). We can make a similar for the Type II+ critical point by noting that $c_i^{cp+} \geq 0$ from Fig. 3-5 (right).

3.2.2. Model comparison for an $\mathcal{H}$-scan

Figure 3-6 shows phase behavior data for an oil-brine-sulfonate-tertiary amyl alcohol system as described by Salter (1977), and the corresponding curvature model results using model parameters listed in Table 3-1. Figure 3-6 (left) shows the solubilization ratios using Eqs. 3-1—3-5 and 3-10, while Fig. 3-6 (right) shows the corresponding phase volume fractions. The phase behavior data is accurately captured by the model, specifically the asymmetric phase transition boundaries and the three-phase data.

Figure 3-7 shows interfacial tension data for the same system described by Salter (1977), and the model interfacial tension results using Eq. 2-4. Figure 3-7 (left) shows the result with tuned scaling constant of $\Omega = 0.87$ mN/m, obtained from Eq. 2-4 based on both interfacial tension and phase behavior data. Figure 3-7 (right) shows the alternative of only defining the model parameters based on phase behavior data, and then estimating the interfacial tensions using Eq. 2-4 with the commonly used value of $\Omega = 0.3$ mN/m. Clearly, this approach would significantly underestimate the interfacial tensions, which would result in an overestimation of oil recovery predictions from a reservoir simulation standpoint.

3.2.3. Model comparison for compositional data

Figure 3-8 shows compositional data for a decane-brine-AOT surfactant system as described by Lekkerkerker et al. (1996), and the corresponding curvature model results using model parameters listed in Table 3-1. The model is able to

accurately capture the location of the invariant point, as well as both two-phase lobes. For the Type II+ lobe, the data is captured by assuming the critical point is located in negative composition space, resulting in a non-vanishing tie-line length as we approach the critical point. This behavior is relevant for systems that exhibit phase separation between a micelle-rich and a micelle-poor phase as the critical point is approached (Kamei et al., 2001).

3.2.4. Model predictability

Austad and Strand studied the three-phase oil and water solubilization ratio as a function of both temperature and pressure for a variety of scans for a sulfonate—dead oil—brine system. Let us define $G_o = \sigma_o^{III}(H_U - H)/H_U$ and $G_w = \sigma_w^{III}(H_L - H)/H_L$. If the model captures the data exactly, then $G_o = G_w = \sigma^*$. Figure 3-9 (top, left) shows σ^* versus the combined G_o and G_w experimental results for six pressure scans at different optimum temperatures (ranging from 55-80°C) and six temperature scans at different optimum pressures (ranging from 50-300 bar). Figure 3-9 (top, left) indicates the model's ability to appropriately scale three-phase data to optimum condition. Figure 3-9 (top, right) shows the same data with the corresponding optimum pressure for temperature scans and optimum temperature for pressure scans, respectively. The data is consistent in that for similar optimum properties, the scans cluster around the same value. For example, the pressure scan data at optimum temperature of 80°C (with optimum pressure of 44.7 bar) clusters similarly compared to the temperature scan data at optimum pressure of 50 bar (with optimum temperature

of 79.8°C). Figure 3-9 (bottom, left) shows the relationship of pressure versus temperature at optimum condition. In order to predict phase behavior away from a single formulation variable scan, σ^* is correlated by the best fit plane to σ^* data in PT space as described previously (Torrealba and Johns, 2017; Khorsandi and Johns, 2016). Relevant correlation parameters are shown in Table 3-2. Figure 3-9 (bottom, right) shows the experimental σ^* are the predicted values using the σ^* correlation, which yields accurate results. Combining the predicted values for optimum solubilization ratio, and using average H_U and H_L parameters (listed in Table 3-1), we are able to accurately predict Type III phase behavior for a number of temperature scans at different pressures (Figure 3-10, left) and pressure scans at different temperatures (Figure 3-10, right).

3.3. Summary

In this chapter, we have presented a robust curvature-based microemulsion phase behavior model, which is coupled with interfacial tensions to allow for a more accurate modeling of fluid interactions. Some specific conclusions are:

- We developed a novel approach to consider variable curvatures in the context of microemulsion phase behavior. This approach allows us to describe spherical, cylindrical and bicontinuous micellar geometries based on the general framework of using prolate spheroids.
- The model is successful in qualitatively and quantitatively capturing physical behavior from typical microemulsion experiments. Some

examples include an $\mathcal{H}$-scan for a fixed overall composition, and a composition-scan for fixed $\mathcal{H}$.

- The model relies on a robust interpolation procedure for the principal curvatures in composition space, based on the principal curvatures from the invariant and critical points.
- The three-phase oil and water solubilization ratios developed from this approach are consistent with those developed by Torrealba and Johns (2017A) from an interfacial tension model, which were based on a principal curvature definition.
- The model is tied with Huh's correlation to present a coupled approach to accurately capture phase behavior and interfacial tensions.
- The model removes all assumptions and limitations in Khorsandi and Johns (2016) model as identified by Torrealba and Johns (2017B).
- The model is shown to have accurate predictive capabilities in the Type III region for a variety of pressure and temperature scans.

3.4. Appendix A: Critical tie-line definition

For the Type II- critical point the critical tie-line is given by σ_w^{cp}, and for the Type II+ critical point the critical tie-line is given by σ_o^{cp}. Based on the definition of $\mathcal{H}_L$ and $\mathcal{H}_U$, we can say,

$$\begin{aligned} \sigma_w^{cp} &= \{\sigma_w^{III} \quad \mathcal{H} = \mathcal{H}_U \\ \sigma_o^{cp} &= \{\sigma_o^{III} \quad \mathcal{H} = \mathcal{H}_L \end{aligned} \qquad (3-A1)$$

A zeroth-order approximation would be to assume a constant value of the critical tie-line based on Eq. 3-A1. This approximation is improved by considering a limiting value for σ_w^{cp} and σ_o^{cp} as $\mathcal{H}$ approaches $-\infty$ and ∞, respectively, as shown below,

$$\begin{aligned} \sigma_w^{cp} &= \{\sigma_{w,\infty}^{cp} \quad \mathcal{H} = -\infty \\ \sigma_o^{cp} &= \{\sigma_{o,\infty}^{cp} \quad \mathcal{H} = \infty \end{aligned} \tag{3-A2}$$

For $-\infty < \mathcal{H} \leq \mathcal{H}_U$, we can estimate c_i^{cp-} using the following simple interpolation function,

$$\begin{aligned} \sigma_w^{cp} &= \sigma_{w,\infty}^{cp} + A_{\sigma_w}^{cp} b_{H-} \quad -\infty < \mathcal{H} \leq \mathcal{H}_U \\ \sigma_o^{cp} &= \sigma_{o,\infty}^{cp} + A_{\sigma_o}^{cp} b_{H+} \quad \mathcal{H}_L \leq \mathcal{H} < \infty \end{aligned} \tag{3-A3}$$

where $A_{\sigma_w}^{cp}$ and $A_{\sigma_o}^{cp}$ are constants defined by evaluating Eq. 3-A3 at the corresponding $\mathcal{H}$ limits based on Eq. 3-A1

3.5. Appendix B: Robust principal curvature interpolation procedure

The interpolation procedure in a Cartesian coordinate space, is based on the following transformation,

$$x = C_o - C_w$$
$$y = C_s \qquad (3-B1)$$

but since $C_o = 1 - C_w - C_s$ for ternary system, we can write $x = 1 - 2C_w - C_s$. In terms of (x, y) coordinates, the surfactant, oil, and water apexes are located in $(0,1)$, $(1,0)$, and $(-1,0)$, respectively. The tie-line for a Type II- system is given by $\sigma_w^\circ = C_w/C_s$. The straight-line equation for the tie-line is given by,

$$x = 1 - y(2\sigma_w^\circ + 1) \qquad (3-B2)$$

The critical point reference point (x^{cp}, y^{cp}) is obtained intersecting Eq. 3-B2 evaluated at $\sigma_w^\circ = \sigma_w^{cp}$ with the $C_S = 1$ straight line (i.e. $y = 1$). Therefore, we can generally define this reference point as,

$$x^{cp} = -2\sigma_w^{cp}$$
$$y^{cp} = 1 \qquad (3-B3)$$

The invariant point reference point (x^{III}, y^{III}) is obtained intersecting Eq. 3-B2 evaluated at $\sigma_w^\circ = \sigma_w^{III}$ with the $C_w = 1$ straight line (i.e. $x = -1 - y$). Therefore, we can generally define this reference point as,

$$x^{III} = -1 - \frac{1}{\sigma_w^{III}}$$
$$y^{III} = \frac{1}{\sigma_w^{III}} \qquad (3-B4)$$

The straight-line going though both (x^{cp}, y^{cp}) and (x^{III}, y^{III}) is defined as,

$$x - x^{cp} = \theta_1 (y - y^{cp}) \qquad (3-B5)$$

where $\theta_1 = (x^{III} - x^{cp})/(y^{III} - y^{cp})$. The reference point (x°, y°) for an arbitrary tie-line σ_w° for which we want to estimate its principal curvatures, is defined by intersecting Eqs. 3-B2 and 3-B5,

$$x^{\circ} = 1 - \theta_2 (2\sigma_w^{\circ} + 1)$$
$$y^{\circ} = \theta_2 \qquad (3-B6)$$

where $\theta_2 = (1 - x^{cp} + \theta_1 y^{cp})/(\theta_1 + 2\sigma_w^{\circ} + 1)$. The distances d between (x^{cp}, y^{cp}) and (x^{III}, y^{III}) and d_1 between (x^{cp}, y^{cp}) and (x°, y°) can be calculated by,

$$d = \sqrt{(x^{cp} - x^{III})^2 + (y^{cp} - y^{III})^2}$$
$$d_1 = \sqrt{(x^{cp} - x^{\circ})^2 + (y^{cp} - y^{\circ})^2} \qquad (3-B7)$$

Finally, we can define a weighing function by $\lambda \equiv d_1/d$. The principal curvatures corresponding to the arbitrary tie-line σ_w° can be calculated by,

$$c_i^- = (1-\lambda)c_i^{cp-} + \lambda c_i^{III} \quad i = 1,2 \qquad (3-B8)$$

Figure 3-2 shows an illustration depicting the relevant reference points in composition space, as well as the resulting phase behavior diagram for a Type II- environment. The procedure for interpolating in a Type II+ system is analogous to the procedure described for a Type II- system.

For a Type II- environment, the interpolation approach described by Khorsandi and Johns (2016) relies on all reference points being intersected with the $C_o = 0$ straight line (i.e. $x = -1 + y$). This assumption limits their implementation for $\sigma_w^{cp} > -1$ and $\sigma_w^{III} < -1$ (note that for $\sigma_w^{\circ} = -1$, the tie-line equation becomes $x = 1 + y$, which is parallel to the $C_o = 0$ straight line, and therefore there is no intersection point). This is important, since for some $\mathcal{H}^* < \mathcal{H}_L$, σ_w^{III} will reach -1, limiting their implementation for $\mathcal{H} > \mathcal{H}^*$. A similar limitation could be described for the Type II+ environment.

Table 3-1. Curvature model parameters for all cases considered.

Data set	σ^*	$\mathcal{H}_U$	$\mathcal{H}_L$	$c_c, \text{Å}^{-1}$	$\sigma_{w,\infty}^{cp}$	$\sigma_{o,\infty}^{cp}$	$c_{i,\infty}^{cp-}$	$c_{i,\infty}^{cp+}$
Example 1	11.4	0.5	-0.5	-0.002	-1	-1	-0.002	0.002
Salter (1977)	11.4	0.85	-0.31	-0.002	-1	-1	-0.001	0.001
Lekkerkerker et al. (1996)	8.2	0.1	-1.0	-0.002	-47	-1	0	0
Austad and Strand (1996)	-	0.43	-0.23	-	-	-	-	-

Table 3-2. Tuned correlation parameters for σ^* predictions.

Data set	$\beta_1, °C^{-1}$	β_2, bar^{-1}	β_3
σ^*, Austad and Strand (1996)	-0.667	-0.042	64.83

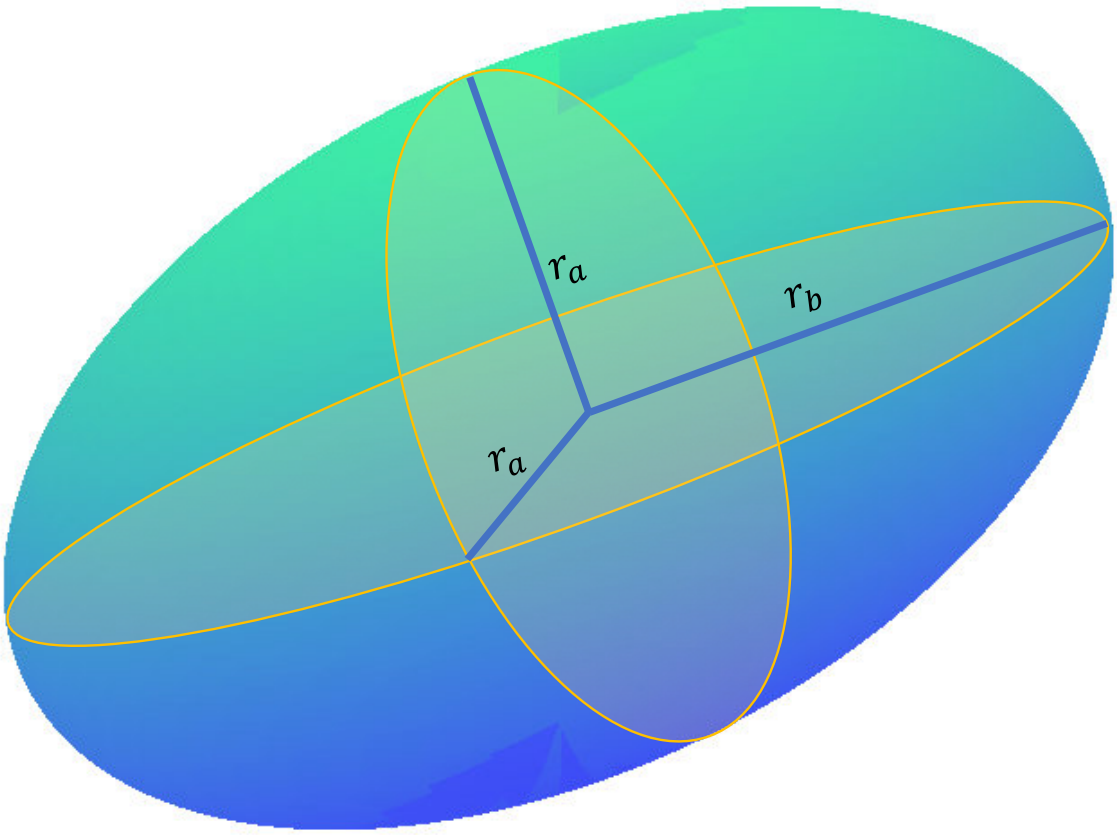

Figure 3-1. Schematic of the general micellar geometry assumed in the curvature model. In the Type III environment, we assume a bicontinuous micellar arrangement, where for both oil and water micelles $r_b = \infty$, and the corresponding value of r_a determines the oil and water solubilization in the three-phase region.

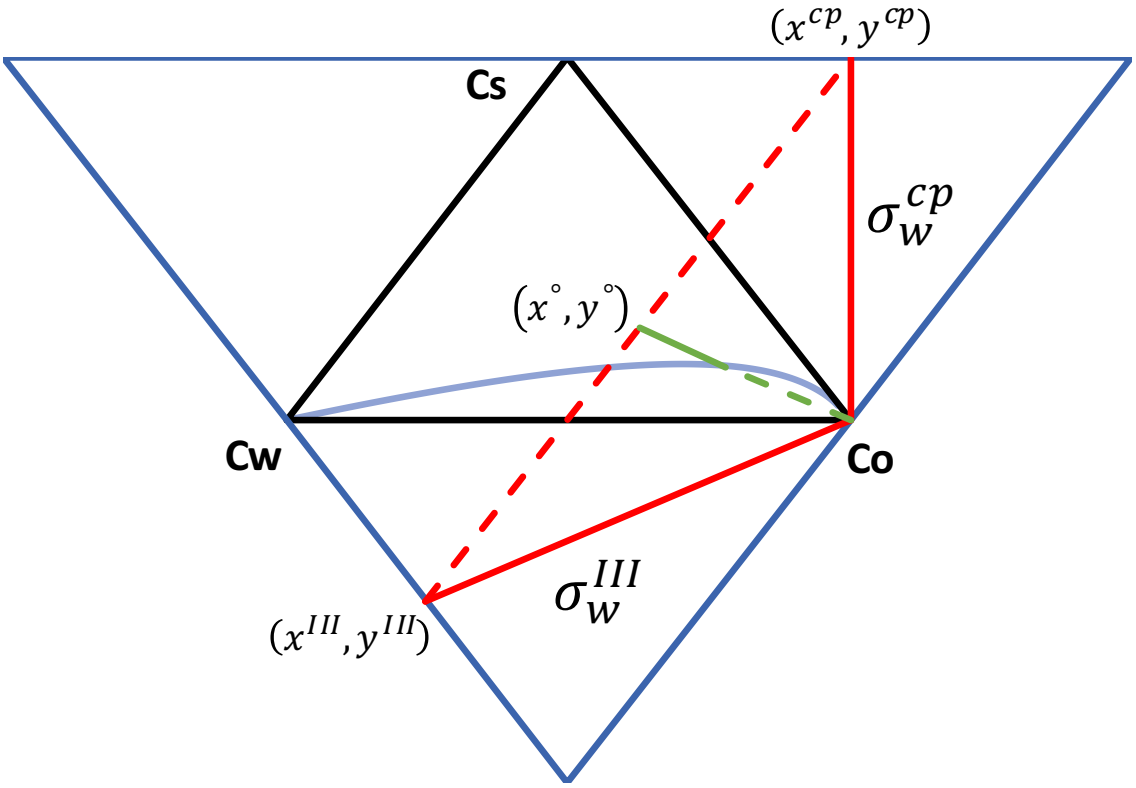

Figure 3-2. Illustration describing key elements in the principal curvature interpolation procedure between the invariant and critical points.

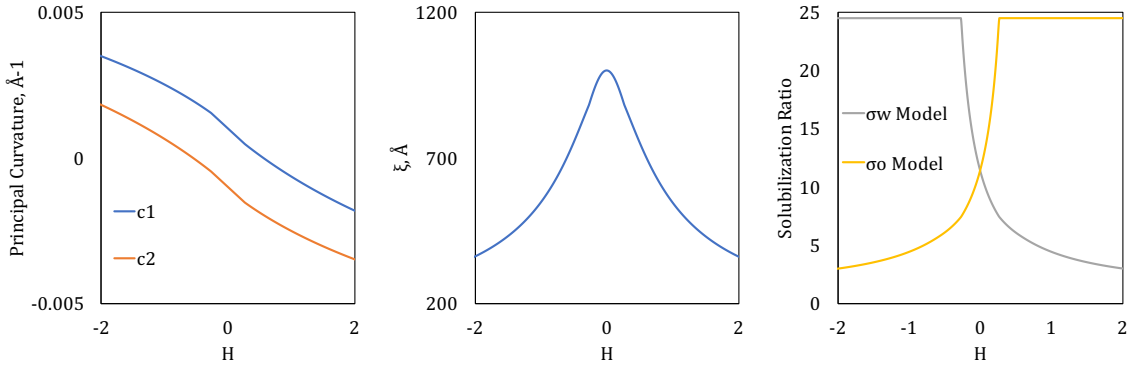

Figure 3-3. Principal curvatures as a function of $\mathcal{H}$ corresponding to a given overall composition in Example 1 (left). Near $\mathcal{H} = 0$ the principal curvatures are straight lines, following Eq. 3-8. Characteristic length scale as a function of $\mathcal{H}$ based on the principal curvatures using Eq. 2-5 (center). Oil and water solubilization ratios as a function of $\mathcal{H}$ using Eqs. 3-1—3-5 and 3-10 (right).

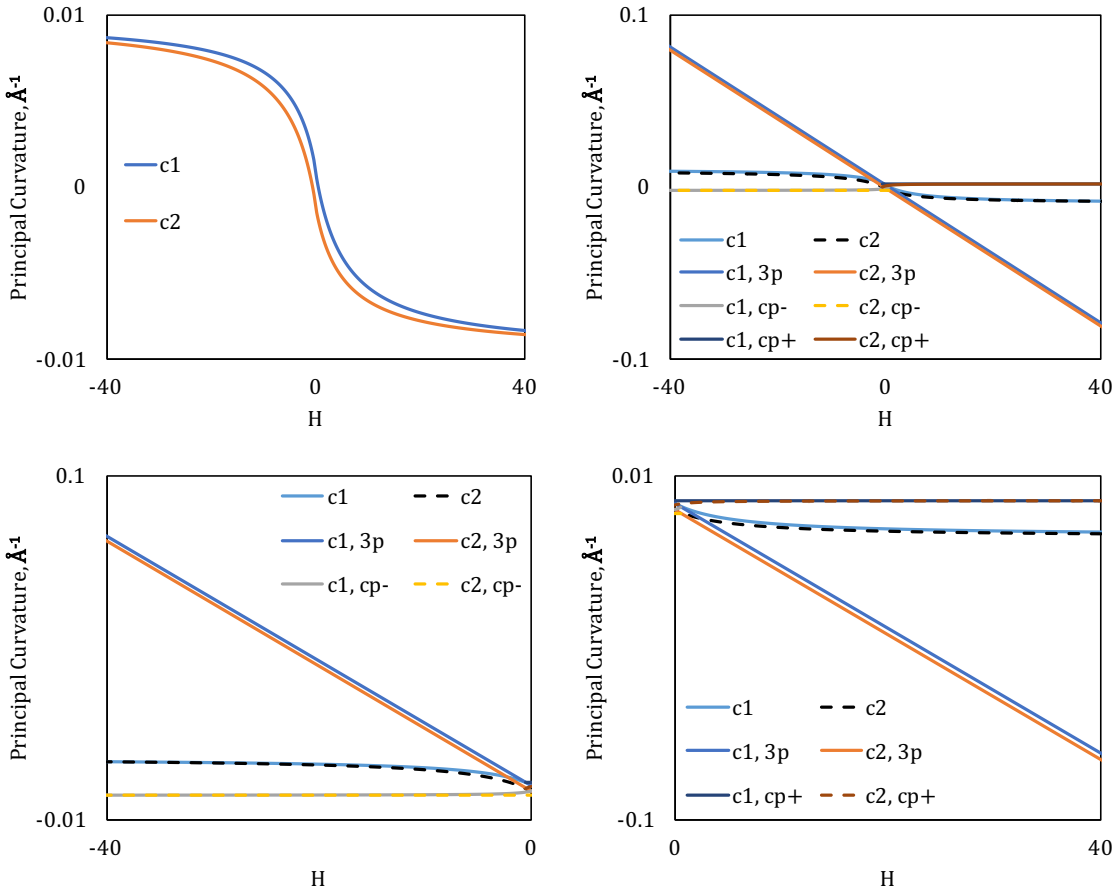

Figure 3-4. Principal curvatures as a function of $\mathcal{H}$ corresponding to a given overall composition in Example 1 for a wide range of $\mathcal{H}$ (top, left), principal curvatures relevant in the interpolation procedure described in Appendix B for a wide range of $\mathcal{H}$ (top, right), zoomed view in the c_i axis for $\mathcal{H} < 0$ (bottom, left) and $\mathcal{H} > 0$ (bottom, right).

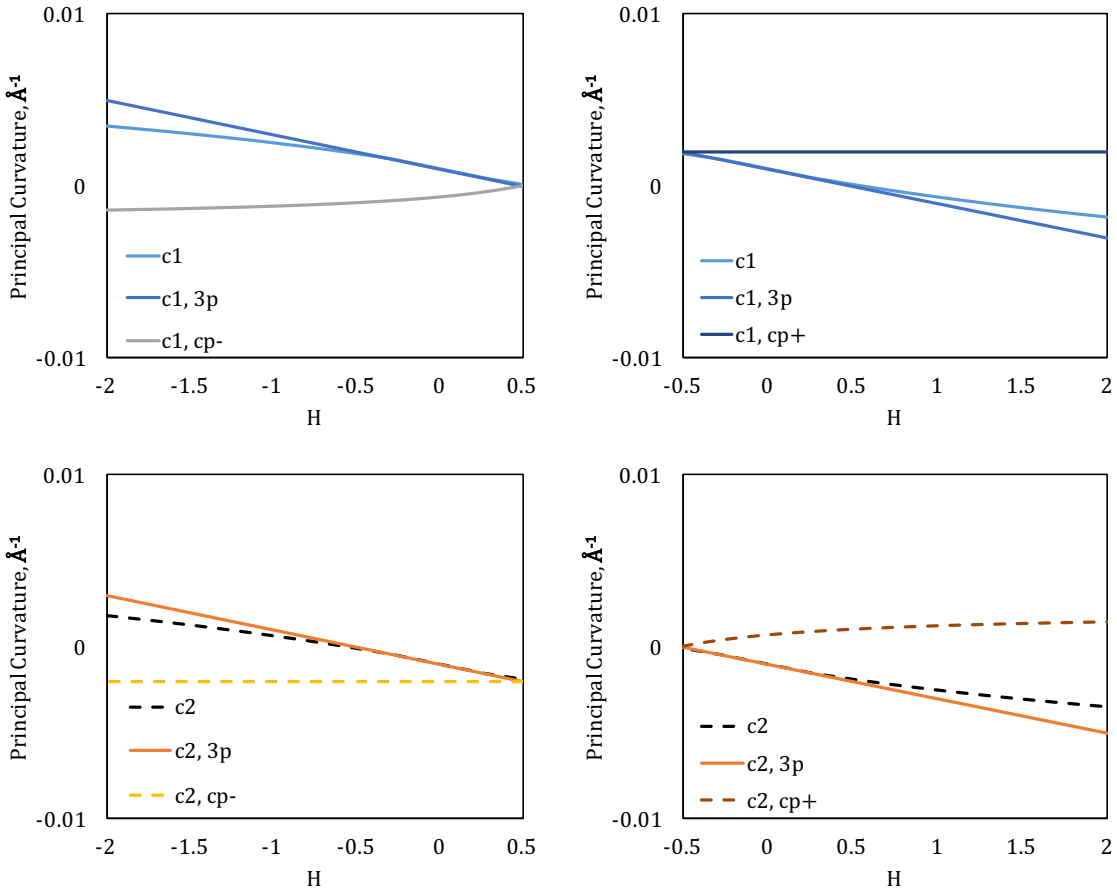

Figure 3-5. All relevant c_1 (top) and c_2 (bottom) principal curvatures in the interpolation procedure for $\mathcal{H} < \mathcal{H}_U$ (left) and $\mathcal{H} > \mathcal{H}_L$ (right) corresponding to Example 1.

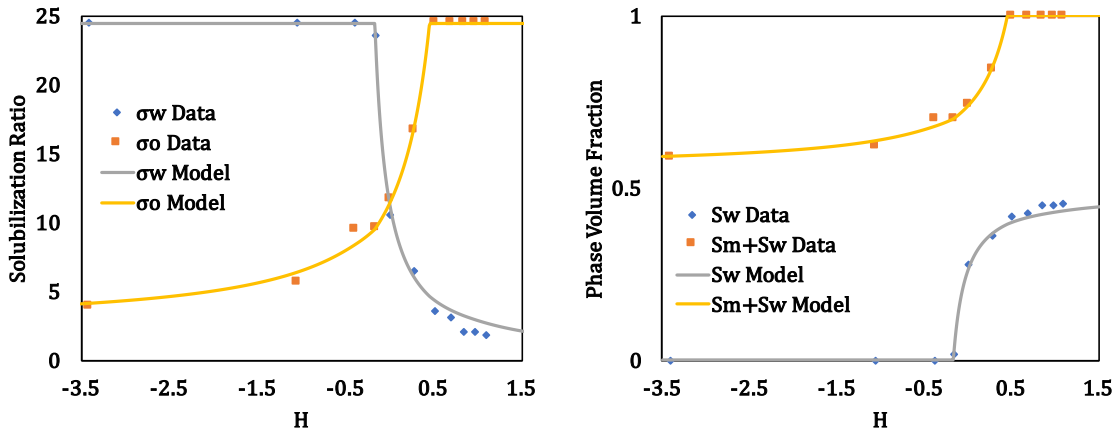

Figure 3-6. Phase behavior experimental data and curvature model results for an $\mathcal{H}$-scan: Oil and water solubilization ratios modeled using Eqs. 3-1—3-5 and 3-10 (left), and corresponding phase volume fractions (right). Data from Salter (1977).

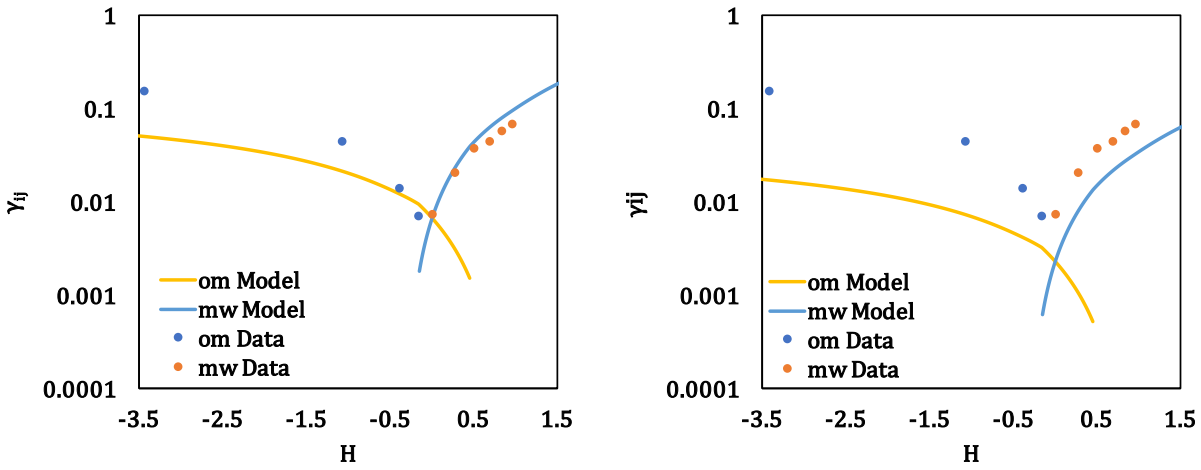

Figure 3-7. Interfacial tension experimental data and curvature model results for an $\mathcal{H}$-scan: interfacial tensions modeled using Eq. 2-4 with a tuned scaling constant Ω of 0.87 mN/m (left), and with the typically used value of 0.3 mN/m (right). Data from Salter (1977).

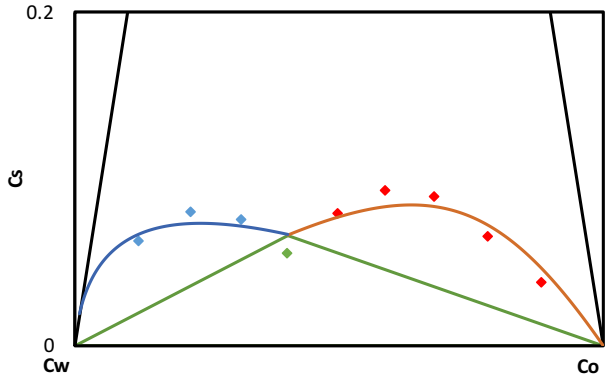

Figure 3-8. Ternary experimental data, and curvature model tuned results for a composition scan using decane at 40°C for a fixed $\mathcal{H}$. Experimental data from Lekkerkerker et al. (1996).

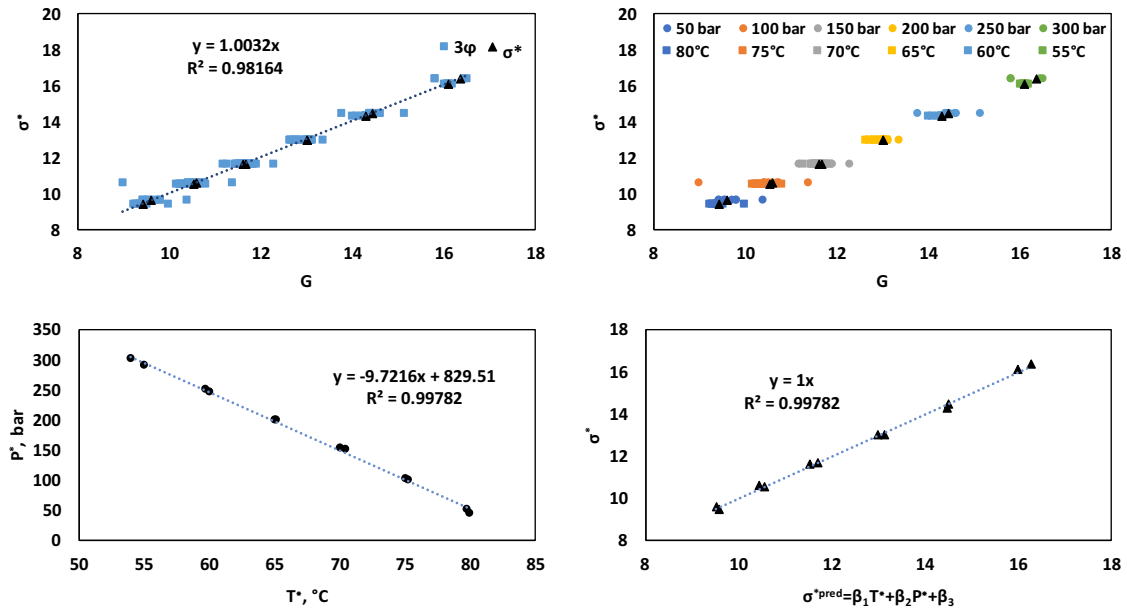

Figure 3-9. Experimental σ^* versus G (top, left) for different temperature and pressure scans as described in the text, and accompanying optimum data for reference (triangles). The same data is shown (top, right) with their corresponding optimum pressure (for temperature scans) and optimum temperature (for pressure scans). Pressure versus temperature at optimum condition (bottom, left) and corresponding experimental σ^* versus predictions for the same temperature and pressure scans (bottom, right). Data from Austad and Strand (1996).

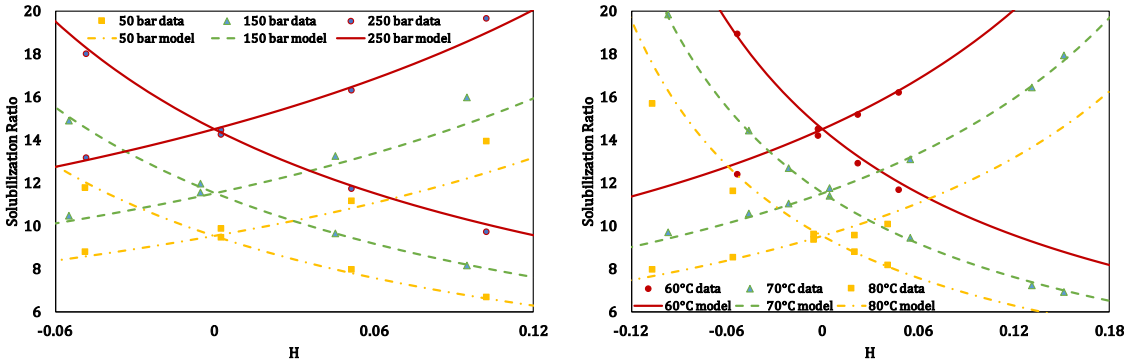

Figure 3-10. Type III phase behavior predictions for different temperature scans at varying pressures (left) and different pressure scans at varying temperatures (right). Data from Austad and Strand (1996).

Chapter 4

Microemulsion Interfacial Tension and Characteristic Length Scale Model Using a Microscopic Curvature Approach and the HLD Concept

In this chapter, we present the first consistent model to predict interfacial tensions for all Winsor types and overall compositions. The interfacial tension between the oil and water phases are linked to the characteristic length definition of Strey (1994) based on HLD. Next, we normalize both γ_{ow} and ξ, which yields simple and practical expressions. The model for γ_{ow} is tested for a wide variety of systems, showing its ability to match and predict experimental data. Both γ_{om} and γ_{mw} are then correlated with HLD based on phase transition boundary conditions, and then are extended to account for compositional changes. These compositionally-dependent interfacial tension models are combined with solubilization ratios using Huh's equation to define a coupled interfacial tension-microemulsion phase behavior model. The predictive capabilities of the model relate to a correlation between the interfacial tension and the solubilization ratio at optimum, where bicontinuous micelles are assumed.

4.1 Methodology

In this section, we present the development of the interfacial tension and characteristic length scale models, as well as the relevant scaling needed for the phase behavior model.

4.1.1. Oil-water interfacial tension

A simple expression for the oil-water interfacial tension can be developed assuming symmetry of the two-phase regions. As shown in the appendix to this chapter, we obtain the equation,

$$\gamma_{ow} = c_{\gamma} HLD^2 + \gamma_{ow}^{min}, \tag{4-1}$$

where c_{γ} and γ_{ow}^{min} are,

$$c_{\gamma} = (2\kappa + \overline{\kappa}){c_c}^2$$

$$\gamma_{ow}^{min} = \overline{\kappa} HLD_U^2 {c_c}^2. \tag{4-2}$$

From this development, γ_{ow}^{min} is the interfacial tension at optimum condition, which is considered to be a function of formulation variables as expressed in Eq. 2-3, and c_{γ} can be used as a tuning parameter accounting for both bending and saddle-splay moduli. The c_{γ} parameter is typically assumed constant.

Further, we can extend the result shown in Eq. 4-1 to define the normalized interfacial tension, as presented below.

$$\gamma_n = \frac{\gamma_{ow} - \gamma_{ow}^{min}}{c_\gamma} = HLD^2. \qquad (4-3)$$

This result says that for any microemulsion system, the normalized interfacial tension should be equal to HLD^2. Equation 4-3 allows to scale different surfactant systems onto the same curve, or predict the interfacial tension for a system if we have an a priori estimate of the γ_{ow}^{min} and c_γ parameters.

The model in Eqs. 4-1 and 4-3 is similar to the model discussed earlier by Leitao et al. (1996), but theirs is presented only as a function of temperature and reduced temperature, whereas we have generalized it in terms of HLD to account for other formulation variables. Further, it the quadratic functionality in HLD is consistent with the findings of Salager et al. (2013A).

4.1.2. Characteristic length scale

From the appendix to this chapter, the following model relating ξ with HLD is defined,

$$\left(\frac{1}{\xi}\right)^2 = c_\xi HLD^2 + \left(\frac{1}{\xi^{max}}\right)^2, \qquad (4-4)$$

where c_ξ and ξ^{max} are,

$$c_\xi = {c_c}^2$$
$$\xi^{max} = \frac{1}{c_c HLD_U}. \qquad (4-5)$$

Similarly, ξ^{max} is the characteristic length scale at optimum condition, which is tied to γ_{ow}^{min} as described in Section 4.1.6, therefore is also considered to be a function of formulation variables. The c_ξ parameter is a tuning parameter, which is typically assumed constant.

We can obtain a similar normalization of the inverse of characteristic length scale as for γ_{ow} by rearranging Eq. 4-4, to obtain the following,

$$\left(\frac{1}{\xi_n}\right)^2 = \frac{\left(\frac{1}{\xi}\right)^2 - \left(\frac{1}{\xi^{max}}\right)^2}{c_\xi} = HLD^2. \qquad (4-6)$$

Equation 4-6 indicates that for any symmetric microemulsion system, the inverse of the normalized characteristic length scale-squared is equal to HLD^2. Combining Eqs. 4-3 and 4-6 results in a simple relationship between the normalized characteristic length scale and interfacial tension,

$$\gamma_n = \left(\frac{1}{\xi_n}\right)^2. \qquad (4-7)$$

Equation 4-7 is an important result, which allows for predicting the characteristic length scale based on interfacial tension data, or vice versa.

4.1.3. Model for three-phase oil-microemulsion and microemulsion-water interfacial tensions

The oil-microemulsion and microemulsion-water interfacial tension models for Type III are based on the bicritical points at HLD_L and HLD_U. That is, at HLD_L the invariant point composition merges to the brine excess phase composition, while at HLD_U the invariant point merges to the oil excess phases composition. Therefore, the following conditions must hold,

$$\gamma_{om}^{3p} = \begin{cases} \gamma_{ow} & HLD = HLD_L \\ 0 & HLD = HLD_U \end{cases}$$

$$\gamma_{mw}^{3p} = \begin{cases} 0 & HLD = HLD_L \\ \gamma_{ow} & HLD = HLD_U \end{cases}. \qquad (4-8)$$

Using the model for γ_{ow} showed in Eq. 2-2, we find that a simple model that satisfies the conditions in Eq. 4-8 is shown below,

$$\gamma_{om}^{3p} = \gamma_{ow}(c_1 = 0) = \frac{{c_c}^2 (HLD - HLD_U)^2 (\kappa + \overline{\kappa})}{2}$$

$$\gamma_{mw}^{3p} = \gamma_{ow}(c_2 = 0) = \frac{{c_c}^2 (HLD - HLD_L)^2 (\kappa + \overline{\kappa})}{2}, \qquad (4-9)$$

where we can show ${c_c}^2(\kappa + \overline{\kappa}) = \gamma_{ow}(HLD_U)/\left(2{HLD_U}^2\right)$ from Eq. 4-2. This observation allows for the estimation of oil-microemulsion and microemulsion-water interfacial tensions from oil-water interfacial tensions, or vice versa.

4.1.4. Compositionally dependent interfacial tensions

Section 4.1.3 showed that oil-microemulsion and microemulsion-water interfacial tension results are only a function of *HLD* since they correspond to the interfacial tensions between the microemulsion and excess phases tied by the three-phase invariant point. This result is extended here to make the oil-microemulsion and microemulsion-water interfacial tensions functions of composition. The oil-microemulsion interfacial tension in the Type III environment has a maximum at the excess oil-microemulsion boundary of the tie triangle and vanishes at the critical point (assuming pure excess phases). These observations are summarized below,

$$\gamma_{om} = \begin{cases} \gamma_{om}^{3p} & \sigma_w^{\circ} = \sigma_w^{3p} \\ 0 & \sigma_w^{\circ} = \sigma_w^{c}, \end{cases} \qquad (4-10)$$

where σ_w° is the water solubilization ratio in the Type II- lobe, given by $\sigma_i^{\circ} = C_i/C_s$ with C_i being the total concentration of component i in the system, and σ_w^{3p} is the tie-triangle water solubilization ratio and σ_w^c is the limiting tie line as we approach the critical point (i.e. critical tie line). An analogous description can be made for γ_{mw}. The simplest expressions that satisfy the required limits are,

$$\gamma_{om} = \gamma_{om}^{3p} e^{-\frac{1}{\sigma_w^{\circ} - \sigma_w^c} + \frac{1}{\sigma_w^{3p} - \sigma_w^c}}$$
$$\gamma_{mw} = \gamma_{mw}^{3p} e^{-\frac{1}{\sigma_o^{\circ} - \sigma_o^c} + \frac{1}{\sigma_o^{3p} - \sigma_o^c}}. \qquad (4-11)$$

For the Type II- environment, the oil-microemulsion interfacial tension reaches a maximum at the oil-water boundary of the ternary diagram, and a minimum at the critical point. That is,

$$\gamma_{om} = \begin{cases} \gamma_{ow} & \sigma_w^\circ = \infty \\ 0 & \sigma_w^\circ = \sigma_w^c. \end{cases} \qquad (4-12)$$

Similar observations can be made for the microemulsion-water interfacial tension in the Type II+ environment. The compositional dependence of IFT in both Type II- and Type II+ environments can be given in its simplest form as,

$$\gamma_{om} = \gamma_{ow} e^{-\frac{1}{\sigma_w^\circ - \sigma_w^c}}$$
$$\gamma_{mw} = \gamma_{ow} e^{-\frac{1}{\sigma_o^\circ - \sigma_o^c}}. \qquad (4-13)$$

where σ_o° is the oil solubilization ratio in the Type II+ lobe. The exponential form in Eqs. 4-11 and 4-13 ensures continuity across phase transition boundaries. The value of σ_w^c and σ_o^c can be considered as tuning parameters from Eqs. 4-11 and 4-13. Further, combining Eqs. 4-9, 4-11, and 4-13 define a consistent model to calculate oil-microemulsion and microemulsion-water interfacial tensions for all Winsor types and overall compositions. The critical tie lines can be estimated from IFT data based on Eqs. 4-11 and 4-13.

4.1.5. Coupling of interfacial tension and phase behavior

The complete interfacial tension model defined in the previous sections can be combined with Eq. 2-4 to predict the phase behavior provided we have properly characterized the relevant interfacial tensions. For the Type III environment, the three-phase oil and water solubilization ratio can be described by,

$$\sigma_o^{3p} = \frac{\Omega}{\gamma_{om}^{3p\,0.5}}$$
$$\sigma_w^{3p} = \frac{\Omega}{\gamma_{mw}^{3p\,0.5}}, \qquad (4-14)$$

where Ω must be selected to satisfy the condition that at $HLD = 0$ we must have $\sigma_o^{3p} = \sigma_w^{3p} = \sigma^*$, with σ^* being the optimum solubilization ratio. Therefore,

$$\Omega = \sigma^* \gamma_{om}^{3p*\,0.5}, \qquad (4-15)$$

where $\gamma_{om}^{3p*} = \gamma_{om}^{3p}(HLD = 0) = {c_c}^2 {HLD_U}^2 (\kappa + \overline{\kappa})/2$. Substitution of Eqs. 4-9 and 4-15 into Eq. 4-14 yields,

$$\sigma_o^{3p} = \sigma^* \left(\frac{HLD_U}{HLD_U - HLD}\right)$$
$$\sigma_w^{3p} = \sigma^* \left(\frac{HLD_L}{HLD_L - HLD}\right). \qquad (4-16)$$

Equation 4-16 provides a simple equation to estimate the oil and water solubilization ratios in the three-phase region (i.e. the invariant point composition), and can be used in conjunction with Eq. 4-9 to simultaneously tune both three-phase IFTs and phase behavior.

4.1.6. Relating γ_{ow}^{min}, ξ^{max} and σ^*

Based on the results from Eqs. 4-2 and 4-5, we can relate the oil-water interfacial tension and the characteristic length scale at optimum by,

$$\gamma_{ow}^{min} = \frac{\overline{\kappa}}{\xi^{max2}}, \qquad (4-17)$$

which is consistent with the scaling discussed by De Gennes and Taupin (1982). At optimum, the volumes of oil and water solubilized in the microemulsion phase are approximately equal (V^*). The principal curvatures in bicontinuous micelles are related to the solubilized volume at optimum as,

$$|c_l| = \frac{A_s}{V^*}, l = 1,2. \qquad (4-18)$$

Using the definition of the I-ratio presented earlier, Eq. 4-18 can be rewritten as,

$$|c_l| = \frac{1}{IL\sigma^*}, l = 1,2. \quad (4-19)$$

Combining the results from Eqs. 2-5 and 4-19 we find,

$$\xi^{max} = IL\sigma^*. \quad (4-20)$$

Substitution of Eq. 4-20 into Eq. 4-17 gives,

$$\gamma_{ow}^{min} = \frac{\overline{\kappa}}{(IL\sigma^*)^2}. \quad (4-21)$$

Equation 4-21 shows how estimate σ^* based on γ_{ow}^{min}, and is different from Huh's correlation at optimum, which considers oil-microemulsion or microemulsion-water IFTs. Figure 4-1 outlines the general flowchart for how to compute interfacial tensions, and the corresponding phase behavior, and additional information on the tuning process is presented in Appendix 4-B.

4.2 Results

In this section, the models for γ_{ow}, γ_{om}, γ_{mw}, and ξ are compared against experimental data. Then, the predictive performance of the coupled interfacial tension-phase behavior is evaluated against experimental data.

4.2.1. Oil-water interfacial tension and characteristic length by Strey (1994)

Strey (1994) studied the interfacial tension between bulk oil-rich and water-rich phases in the water—n-octane—$C_{12}E_5$ system for a temperature scan using a spinning drop technique. Figure 4-2 (top) shows this data as a function of HLD, accompanied by the model results using Eq. 4-1. Figure 4-2 (bottom) shows the results of using Eq. 4-3 to normalize γ_{ow}. Relevant IFT model parameters for all systems considered are listed in Table 4-1.

Strey (1994) also studied the characteristic length scale for the same system as a function of temperature using both freeze fracture electron microscopy and small-angle neutron scattering techniques. Figure 4-3 (top) show the characteristic length scale results as a function of HLD with the corresponding model results by using Eq. 4-4. Figure 4-3 (bottom) shows the result of using Eq. 4-6 to normalize ξ. Figure 4-4 shows the result of combining the normalized the interfacial tension and characteristic length scale. The linear trend seen in Fig. 4-4 verifies the scaling obtained from Eq. 4-7. Relevant characteristic length model parameters for this case are listed in Table 4-2.

4.2.2. Oil-water interfacial tension by Leitao et al. (1996)

Leitao et al. (1996) studied the interfacial tension for a temperature scan between n-octane and water for a variety of systems containing n-alkyl polyglycol ethers with changing surfactant chain length using a spinning-drop tensiometer technique. The top of Fig. 4-5 shows the experimental results for the different surfactant sizes, from C_6E_2 to $C_{12}E_5$, as well as the model results as a function of

HLD, showing an excellent fit. Further, the bottom of Fig. 4-5 shows how all experimental points collapse onto a single curve after normalizing the interfacial tensions.

4.2.3. Characteristic length by Sottmann et al. (1997), oil-water interfacial tension by Sottmann and Strey (1997)

Sottmann et al. (1997) studied the characteristic length scale at optimum condition for a variety of water—n-alkane—C_iE_j systems using small angle neutron scattering, where i denotes the carbon number of the alkyl chain of the surfactant and j denotes the head group size of the surfactant. Further, Sottmann and Strey (1997) studied the interfacial tension between the oil and water phases for a temperature scan for the same water—n-alkane—C_iE_j systems discussed above using a spinning-drop tensiometer technique. Figure 4-6 shows experimental results for γ_{ow}^{min} versus the inverse of ξ^{max2} for all systems described above. As suggested by Eq. 4-17, the slope of the linear relationship in Fig. 4-6 is the saddle-splay modulus, which is approximately constant and within the range for the cases considered by Sottmann and Strey (1997).

Figure 4-7 shows the characteristic length scale versus the solubilization ratio at optimum condition for a variety of water—n-alkane—C_iE_j systems presented by Sottmann et al. (1997). Using the result from Eq. 4-20, and based on the linearity of the relationship presented in Fig. 4-7, we can conclude the product of IL is a constant defined by the slope of the straight-line for all the systems considered.

For the data set presented by Sottmann and Strey (1997), we consider the following formulation variables: inverse of temperature $1/T$, oil equivalent alkane carbon number ($EACN$), carbon number of the alkyl chain (LCL), and surfactant head group size (HCL). Figure 4-8 shows the interfacial tension prediction results using Eq. 2-3, which accurately compare with the experimental data. Further, Fig. 4-9 tests the predictive capability of the model presented in Eq. 4-1 incorporating Eq. 2-3 to estimate γ_{ow}^{min}. The C_8E_3, $EACN = 14$ system is tuned to obtain its γ_{ow}^{min} and c_γ values; all other systems are predicted using the previously tuned c_γ and their corresponding γ_{ow}^{min} predicted from Eq. 2-3. As shown, the described approach is able to accurately predict the entire HLD range considered. Relevant parameters for the definition of Eq. 2-3 are listed in Tables 4-3 and 4-4.

4.2.4. Oil-microemulsion and microemulsion-water interfacial tension by Kunieda and Shinoda (1982)

Kunieda and Shinoda (1982) studied the oil-water, oil-microemulsion, and microemulsion-water interfacial tensions for a temperature scan using a water—n-tetradecane—$C_8H_{17}(OCH_2CH_2)_3OH$ system using a sessile-drop method. Figure 4-10 shows the experimental results for all three interfacial tensions, as well as the model results using Eqs. 4-1 and 4-9 as a function of HLD. The models are able to successfully capture the experimental data. Additionally, we see how the model results for γ_{om}^{3p} and γ_{mw}^{3p} satisfy the phase boundary conditions imposed in Eq. 4-8.

4.2.5. Estimation of phase behavior ternary diagrams based on interfacial tensions

We consider the water-octane-$C_{12}E_4$ system presented by Sottmann and Strey (1997), which corresponds to $\sigma^* = 34.1$ based on the results from Figs. 4-6 and 4-7. Figure 4-11 shows the compositional dependence of the oil-microemulsion interfacial tension for the Type II- lobe at fixed $HLD = 0$ using Eq. 4-11 with different critical tie lines. The maximum value of IFT is that corresponding to the tie triangle IFT and the minimum is obtained as the critical point is approached. For a negative critical tie line, the critical point is in negative composition space, therefore a limiting tie line on the axis is approached, resulting in a non-vanishing IFT. Figure 4-12 shows ternary diagrams for a Type II- environment at fixed $HLD = -0.1$ (left), for a Type III environment at fixed $HLD = 0$ (center), and for a Type II+ environment at fixed $HLD = 0.1$ (right) with the critical lines $\sigma_w^c = \sigma_o^c = 2$ (top), $\sigma_w^c = \sigma_o^c = 0$ (middle), and $\sigma_w^c = \sigma_o^c = -2$ (bottom). The relevance of considering a negative critical tie line is to account for systems that exhibit phase separation between a micelle-rich and a micelle-poor phase as the critical point is approached (Kamei et al., 2001; Bourrel and Schechter, 2010; Khorsandi and Johns, 2016).

4.2.6. Phase behavior predictions based on interfacial tensions

Next, we show the predictability of this coupled interfacial tension-phase behavior model by studying a brine-octane-NPA system presented by Davis and Scriven (1980) where both interfacial tensions and solubilization ratio data are presented

for a salinity scan. Figure 4-13 (top) shows the interfacial tension data, and accompanying tuned model results. Figure 4-13 (middle) shows the phase volume fraction data, with its corresponding model predictions with $\Omega = 0.11$ mN/m calculated using Eq. 2-4, showing excellent predictive capabilities. The optimum solubilization ratio is predicted using the results from Figs. 4-6 and 4-7. Figure 4-13 (bottom) shows the alternative approach, where the commonly-used scaling of $\Omega = 0.3$ mN/m (Ghosh and Johns, 2016A) is used, showing unsatisfactory predictions.

Figure 4-14 shows interfacial tension and phase behavior data for an oil-brine-sulfonate-tertiary amyl alcohol as presented by Salter (1977) for low (left) and high (right) alcohol content. Figure 4-14 (top) shows the interfacial tension data, and accompanying tuned model results. Figure 4-14 (middle) shows the phase volume fraction data, with its corresponding model predictions with $\Omega = 0.99$ mN/m for low alcohol content and $\Omega = 0.91$ mN/m for high alcohol content, showing accurate predictive capabilities. These Ω values are calculated using Eq. 4-15 based on the experimental data for both interfacial tension and solubilization ratio at optimum condition. Figure 4-14 (bottom) shows the alternative approach, where the commonly-used scaling of $\Omega = 0.3$ mN/m is used, showing inaccurate predictive capabilities.

4.3 Summary

We introduced a consistent model that allows to capture and predict relevant interfacial tensions of microemulsion systems for all Winsor types and overall

compositions. This model is coupled with Huh's equation, which allowed us to define a coupled interfacial tension-phase behavior model. The main conclusions are:

- The model is developed considering micellar curvatures for the definition of interfacial tensions, making the phase behavior estimation physically representative.
- The presented approach allows for a consistent definition of all relevant interfacial tension in microemulsion systems for all HLD and composition conditions, and offers accurate predictions of the corresponding phase behavior.
- The interfacial tension between oil and water is tied to HLD by using film bending energy arguments and empirical relations for microscopic curvatures. This oil-water interfacial tension is found to be quadratic with HLD. Similarly, the characteristic length scale is tied to HLD following empirical expressions for the characteristic length scale and principal curvatures; the characteristic length scale is found to scale with the inverse of HLD. Comparison to experimental data shows excellent results.
- The approach allows to predict oil-water interfacial tensions at optimum and away from optimum condition for a wide range of cases, which can minimize the number of experiments needed for a given system and allow for accurate estimations away from experimental conditions.
- Models for the oil-microemulsion and microemulsion-water interfacial tensions are developed based on phase transition boundary conditions,

which show accurate results when compared to experimental data. These models are extended to account for compositional changes.

- Using Huh's equation, the interfacial tension is linked to phase behavior in order to present a coupled model for all microemulsion phase environments.
- The oil-water interfacial tension, characteristic length scale and solubilization ratio are tied at optimum condition under the assumption of bicontinuous micellar arrangement, which allows for increased predictability of the coupled interfacial tension-phase behavior model.

4.4 Appendix A: Interfacial tension and characteristic length scale models

The mean and principal curvatures (i.e. H, c_1 and c_2) are intensive state functions. Based on the Gibbs phase rule, the intensive state of a three-component system in the three-phase region is fully determined by fixing pressure and temperature (or any two intensive state parameters). For both principal curvature and HLD we can write,

$$dc_1 = \left(\frac{\partial c_1}{\partial T}\right)_P dT + \left(\frac{\partial c_1}{\partial P}\right)_T dP$$

$$dc_2 = \left(\frac{\partial c_2}{\partial T}\right)_P dT + \left(\frac{\partial c_2}{\partial P}\right)_T dP \qquad (4-A1)$$

$$dHLD = \left(\frac{\partial HLD}{\partial T}\right)_P dT + \left(\frac{\partial HLD}{\partial P}\right)_T dP.$$

Strey (1994) gave empirical relationships for the mean curvature and principal curvatures for a temperature-scan, under constant pressure conditions. After integration, for a temperature-scan we find,

$$\begin{aligned} c_1 - c_{1,ref} &= \left(\frac{\partial c_1}{\partial T}\right)_P \left(T - T_{ref}\right) \\ c_2 - c_{2,ref} &= \left(\frac{\partial c_2}{\partial T}\right)_P \left(T - T_{ref}\right) \\ HLD - HLD_{ref} &= \left(\frac{\partial HLD}{\partial T}\right)_P \left(T - T_{ref}\right), \end{aligned} \qquad (4 - A2)$$

where $(\partial HLD/\partial T)_P$ has been shown to be constant, and can be correlated as a linear function with pressure for changing pressure conditions (Ghosh and Johns, 2016B). By combining the principal curvature equations with the expression for HLD, we can express the principal curvatures as follows,

$$\begin{aligned} c_1 - c_{1,ref} &= c_c\left(HLD - HLD_{ref}\right) \\ c_2 - c_{2,ref} &= c_c\left(HLD - HLD_{ref}\right), \end{aligned} \qquad (4 - A3)$$

where $c_c = (\partial c_1/\partial HLD)_P = (\partial c_2/\partial HLD)_P$ under the assumption of symmetric curvature dependence on HLD at constant pressure (Leitao et al., 1996). From the definition of mean curvature, we can write $dH = (dc_1 + dc_2)/2$, and following a similar development as above, we obtain,

$$H - H_{ref} = c_c\left(HLD - HLD_{ref}\right) \qquad (4-A4)$$

Following the observations by Strey (1994), we consider the following reference conditions,

$$\begin{aligned} c_1 = 0 \quad HLD = HLD_L \\ c_2 = 0 \quad HLD = HLD_U \\ H = 0 \quad HLD = 0, \end{aligned} \qquad (4-A5)$$

where HLD_L and HLD_U are the HLD where the invariant point merges with the brine and oil excess phases, respectively. Combining Eqs. 4-A3 and 4-A4 with the reference values in 4-A5, we obtain,

$$\begin{aligned} c_1 = c_c(HLD - HLD_L) \\ c_2 = c_c(HLD - HLD_U) \\ H = c_c HLD \end{aligned} \qquad (4-A6)$$

Substitution of Eq. 4-A6 into Eq. 2-2 gives,

$$(4-A7)$$

$$\gamma_{ow} = {c_c}^2(2\kappa + \overline{\kappa})HLD^2 + \overline{\kappa}{c_c}^2(HLD_L + HLD_U)HLD - \overline{\kappa}{c_c}^2 HLD_L HLD_U.$$

The desired result (Eq. 4-1) is obtained from Eq. 4-A7 under the assumption of symmetry in the phase transition boundaries (i.e. $HLD_L = -HLD_U$).

Similarly, an equation for the characteristic length can be obtained by substitution of Eq. 4-A into Eq. 2-5,

$$\xi = \frac{\sqrt{2}/(c_c)}{(HLD_U^2 + HLD_L^2 - 2HLD(HLD_U + HLD_L) + 2HLD^2)^{0.5}}. \qquad (4-A8)$$

The desired result (Eq. 4-4) is obtained from Eq. 4-A8 assuming $HLD_L = -HLD_U$.

4.5 Appendix B: Model coefficients definition

This appendix gives a detailed explanation of how to use the approach described in this chapter to tune interfacial tensions and predict phase behavior. The approach relies on having available γ_{ow}, γ_{om}, and γ_{mw} experimental data. The following are relevant steps in our computation:

Based on the available γ_{ow} data, define the model parameters in Eq. 4-1 (i.e. c_γ and γ_{ow}^{min}). Further, using γ_{om}, and γ_{mw} data in the Type III environment, define the model parameters in Eq. 4-9 (i.e. HLD_L and HLD_U). This step completely defines our interfacial tension model for all HLD and composition conditions. The relevant model parameters can be calculated if γ_{om} data is available in the Type

II- environment and γ_{mw} data is available in the Type II+ environment by using Eq. 4-9.

The phase behavior coupling is defined through Eq. 2-4, which relies on the scaling constant Ω. In practice, the value of Ω is traditionally taken to be 0.3 mN/m (Ghosh and Johns, 2016A). However, if optimum solubilization and interfacial tension data is available for the system under consideration, Eq. 4-11 can provide a more accurate value.

Combining Eqs. 2-3 and 4-21 gives the model predictive capabilities. For Eq. 4-21 to be fully defined, we need to know the value of the ratio $\overline{\kappa}/(IL)^2$, which for the systems considered is around 0.13 mN/m.

Table 4-1. IFT model parameters for all systems considered.

Data set	γ_{ow}^{min}	c_γ	HLD_U	HLD_L
Strey (1994)	4.0E-4	8.7	-	-
Leitao et al. (1996), C_6E_2	8.2E-2	18.7	-	-
Leitao et al. (1996), C_8E_3	1.5E-2	15.9	-	-
Leitao et al. (1996), $C_{10}E_4$	2.8E-3	14.1	-	-
Leitao et al. (1996), $C_{12}E_5$	4.8E-4	9.1	-	-
Sottmann and Strey (1997)	1.0E-1	9.7	-	-
Kunieda and Shinoda (1982)	1.2E-1	10.7	0.1	-0.1
Davis and Scriven (1980)	5.0E-1	1.3	0.8	-0.8
Salter (1977), low alcohol	2.0E-3	4.0E-2	0.3	-0.3
Salter (1977), high alcohol	1.1E-2	8.0E-2	0.5	-0.5

Table 4-2. Characteristic length model parameters for all systems considered.

Data set	c_ξ	ξ^{max}
Strey (1994)	0.015	1.0E3

Table 4-3. Reference values corresponding to the system by Sottmann and Strey (1997).

$log(\gamma_{ow,ref}^{min})$	$X_{1,ref}^* = LCL_{ref}^*$	$X_{2,ref}^* = HCL_{ref}^*$	$X_{3,ref}^* = EACN_{ref}^*$	$X_{4,ref}^* = 1/T_{ref}^*$
-1.34	8	3	12	3.6E-2°C^{-1}

Table 4-4. Relevant partial derivatives needed to define the correlation for log of (γ_{ow}^{min}) for the system by Sottmann and Strey (1997).

$\left(\frac{\partial log(\gamma_{ow}^{min})}{\partial X_1^*}\right)_{X_k^* \neq X_1^*}$	$\left(\frac{\partial log(\gamma_{ow}^{min})}{\partial X_2^*}\right)_{X_k^* \neq X_2^*}$	$\left(\frac{\partial log(\gamma_{ow}^{min})}{\partial X_3^*}\right)_{X_k^* \neq X_3^*}$	$\left(\frac{\partial log(\gamma_{ow}^{min})}{\partial X_4^*}\right)_{X_k^* \neq X_4^*}$
-3.7E-1	7.8E-2	1.2E-1	-18.8°C

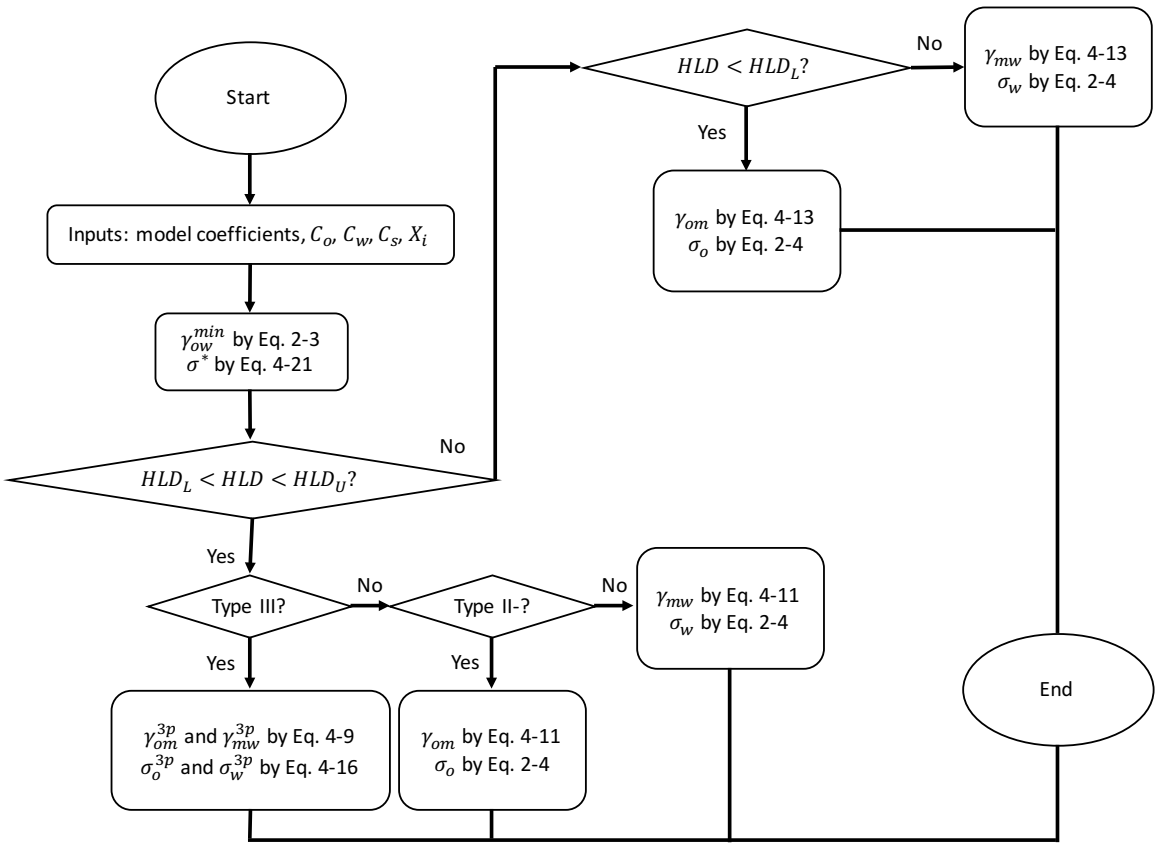

Figure 4-1. General flow chart for coupled interfacial tension-phase behavior algorithm.

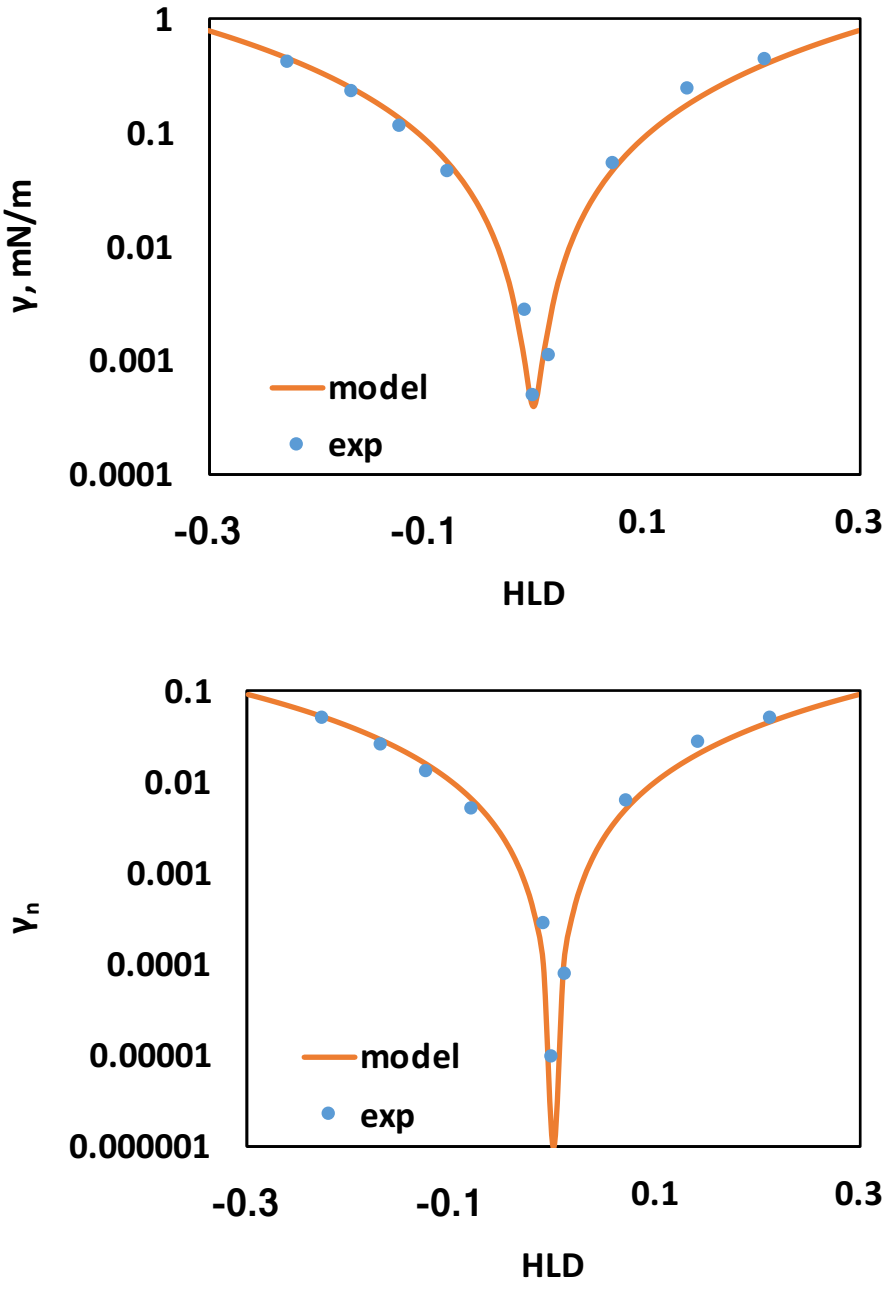

Figure 4-2. Interfacial tension between the oil and water phases using Eq. 4-1 (top) and normalized interfacial tension using Eq. 4-3 (bottom) as a function of HLD for a water—n-octane—$C_{12}E_5$ system. Experimental data from Strey (1994).

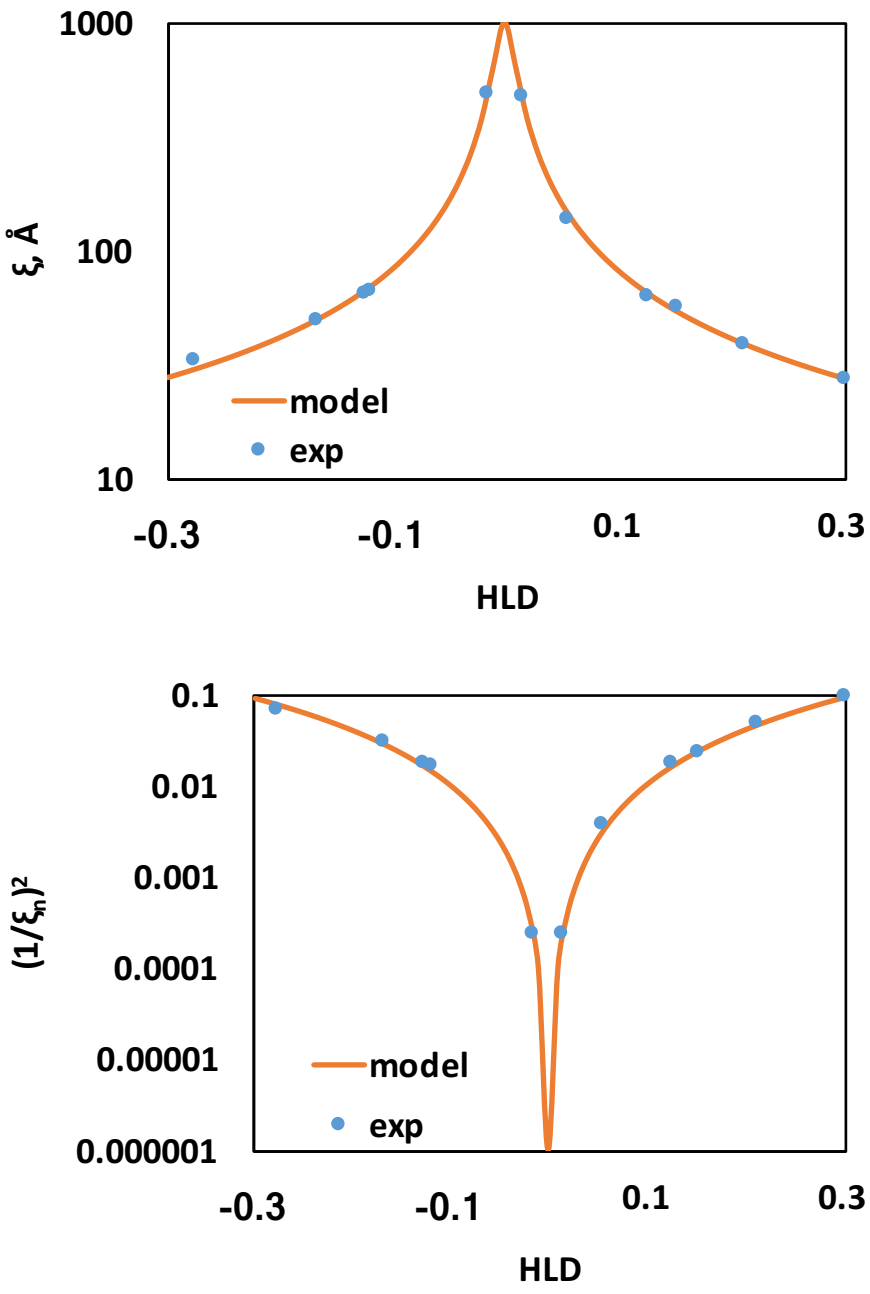

Figure 4-3. Characteristic length scale using Eq. 4-4 (top) and inverse of the normalized characteristic length scale square using Eq. 4-6 (bottom) as a function of HLD for a water—n-octane—$C_{12}E_5$ system. Experimental data from Strey (1994).

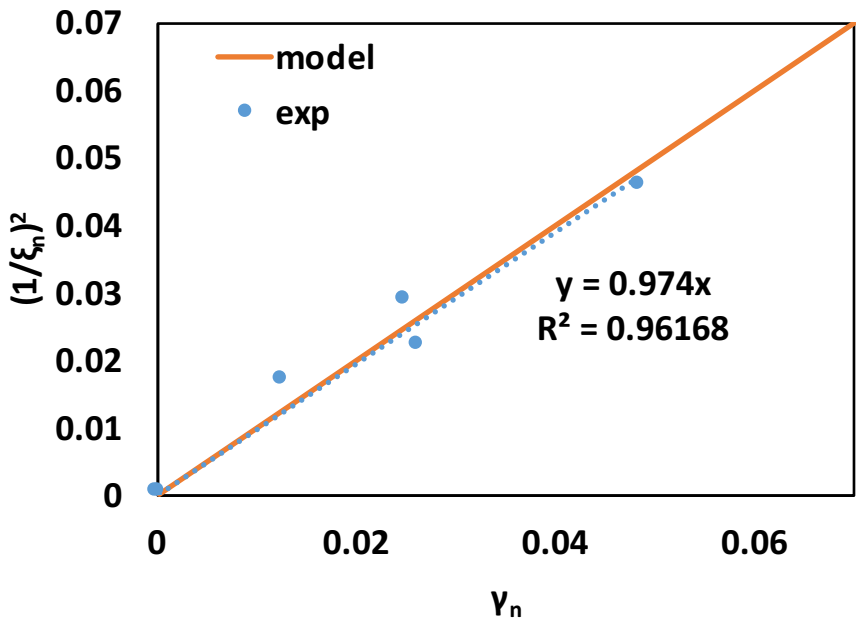

Figure 4-4. Inverse of normalized characteristic length square as a function of normalized interfacial tension using Eq. 4-7 for a water—n-octane—$C_{12}E_5$ system. Experimental data from Strey (1994).

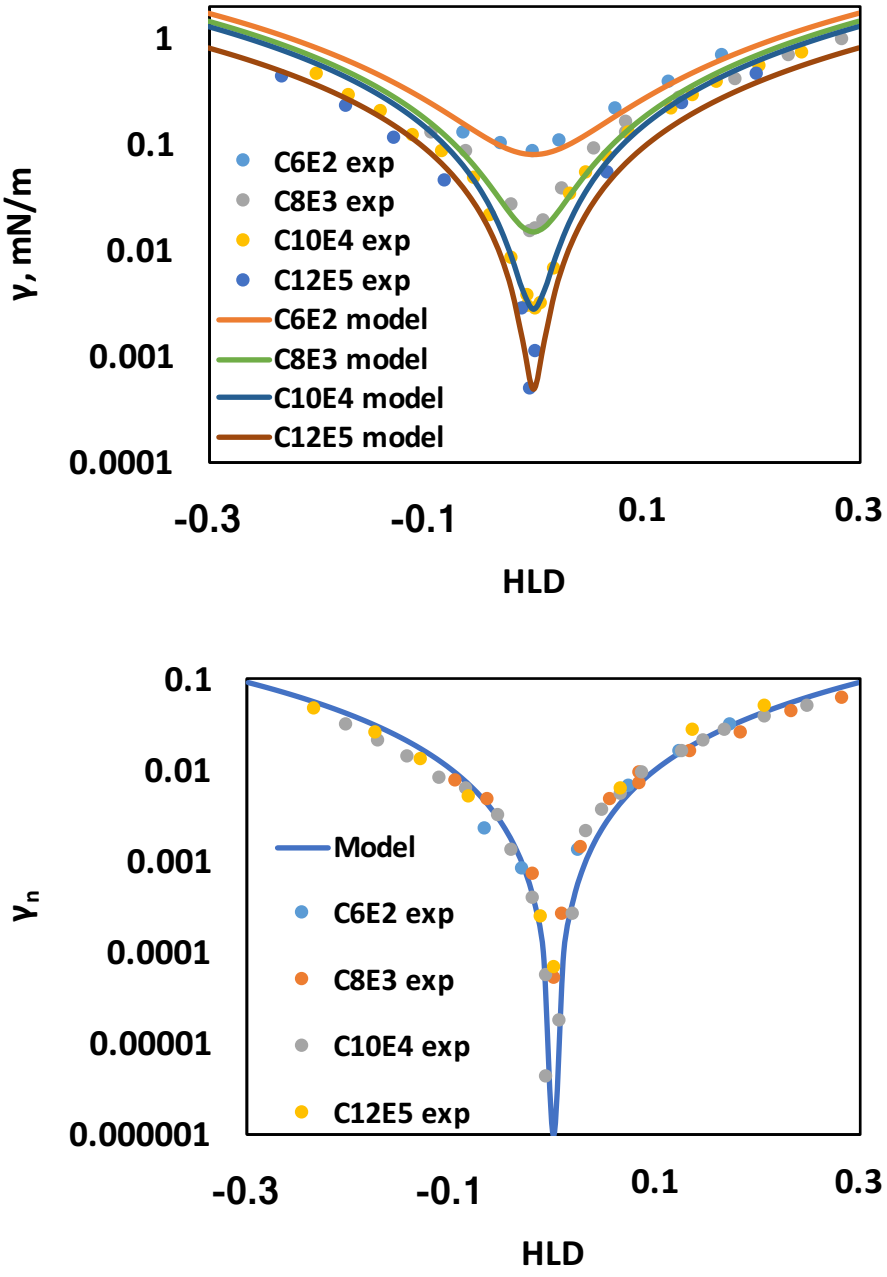

Figure 4-5. Interfacial tension between the oil and water phases using Eq. 4-1 (top) and normalized interfacial tension using Eq. 4-3 (bottom) as a function of HLD for different water—n-octane—C_iE_j systems. Experimental data from Leitao et al. (1996).

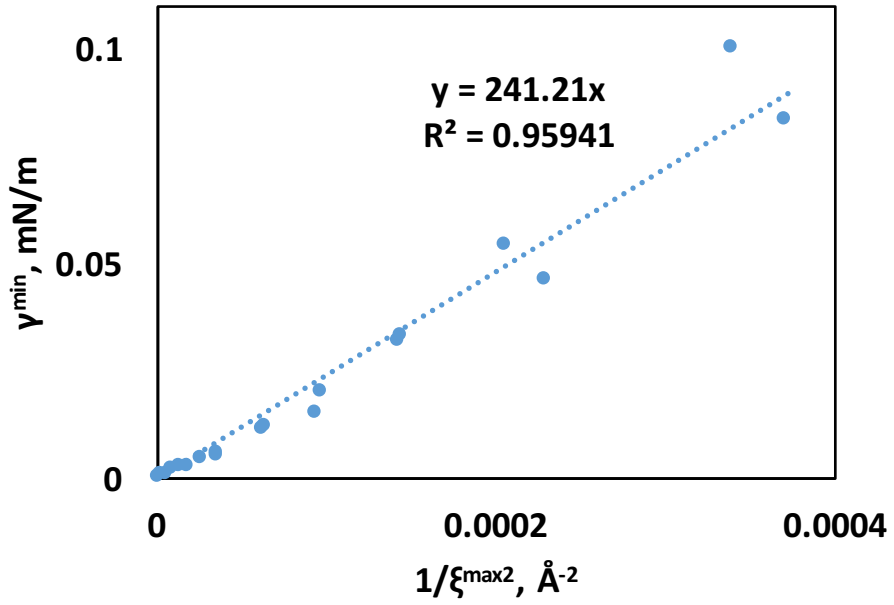

Figure 4-6. Oil-water interfacial tension versus the inverse of the characteristic length scale square, both at optimum condition. Experimental data from Sottmann and Strey (1997) and Sottmann et al. (1997).

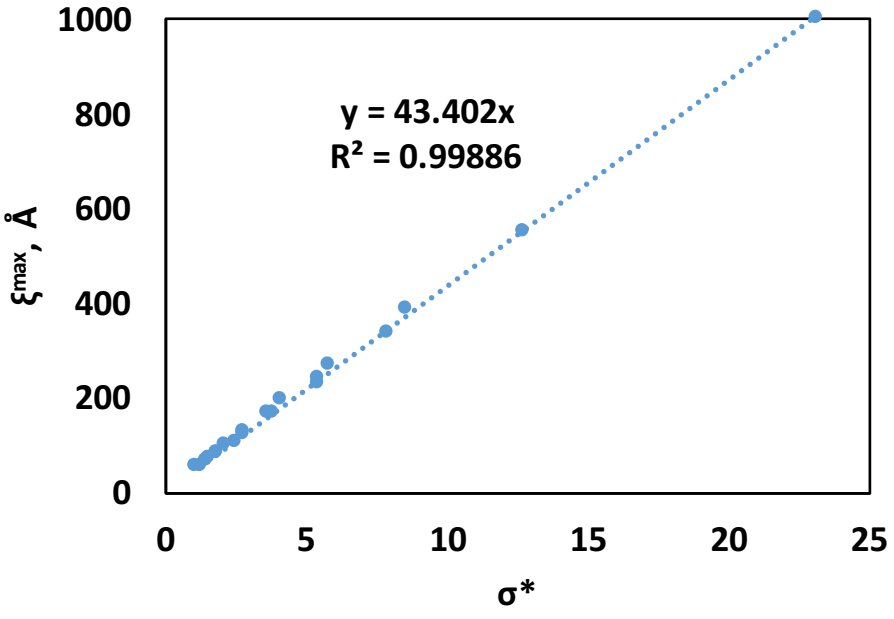

Figure 4-7. Characteristic length scale as a function of solubilization ratio, both at optimum condition. Experimental data from Sottmann et al. (1997).

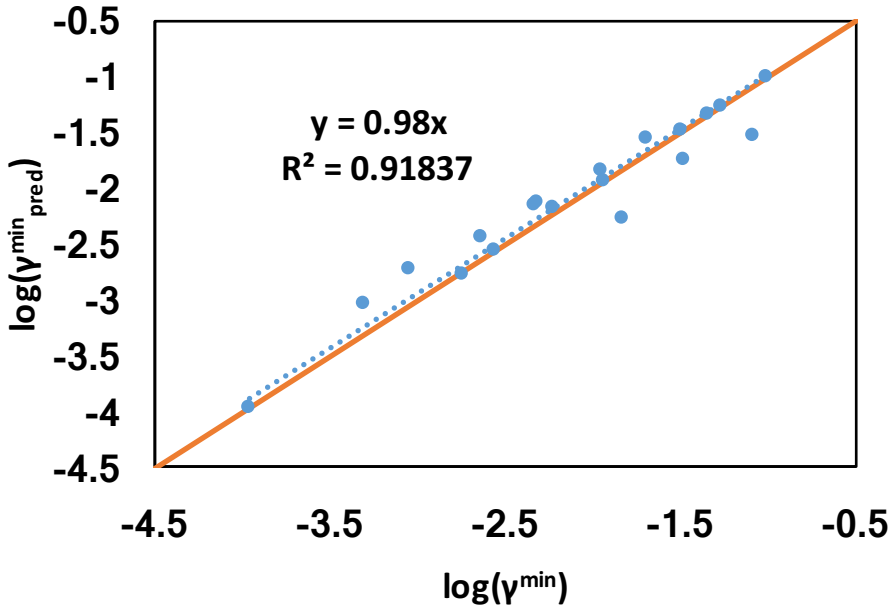

Figure 4-8. Comparison between predicted values of the oil-water interfacial tension at optimum using Eq. 2-3, and the corresponding experimental results. Experimental data from Sottmann and Strey (1997).

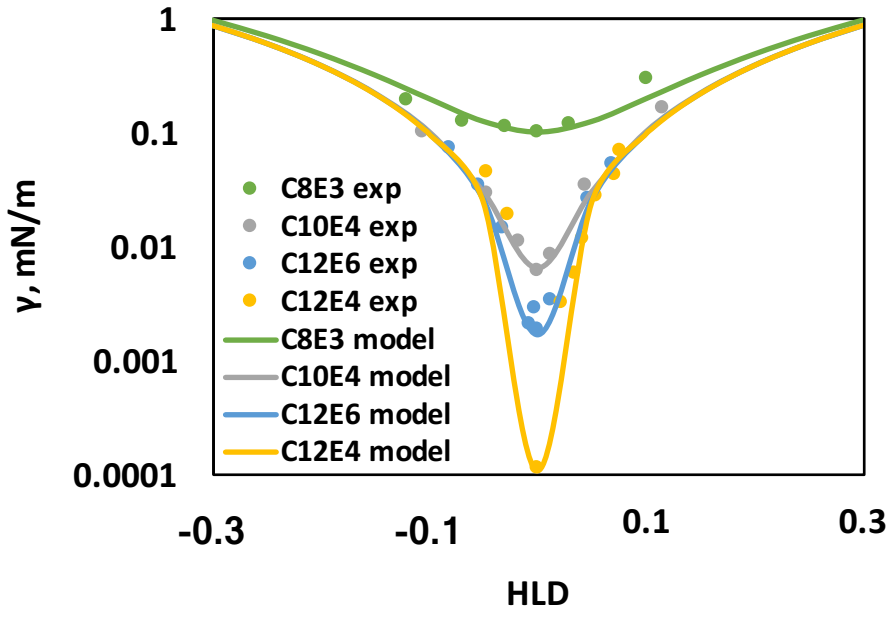

Figure 4-9. Oil-water interfacial tension model using Eq. 4-1 and experimental results as a function of HLD for different water—n-alkane—C_iE_j systems. The C_8E_3, $EACN = 14$ system is tuned and all others are predicted as described in the text. Experimental data from Sottmann and Strey (1997).

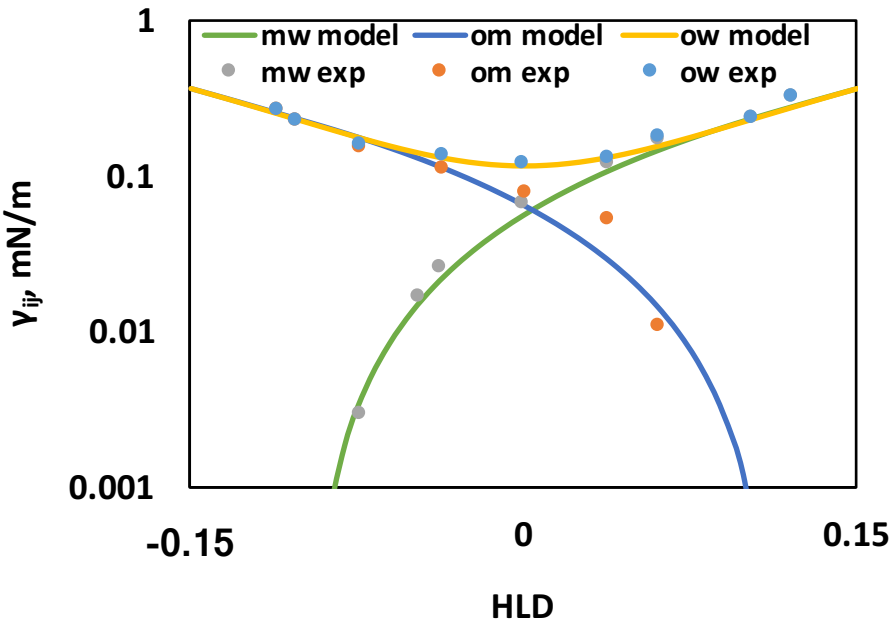

Figure 4-10. Interfacial tension between the oil and water, the microemulsion and water, and the oil and microemulsion phases as a function of HLD using Eqs. 4-1 and 4-9 for a water—n-tetradecane—$C_8H_{17}(OCH_2CH_2)_3OH$ system. Experimental data from Kunieda and Shinoda (1982).

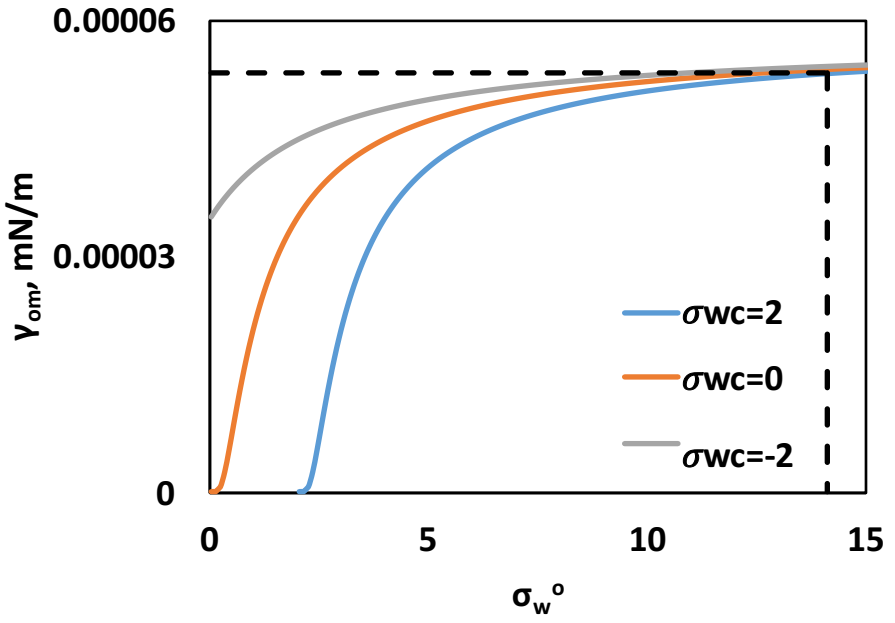

Figure 4-11. Oil-microemulsion interfacial tension as a function of water solubilization ratio in the Type II- lobe with the critical lines $\sigma_w^c = 2$, $\sigma_w^c = 0$, and $\sigma_w^c = -2$ at fixed $HLD = 0$.

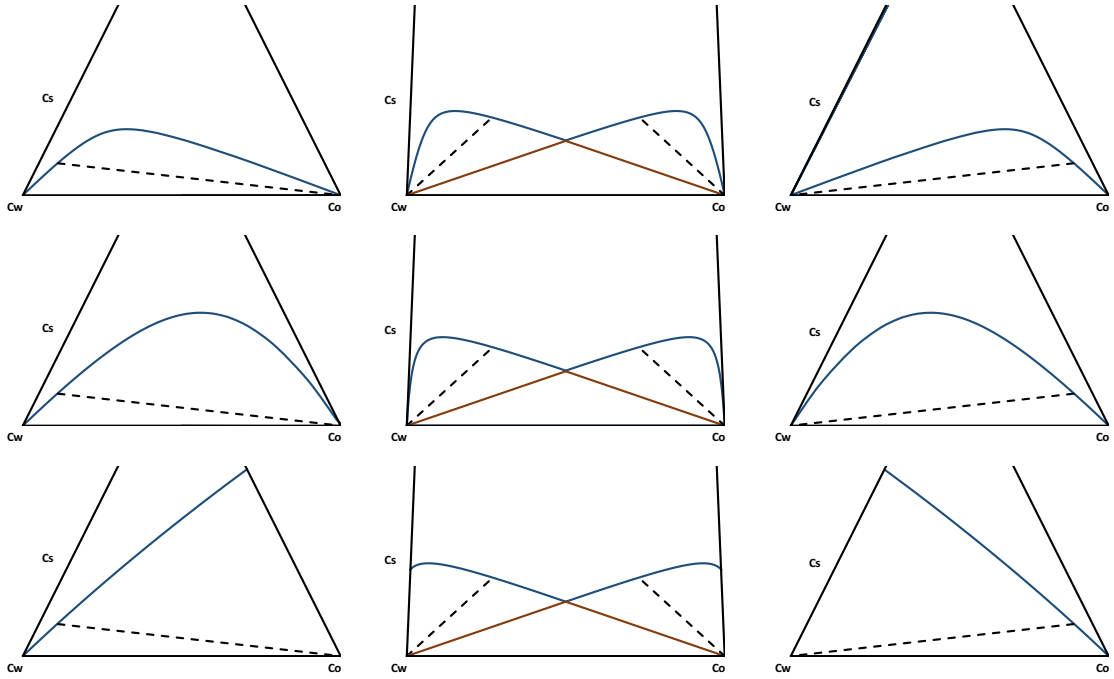

Figure 4-12. Ternary diagrams corresponding to $HLD = -0.1$ (left), $HLD = 0$ (center), and $HLD = 0.1$ (right) with the critical lines $\sigma_w^c = \sigma_o^c = 2$ (top), $\sigma_w^c = \sigma_o^c = 0$ (middle), and $\sigma_w^c = \sigma_o^c = -2$ (bottom).

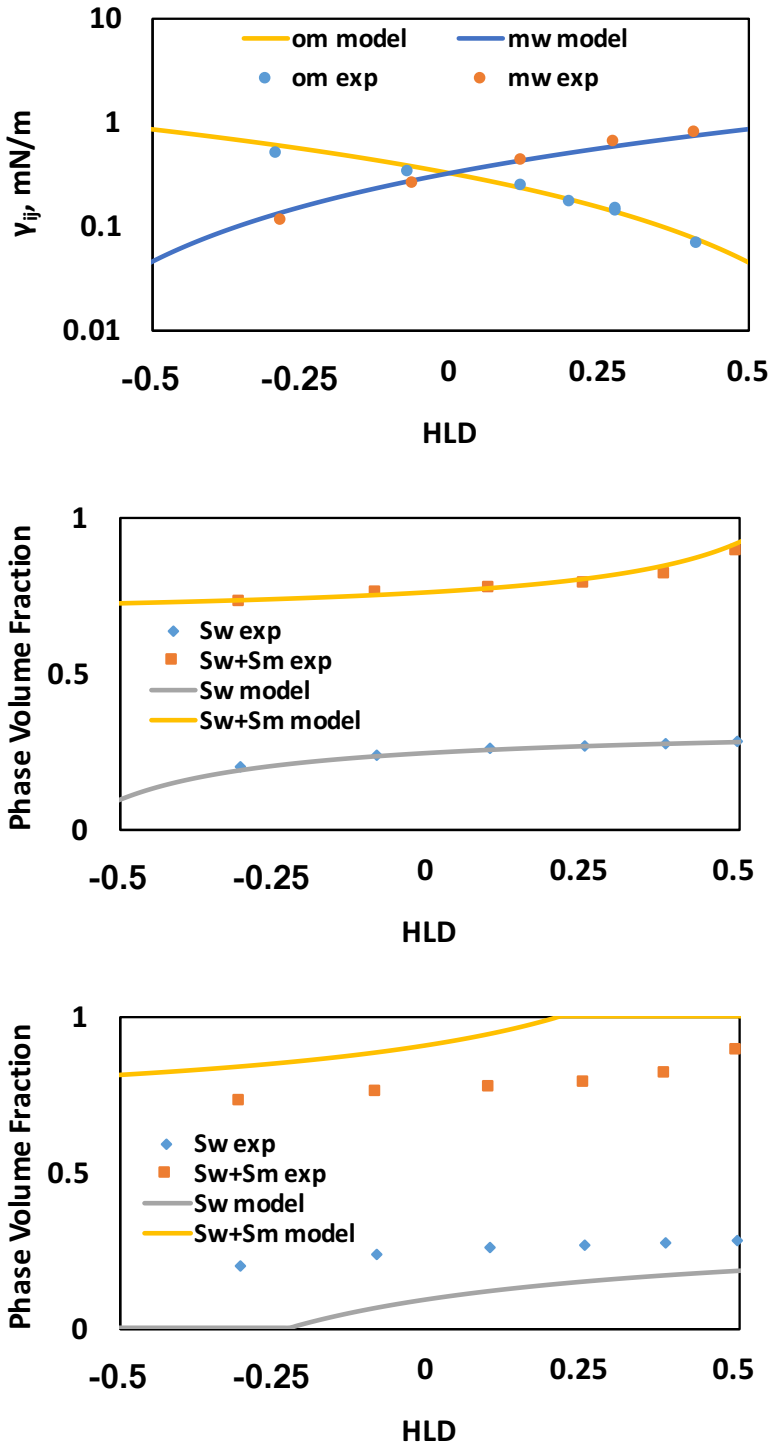

Figure 4-13. Relevant interfacial tension experimental and tuned model results using Eq. 4-9 (top), the accompanying phase behavior experimental and model prediction results using Eq. 2-4 with $\Omega = 0.11$ mN/m calculated using Eq. 4-15 (middle), and the alternative prediction by considering the commonly-used scaling value of $\Omega = 0.3$ mN/m (bottom). Experimental data from Davis and Scriven (1980).

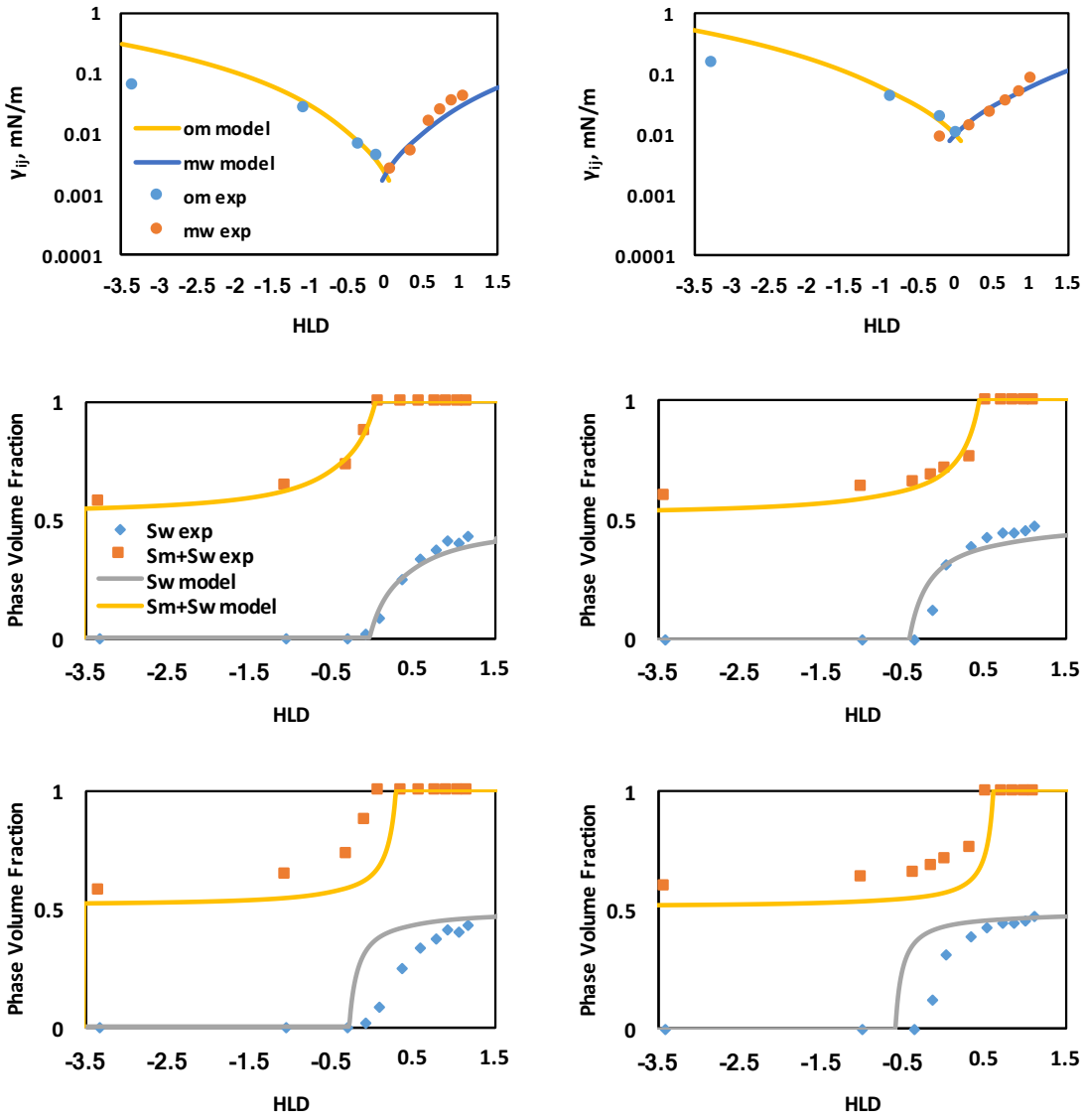

Figure 4-14. Oil-microemulsion and microemulsion-water interfacial tension data and model tuned results (top), and phase volume fraction data and model predictions using the estimated value of Ω (middle) and the commonly used value of $\Omega = 0.3$ mN/m (bottom) for low alcohol content (left) and high alcohol content (right). Data from Salter, 1977.

Part III

Chemical Potential-Based Methods

Chapter 5

Microemulsion Phase Behavior Model Using Empirical Trends in Chemical Potentials

Recent contributions to the petroleum engineering literature have used the hydrophilic-lipophilic difference net-average curvature ($HLD - NAC$) model to develop a phase behavior Equation of State (EoS) to fit experimental data and predict phase behavior away from tuned data. The model currently assumes spherical micelles, which may yield errors in the bicontinuous region where micelles transition into cylindrical and planar shapes.

This chapter develops a new phase behavior EoS model based on empirical trends in the chemical potentials (referred to as the CP EoS model) that eliminates many of the above assumptions. The model is linked to HLD and can be easily tuned to available experimental data (either an HLD-scan at fixed composition or variable composition data at fixed HLD). The new model is extended to account for surfactant partitioning into the excess phases and eliminates the use of the *NAC* equations, which rely on spherically-shaped micelles.

5.1 Methodology

In this section, we will introduce the fundamental ideas for the new phase behavior model, such as how the oil and water solubilization ratios in the microemulsion phase differ from Type III to Type II- or Type II+ (Torrealba and Johns, 2017B).

5.1.1. Model development with pure excess phases

For a type III microemulsion environment, we can write the oil and surfactant chemical potentials between the oil and microemulsion phase, to obtain Eq. 5-1,

$$\begin{aligned} ln(\bar{\gamma}_{oo}C_{oo}) &= ln(\bar{\gamma}_{om}C_{om}) \\ ln(\bar{\gamma}_{so}C_{so}) &= ln(\bar{\gamma}_{sm}C_{sm}). \end{aligned} \qquad (5-1)$$

Most microemulsion phase behavior data measured for the petroleum engineering literature is presented as phase solubilization ratios. The solubilization ratio of component i in phase j is defined as $\sigma_{ij} \equiv C_{ij}/C_{sj}$, where the surfactant component is used as the reference component. Then, algebraic manipulation of Eq. 5-1 yields the following expression,

$$\sigma_{om} = \frac{\bar{\gamma}_{sm}\bar{\gamma}_{oo}\sigma_{oo}}{\bar{\gamma}_{om}\bar{\gamma}_{so}}. \qquad (5-2)$$

Substitution of the definition of HLD into $\bar{\gamma}_{so}$ gives,

$$\sigma_{om} = \frac{\bar{\gamma}_{sm}\bar{\gamma}_{oo}\sigma_{oo}}{\bar{\gamma}_{om}\bar{\gamma}_{sw}} e^{HLD}. \qquad (5-3)$$

Following a similar development for the water solubilization ratio in the microemulsion phase we obtain,

$$\sigma_{wm} = \frac{\bar{\gamma}_{sm}\bar{\gamma}_{ww}\sigma_{ww}}{\bar{\gamma}_{wm}\bar{\gamma}_{so}} e^{-HLD}. \qquad (5-4)$$

At $HLD = 0$, we assume $\sigma_{om} = \sigma_{wm} = \sigma^*$, with σ^* being the optimum solubilization ratio. Figure 5-1 shows examples of $ln\,(\frac{\sigma_{om}}{\sigma^*})$ and $ln\,(\frac{\sigma_{wm}}{\sigma^*})$ versus HLD for a temperature scan at different pressures using a dodecyl-orthoxylene sulfonate surfactant, a dead oil, and a brine, as measured by Austad and Strand (1996) for pressures between 50 to 250 bars. Based on these trends, we propose the following form for σ_{om} and σ_{wm} in the type III region,

$$\begin{aligned} \sigma_{om} &= \sigma^* e^{\Omega_o^{III} HLD} \\ \sigma_{wm} &= \sigma^* e^{-\Omega_w^{III} HLD}, \end{aligned} \qquad (5-5)$$

where the constant parameters Ω_o^{III} and Ω_w^{III} are introduced to provide improved fits of solubility ratio within the type III region. Let us define $G_o = \sigma_{om}/e^{\Omega_o^{III} HLD}$. For a three-component system, the relevant formulation variables to determine the intensive state in the three-phase region are pressure and temperature. For

our model to accurately predict outside the range of experimental observation, we should define a correlation of the form,

$$G_o^{pred} = \beta_1 T + \beta_2 P + \beta_3 \qquad (5-6)$$

where β_i are the tuning constants defining a G_o plane in TP space. Figure 5-2 (top) shows the G_o results versus the corresponding predictions using Eq. 5-6 for six different temperature scans at various pressures ranging from 50-300 bar. Interestingly enough, the scaling proposed in Eq. 5-5 clusters all pressure scans around the corresponding optimum value (which is shown for reference). This is an important result, as it suggests that by considering the proper scaling, all three-phase data can be estimated from the optimum value. Further, it motivates us to consider a similar correlation for the optimum solubilization ratio. Figure 5-2 (bottom) shows the σ^* experimental results versus the corresponding predictions using the same form of Eq. 5-6 using parameters obtained from tuning to three-phase data (i.e. same parameters as in Fig. 5-2, top) and to optimum solubilization data, yielding comparable results. The use of such correlation for σ^* allows us to practically estimate phase behavior away from the conditions of a single formulation variable scan. However, further work should be made to better understand the nature of these correlations as we increase the number of components in the system, and therefore the number of relevant formulation variables.

Equation 5-5 also allows for the calculation of the HLD phase transition boundaries at a fixed composition with,

$$HLD_L = -\frac{\ln\left(\frac{\overset{\circ}{\sigma}_{wm}}{\sigma^*}\right)}{\Omega_w^{III}}$$

$$HLD_U = \frac{\ln\left(\frac{\overset{\circ}{\sigma}_{om}}{\sigma^*}\right)}{\Omega_o^{III}}, \qquad (5-7)$$

where $\sigma_{im}^o = C_i/C_s$ and C_i is the overall volumetric composition of component i and the subscript *L* refers to the lower boundary (type III—type II-) and *U* the upper boundary (type III—type II+). Equation 5-7 implies that for $HLD \to \infty$, the invariant point (i.e. the composition of the three-phase microemulsion) approaches the type II- critical point (i.e. the oil apex of the ternary diagram), and for $HLD \to -\infty$, the invariant point approaches the type II+ critical point (i.e. the water apex of the ternary diagram). That is, the model assumes the three-phase region is always present, but it becomes differentially small in the ternary diagram as we approach $HLD \to \pm\infty$. This limitation is removed in Sec. 5.1.2 for the case where the model is extended to account for surfactant partitioning.

Now consider the oil solubilization for a type II- microemulsion. In this case, we know σ_{om} should approach the type III oil solubilization as we approach HLD_L to preserve continuity. In addition, we assume the critical point of the type II- lobe is located at the pure oil apex, which means the critical point oil solubilization ratio (σ_{om}^{cp}) is infinity, and the limiting tie line at the critical point is

along the surfactant-oil axis (i.e. $\sigma_{wm}^{o} = 0$ at the type II- critical point). Equation 5-8 presents a simple expression for the type II- oil solubilization ratio, which honors the described limits,

$$\sigma_{om} = \frac{K_o}{\sigma_{wm}^{o}}\left(1 - e^{\Omega_o^{II}(HLD - HLD_L)}\right) + \sigma^* e^{\Omega_o^{II}(HLD - HLD_L)} e^{\Omega_o^{III} HLD}, \qquad (5-8)$$

where K_o and Ω_o^{II} are constant parameters that can be adjusted to improve fits to experimental data. Similarly, for a type II+ microemulsion, the following expression for the water solubilization ratio in the microemulsion phase is,

$$\sigma_{wm} = \frac{K_w}{\sigma_{om}^{o}}\left(1 - e^{\Omega_w^{II}(HLD_U - HLD)}\right) + \sigma^* e^{\Omega_w^{II}(HLD_U - HLD)} e^{-\Omega_w^{III} HLD}, \qquad (5-9)$$

where K_w and Ω_w^{II} are constant parameters. Equations 5-8 and 5-9 are consistent with the Gibbs phase rule: for a three-component, two-phase system, the intensive state is determined by fixing three independent variables. We could either set pressure, temperature and the corresponding tie-line parameter (σ_{wm}° for Type II- or σ_{om}° for Type II+) or HLD, σ^* and the corresponding tie-line parameter.

The CP EoS model based on Eqs. 5-5, 5-8 and 5-9 is consistent across all phase environments. For phase behavior symmetry (where $\sigma_{om}(HLD) = \sigma_{wm}(-HLD)$ for a water-oil-ratio of 1) we set $K \equiv K_o = K_w$, $\Omega^{II} \equiv \Omega_o^{II} = \Omega_w^{II}$ and $\Omega^{III} \equiv \Omega_o^{III} = \Omega_w^{III}$. Further, we can simplify the model by setting $\Omega \equiv \Omega^{II} = \Omega^{III}$. In

the simplest form, the model reduces to a two-parameter model (i.e. the K and Ω constant parameters), whereas in the most flexible form, the model has six constant parameters (i.e. Ω_i^{III}, Ω_i^{II} and K_i with $i = o, w$).

5.1.2. Model development with impure excess phases

So far, the CP EoS model is only capable of capturing the surfactant component in the microemulsion phase; however, sufficient experimental data supports otherwise (Wade et al., 1978; Koukounis et al., 1983; Torrealba and Johns, 2016). In this section, we allow the surfactant component to partition into the excess phases while keeping immiscibility between the oil and water components. For the type II- region, the critical point is at the oil excess phase composition, which has an oil composition of C_{oo}, and a surfactant composition of $C_{so} = 1 - C_{oo}$. As we approach the critical point of the type II- region (i.e. as σ_{wm}^{o} approaches the limiting tie-line at the critical point) the oil solubilization ratio must approach a maximum value given by the critical point oil solubilization ratio (σ_{om}^{cp}), which is $\sigma_{om}^{cp} = C_{oo}/(1 - C_{oo})$. This limit occurs because the critical point is located at the oil excess phase composition; alternatively, as σ_{wm}^{o} goes to its maximum value of $\sigma_{wm}^{cp} = C_{ww}/(1 - C_{ww})$, the oil solubilization approaches zero (corresponding to oil immiscibility at the water excess phase). These arguments in terms of limiting tie-lines are consistent with the approach outlined by Khorsandi and Johns (2016) for pure excess phases. Analogous observations hold for the type II+ region. By combining these observations with Eqs. 5-8 and

5-9, we obtain the extended model that allows for the removal of the pure excess phases assumption as shown by Eq. 5-10.

$$\sigma_{om} = \frac{\kappa_o\left(1 - e^{\Omega_o^{II}(HLD_L^* - HLD_L)}\right)}{\sigma_{wm}^o + \frac{\kappa_o}{\sigma_{om}^{cp}}} + \sigma_{om}^{III} e^{\Omega_o^{II}(HLD_L^* - HLD_L)}$$

$$\sigma_{wm} = \frac{\kappa_w\left(1 - e^{\Omega_w^{II}(HLD_U - HLD_U^*)}\right)}{\sigma_{om}^o + \frac{\kappa_w}{\sigma_{wm}^{cp}}} + \sigma_{wm}^{III} e^{\Omega_w^{II}(HLD_U - HLD_U^*)}, \qquad (5-10)$$

where for the oil component $\sigma_{om}^{III} = \sigma_{om}^{cp}$ and $HLD_U^* = HLD_U\left(\sigma_{om}^{cp}\right)$ if $\sigma^* e^{\Omega_o^{III} HLD} > \sigma_{om}^{cp}$ (i.e. if the invariant point falls below the limiting tie line), otherwise $\sigma_{om}^{III} = \sigma^* e^{\Omega_o^{III} HLD}$ and $HLD_U^* = HLD$. Similarly, for the water component $\sigma_{wm}^{III} = \sigma_{wm}^{cp}$ and $HLD_L^* = HLD_L\left(\sigma_{wm}^{cp}\right)$ if $\sigma^* e^{-\Omega_w^{III} HLD} > \sigma_{wm}^{cp}$, otherwise $\sigma_{wm}^{III} = \sigma^* e^{-\Omega_w^{III} HLD}$ and $HLD_L^* = HLD$. In the limit of pure excess phases, Eq. 5-10 reduces to Eqs. 5-8 and 5-9, demonstrating consistency in the model. Equation 5-10 allows for the definition of a critical micelle concentration (CMC), which is a function of WOR. Equation 5-10 for impure excess phases is currently limited by having a constant surfactant concentration with HLD in the excess phases, but this could be extended to incorporate a surfactant partitioning model that is a function of HLD.

5.2 Results

In this section, we validate the CP EoS model against experimental data corresponding to various surfactant-oil-brine systems. Further, we benchmark the

CP EoS model against the HLD-*NAC* EoS model for various HLD-scans as well as for a composition-scan.

5.2.1. Predictability under changing pressure conditions

Figure 5-3 (left) compares experimental data and the fits from the CP EoS model for a dodecyl-orthoxylene sulfonate surfactant, dead oil, and brine system for a temperature scan at different pressures ranging from 50 to 250 bar, as measured by Austad and Strand (1996). The model was tuned to the results at 50 bar. Other data shown are predicted for the remaining pressures. The model replicates the tuned results well, and provides a good prediction for other pressures. Relevant model parameters for all cases tuned with the CP EoS model can be found in Table 5-2, and the HLD scaling parameter for all temperature scans in this chapter is $(\partial HLD/\partial T)_{X_k \neq T} = 0.01°C^{-1}$.

Figure 5-3 (right) shows the same data using the HLD-*NAC* EoS model, where tuning was also made at 50 bar, and predictions are presented for the other pressures. The water solubilization ratios are accurately captured by the predictions from the model, but the oil solubilization ratios are not captured as well. This is because the current HLD-*NAC* EoS model assumes a constant I-ratio and characteristic length in the Type III region that control both oil and water solubilization ratios, while the CP EoS model allows for two decoupled parameters in the type III region: one controlling the oil solubilization ratio (i.e. Ω_o^{III}) and one controlling the water solubilization ratio (i.e. Ω_w^{III}). Relevant model

parameters for all cases tuned with the HLD-*NAC* EoS model can be found in Table 5-3.

5.2.2. Predictability under changing oil EACN conditions

Figure 5-4 gives the phase behavior results for a salinity scan for a surfactant mixture containing 1.5 wt.% of TDA-13PO-SO_4 as the principal surfactant, 0.5 wt.% $C_{15\text{-}18}$ IOS as the co-surfactant, 3.0 wt.% IBA as a co-solvent, and a WOR of 1, for three oil compositions ranging from octane to dodecane as shown by Roshanfekr (2010). The CP EoS model was tuned to the decane data, honoring phase behavior transitions from type III to type II regions, and then was used to predict the results for octane and dodecane. For octane, both the phase volume fraction data and phase transition boundaries are accurately predicted, while for dodecane only the phase volume fraction data is accurately predicted. Future extensions of the model could consider Ω_o^{III} and Ω_w^{III} parameters to be function of EACN, which may allow for capturing of phase boundaries under significantly different formulation variable conditions. The HLD scaling parameter for all salinity scans in this chapter is $(\partial HLD/\partial ln(S))_{X_k \neq ln(S)} = 1$.

5.2.3. Capturing asymmetric phase boundaries

Figure 5-5 shows the data from Bennett et al. (1981) for a salinity scan using a mixture of sulfonate with isobutanol, n-hexadecane, and brine. The CP EoS model with four tuning parameters ($\Omega_i^{II} = \Omega_i^{III}$ with $i = o, w$) is able to capture both phase transition boundaries as well as the location of the experimental

optimum (i.e. the intersection of oil and water solubilization ratio data) as shown by Fig. 5-5 (top). Alternatively, because of the assumption of symmetry, the HLD-*NAC* EoS model with only three tuning parameters (C_k^-=C_k^+ with $k = 1,2$) did not capture both phase transition boundaries and the experimental optimum simultaneously. Figure 5-5 (middle) shows the HLD-*NAC* EoS model results where the optimum is fit, but the phase transition boundaries are not exactly satisfied; Fig. 5-5 (bottom) shows the HLD-*NAC* EoS model results where the phase transition boundaries are honored, but the optimum condition experimental location is missed.

5.2.4. Application to a complex crude system

Figure 5-6 shows the phase behavior experimental data and model results for a salinity scan for a petroleum sulfonate surfactant with isopentyl alcohol as cosolvent, Daqing crude oil and brine system and a water-oil-ratio (WOR) of 3, as presented by Xiren and Shutang (1988). The model is tuned to honor the phase transition boundaries, and it also accurately captures the phase volume fractions in the type II- and type II+ regions.

5.2.5. Dimensionless correlation length

Figure 5-7 shows the dimensionless correlation length for the octane data from Roshanfekr (2010) as described above, and the CP EoS and the HLD-*NAC* EoS model results. The dimensionless correlation length (ξ_D) is calculated by,

$$\frac{1}{\xi_D} = \frac{1}{\sigma_{om} + 0.5} + \frac{1}{\sigma_{wm} + 0.5}, \qquad (5-11)$$

which is similar to the definition derived in Khorsandi and Johns (2016). As previously described, the Khorsandi and Johns (2016) EoS assumes a constant dimensionless correlation length in the three-phase region, since it relies on the *NAC* for the three-phase solubilization ratios. However, for the same three-phase region, the CP EoS model predicts a variable dimensionless correlation length, with a maximum at optimum condition, which is consistent with observations from scattering experiments of microemulsion systems (Strey, 1994).

5.2.6. Composition-scan data

Lekkerkerker et al. (1996) conducted phase behavior studies using the double chain anionic surfactant AOT (which does not require a co-surfactant to form a microemulsion), brine (containing 0.6% NaCl), and n-decane at 40°C. Figure 5-8 shows compositional data for fixed HLD. The CP EoS model (Figure 5-8, left) is able to satisfactorily represent the phase boundaries, as well as provide good fits of the binodal curves for both type II- and type II+ microemulsion environments. For reference, the same system is tuned using the HLD-*NAC* EoS model (Figure 5-8, right). The model captures the correct trend in the two-phase lobes, but does not replicate the compositional experimental data as accurately as the CP EoS model because all CP EoS model two-phase parameters (Ω_i^{II} and K_i with $i = o, w$) can be defined at constant HLD. However, the HLD-*NAC* EoS model two-phase parameters (C_k^- and C_k^+ with $k = 1,2$) cannot be independently tuned since

we would only have one data point for the critical correlation length for each two-phase lobe (in our tuning, we assumed $C_1^- = C_1^+ = 1$, and calculated the corresponding C_2^- and C_2^+). In order to define both parameters independently, an additional HLD condition needs to be considered.

Burauer et al. (1999) studied the phase behavior of an ethylene glycol monobutyl ether (C_4E_1) surfactant, water, and n-dodecane at 52°C. Figure 5-9 shows compositional data for fixed HLD, and the accompanying results using the CP EoS phase behavior model for impure excess phases described by Eq. 5-10. The surfactant concentration in the excess phases for the system are $C_{so} = 0.16$ and $C_{sw} = 0.11$. The results show the capacity of the CP EoS model to accurately capture complex phase behavior in the presence of surfactant partitioning. In general, the surfactant concentration in the excess phases should be determined as a function of HLD in order to accurately represent the partitioning phenomena.

5.3 Summary

A new phase behavior EoS model was introduced based on an empirical formulation suggested by changes in chemical potentials (CP) with HLD. The CP EoS model relies on the HLD measure for surfactant affinity quantification, which captures a broad range of formulation state variables. Some specific conclusions are the following:

- The CP EoS phase behavior model satisfactorily tunes experimental data (including crude oil) for an HLD-scan and ternary diagram data. Tuning

honors phase boundaries between the type III and type II regions, while accurately capturing experimental phase volume fractions.

- For the cases considered, the CP EoS model offered improved tuning and predictions than the HLD-*NAC* EoS model.
- The new model eliminates the need for the *NAC* equations, does not assume a constant correlation length in the three-phase region, or that micelles are spherical in shape.
- The CP EoS model was extended to incorporate surfactant partitioning into the excess phases, which allows for a more complete description of the phase behavior of surfactant-oil-brine systems.

5.4 Appendix

The chemical potential for the surfactant in both oil and water excess phases can be written as,

$$\mu_{so} = \mu_s^{\circ} + RTln(\bar{\gamma}_{so}C_{so})$$
$$\mu_{sw} = \mu_s^{\circ} + RTln(\bar{\gamma}_{sw}C_{sw}). \qquad (5-A1)$$

At equilibrium, the chemical potential of each component is equal across all phases, which allows us to write the following,

$$ln\left(\frac{\bar{\gamma}_{sw}}{\bar{\gamma}_{so}}\right) = ln(K_{ow}^{s}), \qquad (5-A2)$$

where $K_{ow}^{s} = C_{so}/C_{sw}$. The change in HLD can be expressed as the change in surfactant partitioning between the excess phases as shown below,

$$dHLD = dln(K_{ow}^{s}). \qquad (5-A3)$$

Following integration from a reference state, we obtain,

$$HLD - HLD_{ref} = ln\left(\frac{K_{ow}^{s}}{K_{ow,ref}^{s}}\right). \qquad (5-A4)$$

The HLD_{ref} is usually set at zero, therefore $K_{ow,ref}^{s}$ corresponds to the surfactant partitioning at optimum condition, which can be simplified by assuming $K_{ow,ref}^{s} = 1$; however, if there is available data suggesting preferential partitioning (e.g. as in the case of nonionic surfactants) $K_{ow,ref}^{s}$ should be selected accordingly. Combining the results from Equations 5-A2 and 5-A4, we can write the HLD analogously as follows,

$$HLD = ln\left(\frac{\bar{\gamma}_{sw}}{\bar{\gamma}_{so}}\right). \qquad (5-A5)$$

Table 5-1. Tuned correlation parameters for both G_o and σ^* predictions.

Data set	$\beta_1, °C^{-1}$	β_2, bar^{-1}	β_3
G_o, Austad and Strand (1996)	-0.017	0.024	9.84
σ^*, Austad and Strand (1996)	-0.714	-0.047	68.94

Table 5-2. Tuned CP EoS model parameters based on all data sets considered.

Data set	Ω_o^{III}	Ω_w^{III}	Ω_o^{II}	Ω_w^{II}	K_o	K_w
Austad and Strand (1996)	3.6	4.1	-	-	-	-
Xiren and Shutang (1988)	1.0	0.37	1.0	0.37	0.1	1.34
Decane, Roshanfekr (2010)	3.6	3.0	8.0	3.0	140.0	50.0
Octane, Roshanfekr (2010)	2.4	2.4	0.0	0.0	1.0	1.0
Bennett et al. (1981)	2.6	6.2	2.6	6.2	15.0	2.5
Lekkerkerker (1996)	4.9	6.0	7.0	4.9	28.0	21.6
Burauer et al. (1999)	0.9	1.4	3.0	0.014	10	0.1

Table 5-3. Tuned HLD-*NAC* EoS model parameters based on all data sets considered.

Data set	l-ratio	C_1^-	C_2^-	C_1^+	C_2^+
Austad and Strand (1996)	0.34	-	-	-	-
Bennett et al. (1981) preserving optimum condition	0.48	0.8	1.0	0.8	1.0
Bennett et al. (1981) preserving phase boundaries	0.5	0.55	1.0	0.55	1.0
Octane, Roshanfekr (2010)	0.12	1.0	4.0	1.0	4.0
Decane at 40°C, Lekkerkerker (1996)	0.39	1.0	0.94	1.0	1.8

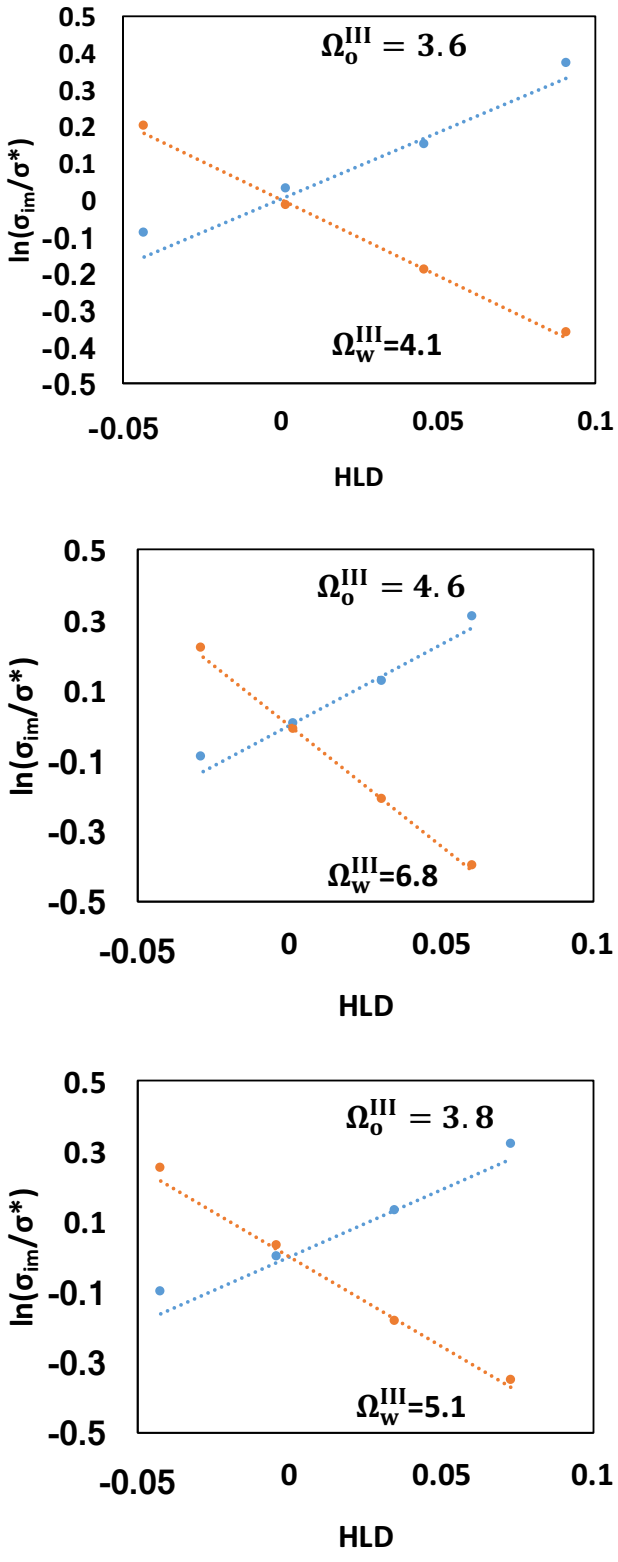

Figure 5-1. Observed linear relationship between $\ln\left(\frac{\sigma_{im}}{\sigma^*}\right)$ and HLD, for different temperature scans at 50 bar (top), 150 bar (middle), and 250 bar (bottom). Experimental data from Austad and Strand (1996).

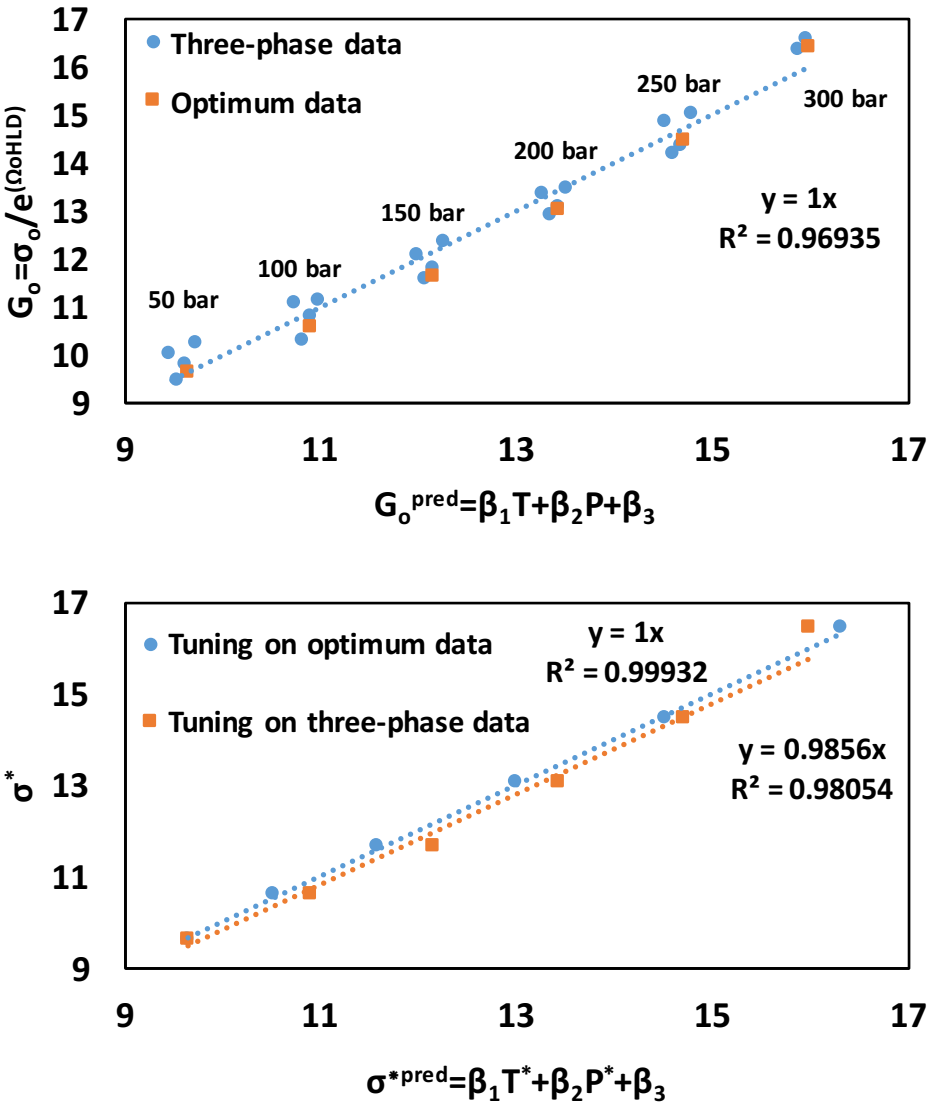

Figure 5-2. Experimental value for the G_o function versus the predicted value for the three-phase data tuned on three-phase data accompanied by the optimum value for reference (top) and calculated optimum solubilization versus the predicted value using both tuning to the optimum data and three-phase data (bottom). Experimental data corresponding to various temperature scans at changing pressures from Austad and Strand (1996). Relevant parameter are listed in Table 5-1.

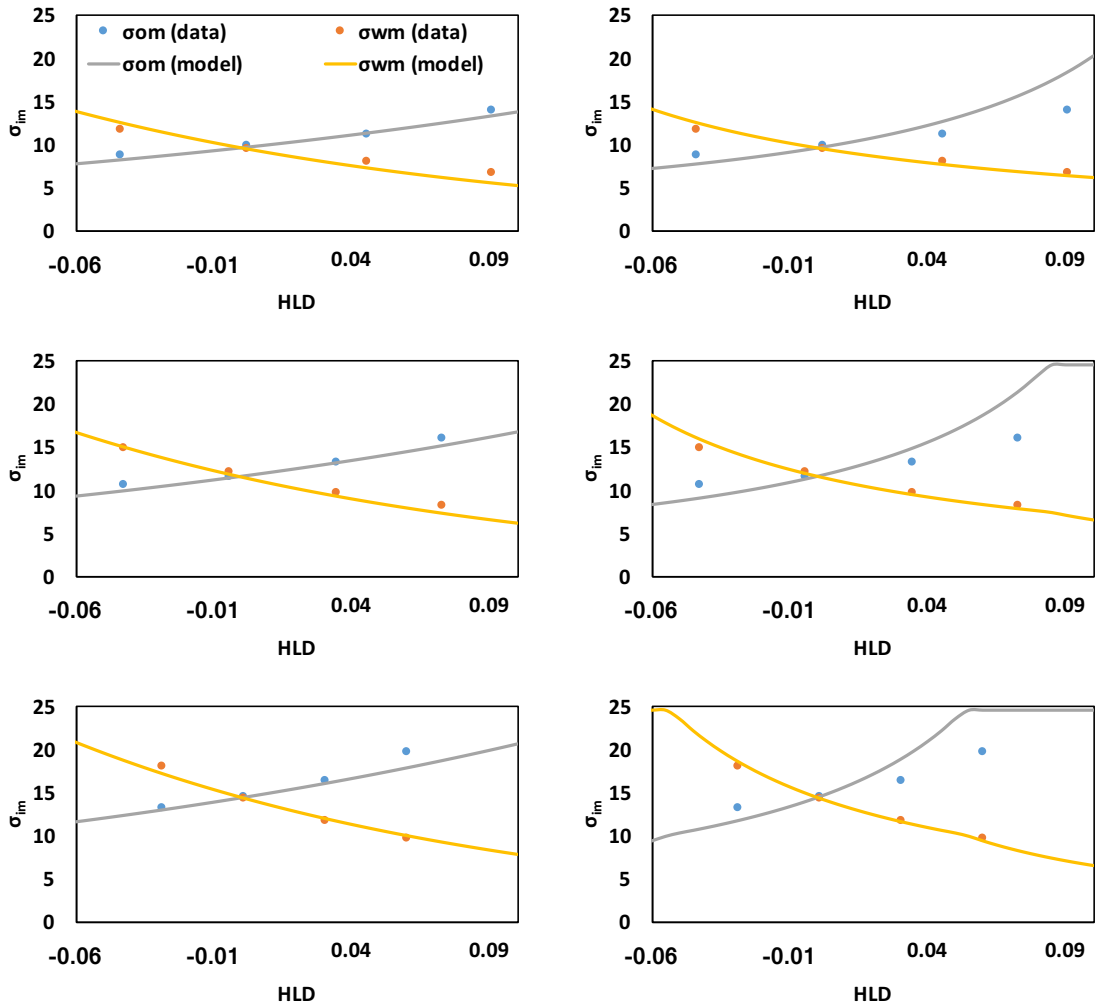

Figure 5-3. Solubilization ratio experimental data, and comparison to CP (left) and *HLD-NAC* (right) EoS model results. The models were tuned to the 50 bar data (top), and predictions are shown for all other cases: 150 bar (middle), and 250 bar (bottom). Experimental data from Austad and Strand (1996).

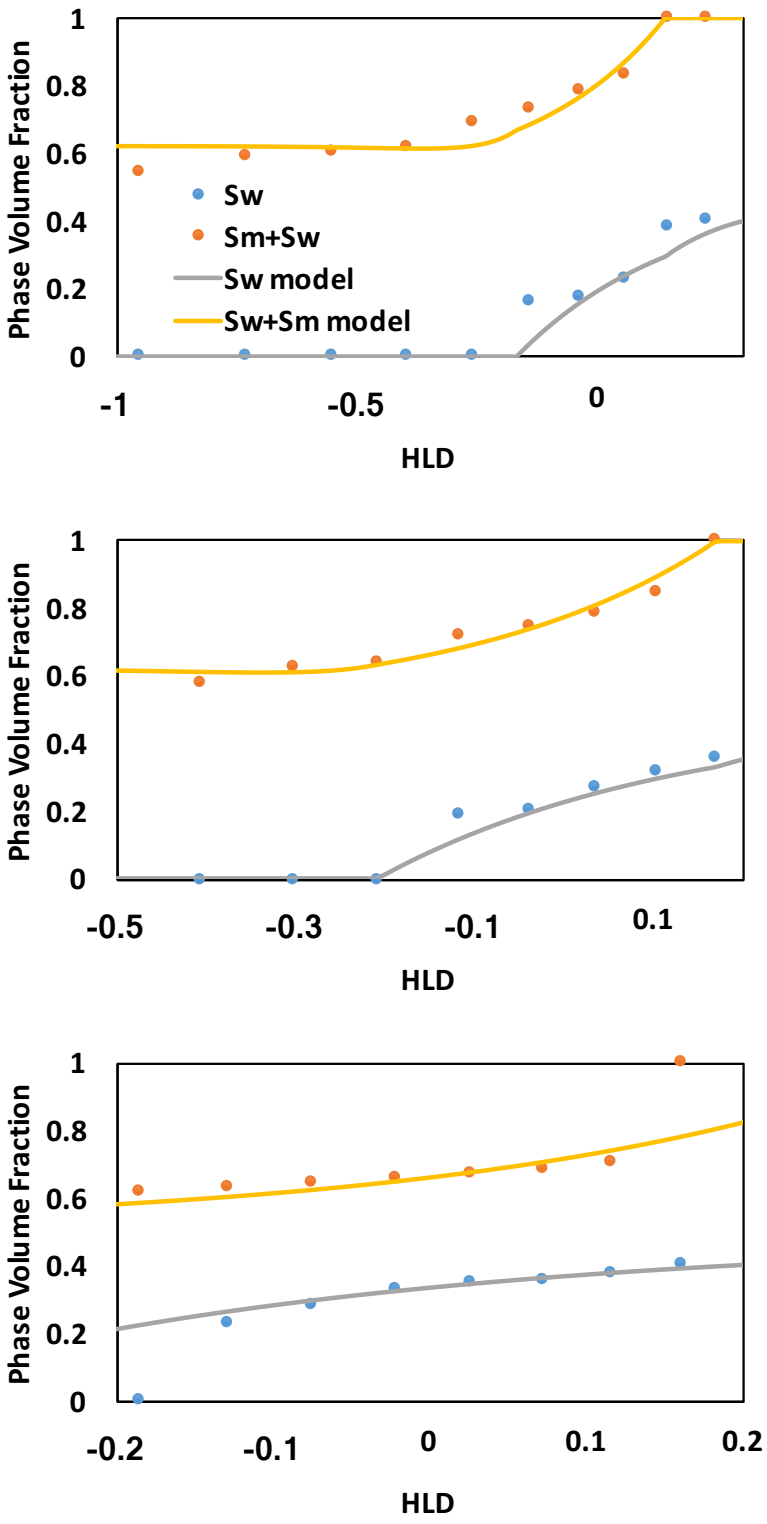

Figure 5-4. Phase behavior experimental data, and CP EoS model results for a salinity scan using octane (top), decane (middle), and dodecane (bottom). The model was tuned using the decane data, and predicted the results for octane and dodecane. Experimental data from Roshanfekr (2010).

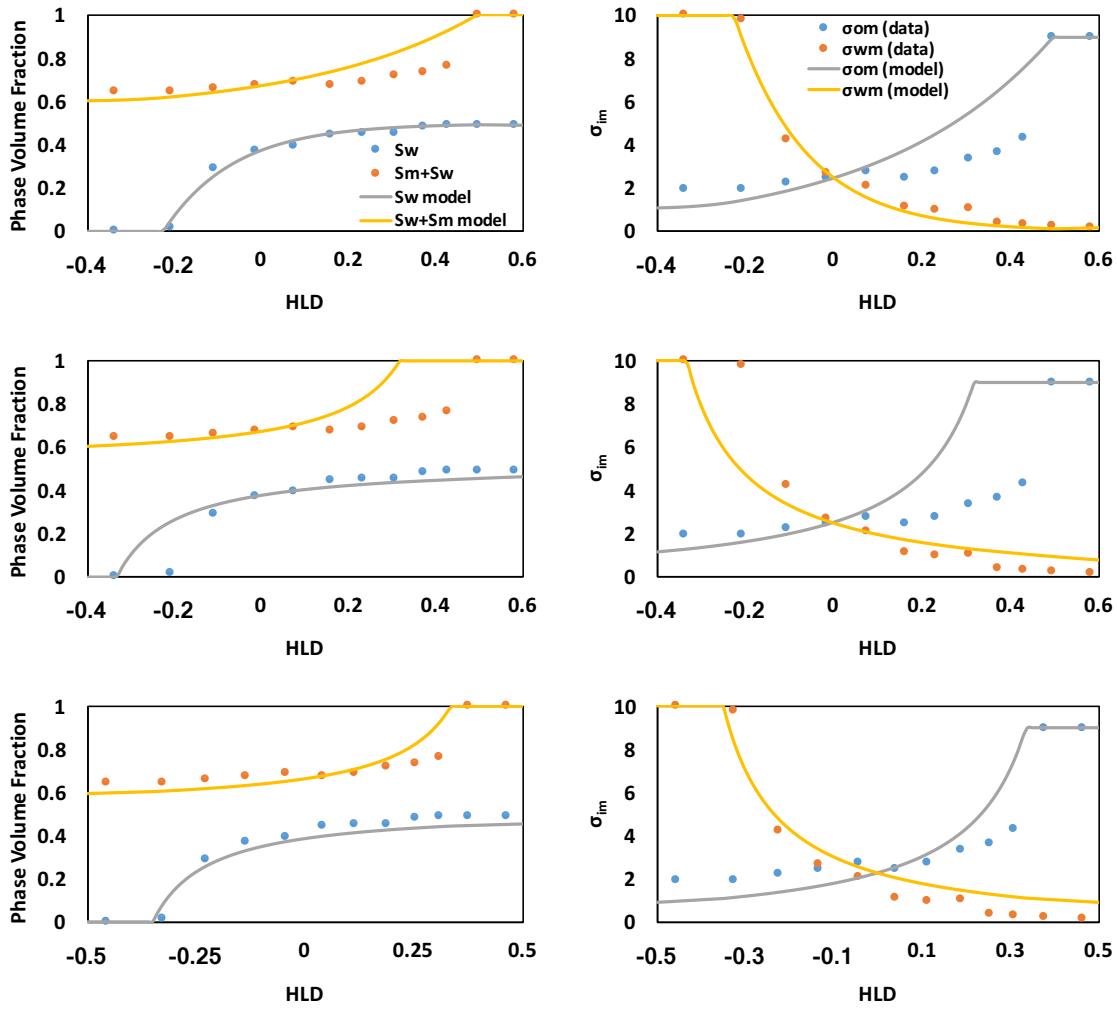

Figure 5-5. Phase volume fractions (left) and solubilization ratios (right) from experimental data and CP EoS model tuned results (top), HLD-*NAC* EoS model tuned results preserving optimum condition (middle), and HLD-*NAC* EoS model tuned results preserving phase boundaries (bottom) for a salinity scan. Experimental data from Bennett et al. (1981).

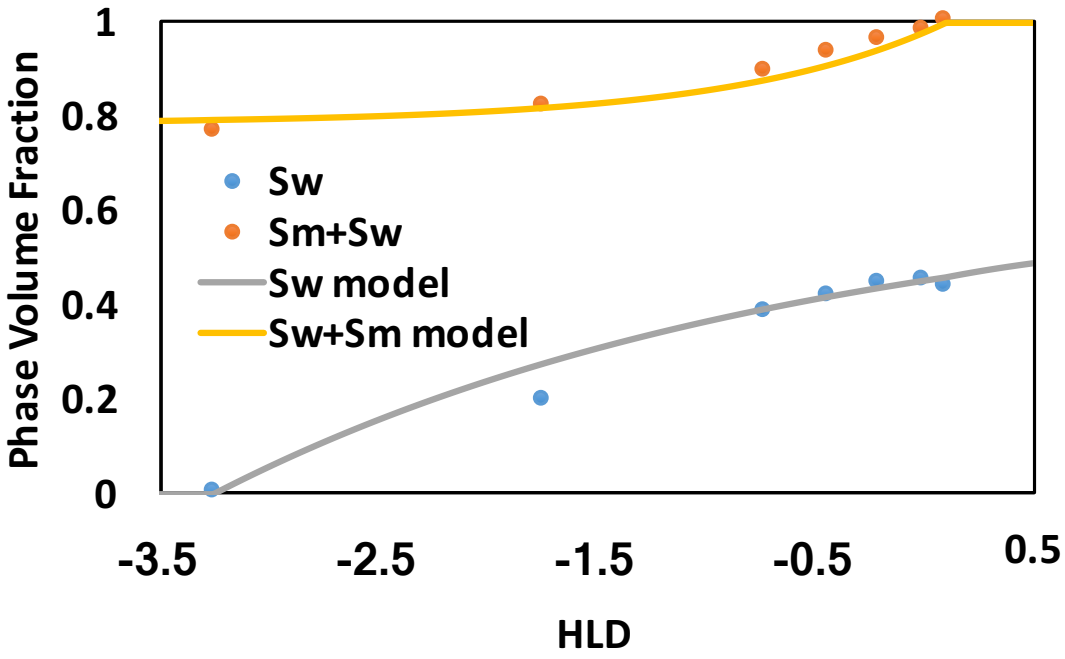

Figure 5-6. Phase behavior experimental data compared to the CP EoS model tuned results for a salinity scan, tuned on phase transition boundaries. Experimental data from Xiren and Shutang (1988).

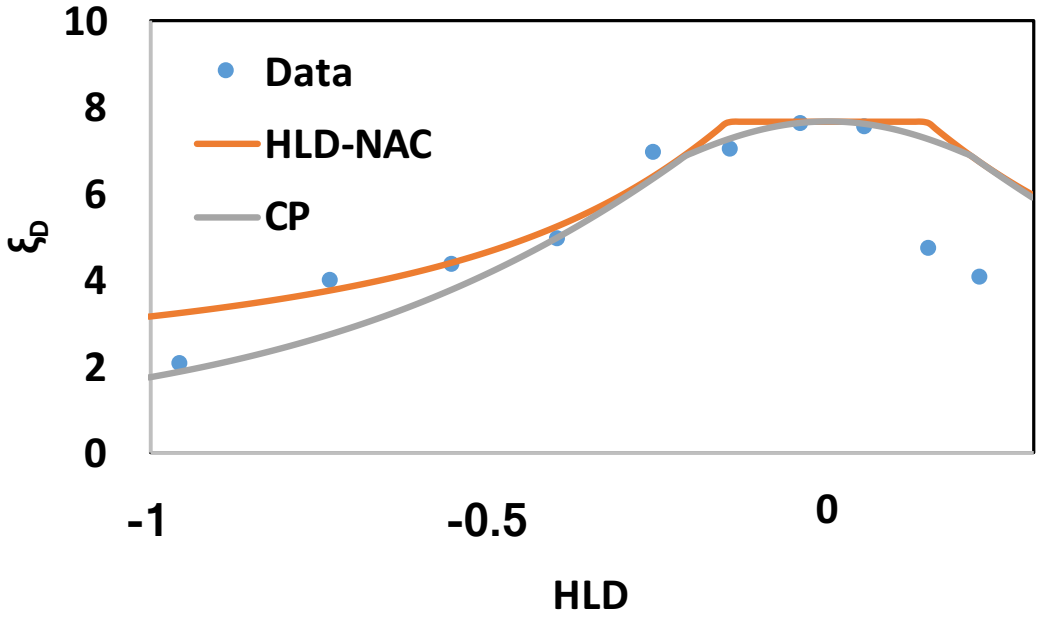

Figure 5-7. Dimensionless correlation length data and results of CP and HLD-*NAC* EoS models. Experimental data from Roshanfekr (2010).

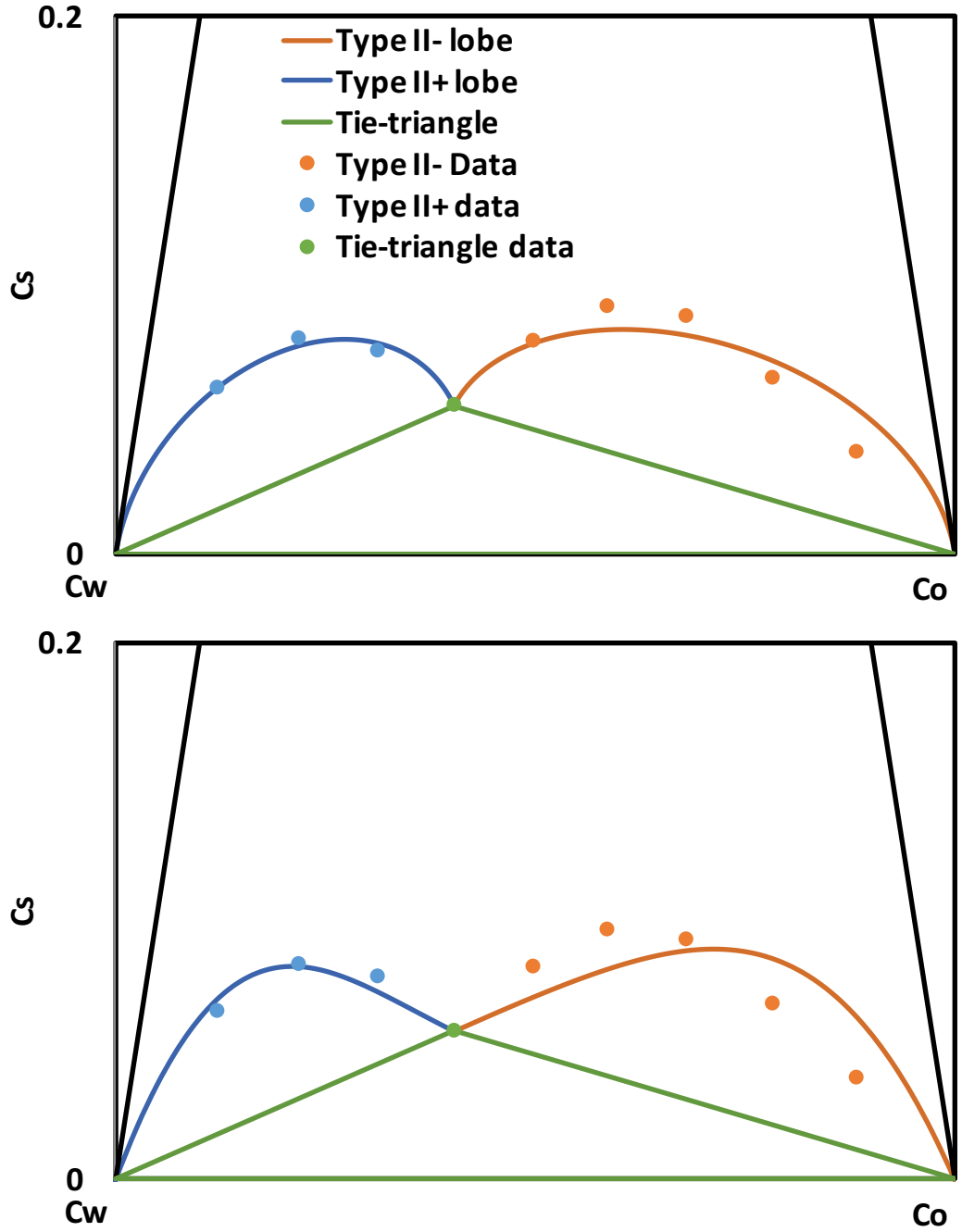

Figure 5-8. Ternary experimental data, and CP EoS model (assuming pure excess phases) tuned results (top) and HLD-*NAC* EoS model tuned results (bottom) for a composition scan using decane at 40°C for a fixed HLD. Experimental data from Lekkerkerker et al. (1996).

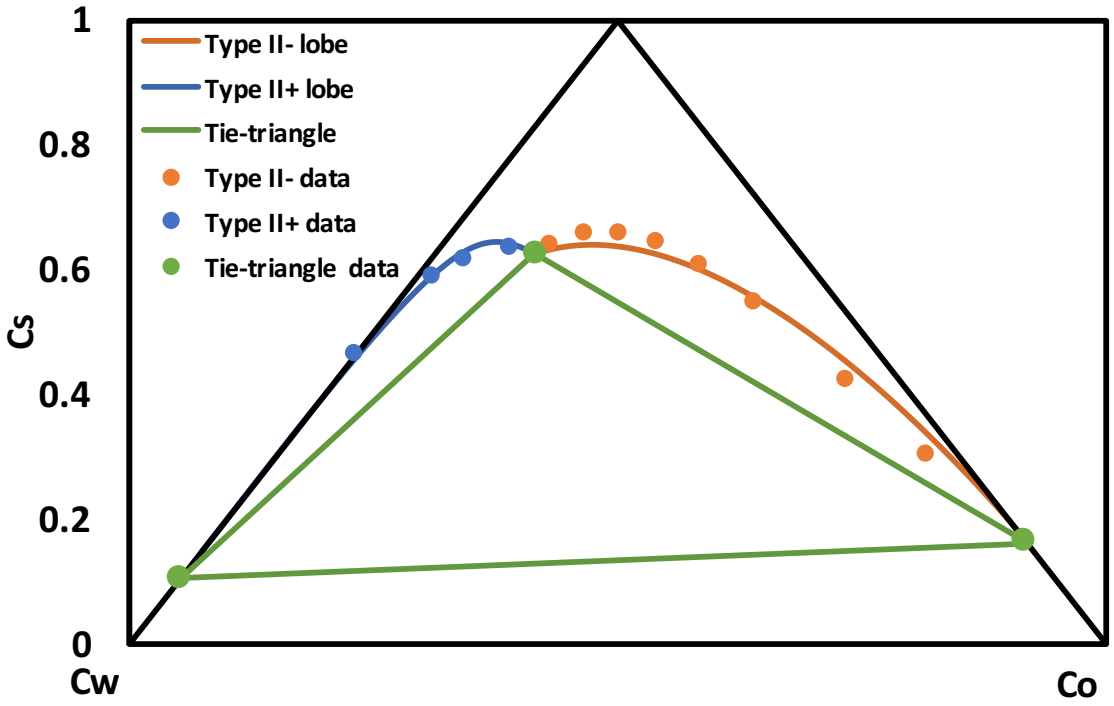

Figure 5-9. Ternary experimental data, and CP EoS model (with impure excess phases) tuned results for a composition scan using dodecane at 52°C for a fixed HLD. Experimental data from Burauer et al. (1999).

Chapter 6

Partition Coefficient Relations for Improved Equation-of-State Description of Microemulsion Phase Behavior

This chapter presents a novel way to estimate partitioning of surfactant from the microemulsion into both excess phases, as well as the oil and water partitioning between the microemulsion into the corresponding excess phase. Mathematical development of the surfactant partitioning coefficients in terms of HLD is presented first, and then using a similar argument the approach is extended for oil and water partitioning. These coefficients are then calculated and correlated to HLD for a number of experiments. Based on that correlation, a method is presented that allows for a complete phase behavior description based on K-values, including the removal of the pure excess assumption using the recently developed CP phase behavior model. These results could also be potentially used in other equations-of-state, such as the HLD-NAC improved approach by Khorsandi and Johns (2016).

6.1 Methodology

For a ternary system, there are six independent K-values to determine the phase compositions of a three-phase region, while there are only three independent K-values for a two-phase region. If oil is assumed to not exist in the excess water phase, and water is absent from the excess oil phase, then there are only four

independent K-values describing the three-phase region, and two independent K-values in the two-phase regions. For example, we could select the following four independent K-values to represent the three-phase region: $K_{wm}^{s} = C_{sw}/C_{sm}$, $K_{om}^{s} = C_{so}/C_{sm}$, $K_{mo}^{o} = C_{om}/C_{oo}$, and $K_{mw}^{w} = C_{wm}/C_{ww}$, where the subscripts in the volumetric concentrations (C_{ij}) indicate the component *i* first and phase *j* next. Two of these K-value expressions can be simplified since there is only surfactant and one of the other components (oil or water) in the excess phases. That is, $K_{mo}^{o} = C_{om}/(1 - C_{so})$ and $K_{mw}^{w} = C_{wm}/(1 - C_{sw})$.

Salager et al. (2000) introduced the hydrophilic-lipophilic deviation (HLD), which is the dimensionless free energy of transfer of a surfactant molecule from the oil phase to the water phase. The change in HLD is related to the change in surfactant partitioning between the oil and water excess phases; therefore, after an appropriate integration, HLD can be expressed as follows,

$$HLD - HLD_{ref} = ln\left(\frac{K_{ow}^{s}}{K_{ow,ref}^{s}}\right), \qquad (6-1)$$

where $K_{ow}^{s} = K_{om}^{s}/K_{wm}^{s}$. HLD is a state function (Salager et al., 2000), and as such any change in HLD owing to changes in N independent formulation variables X_i can be expressed by,

$$dHLD = \sum_{i=1}^{N}\left(\frac{\partial HLD}{\partial X_i}\right)_{X_k \neq X_i} dX_i. \qquad (6-2)$$

Changes in HLD can be obtained by integration of Eq. 6-2, where the optimum condition (i.e. $HLD_{ref} = 0$) is a convenient reference state.

HLD, like other state functions in thermodynamics, is useful because it provides a convenient way to present experimental results compared to a certain reference state (typically optimum). Its definition does not provide new information, similar to say the definition of enthalpy. The definition of HLD and its usefulness comes from the observed experimental results that the partial derivatives in Eq. 6-2 are relatively constant over the range of interest. Thus, it is easy to integrate Eq. 6-2 and assign a reference state of interest (i.e. optimum).

The number of independent parameters *N* in Eq. 6-2 is restricted by the Gibbs phase rule. Assuming no chemical reactions and five components (surfactant, two brine components, and two oil components), the Gibbs phase rule gives a degree of freedom of four for the three-phase region. This means that HLD can be taken as a function of salinity, oil EACN, T and P. The brine components could consist of two different salinities (e.g. brine and distilled water), while the oil could be a mixture of two different hydrocarbons (e.g. methane and decane). Other components could also be added as needed. If we allow for two surfactant components, then the degree of freedom increases by one and HLD would also be a function of a surfactant parameter, such as the EO chain length.

The chemical potential of component i in phase j is given by,

$$\mu_{ij} = \mu_i^{\circ} + RTln\left(\bar{\gamma}_{ij}C_{ij}\right) \qquad (6-3)$$

where μ_{ij} and C_{ij} are the chemical potential and the volumetric composition of component i in phase j; μ_i° is the reference chemical potential for pure component i. For convenience, we defined $\bar{\gamma}_{ij} = \gamma_{ij}\rho_{ij}/\rho_j$, with γ_{ij} and ρ_{ij} being the chemical potential and molar density of component i in phase j, and ρ_j is the molar density of phase j.

Optimum condition in enhanced oil recovery is strictly defined at the point of equal oil-microemulsion and microemulsion-water interfacial tensions (IFT). Some also assign equal water and oil solubilities in the microemulsion phase as the definition of optimum, but this is not generally correct. Huh's correlation (Huh, 1979) would indicate the two definitions are equivalent, but there are special surfactant systems where there would be one scaling constant for the oil-microemulsion IFT and a different one for the microemulsion-water IFT, therefore yielding different oil and water solubilities at optimum. In phase behavior, IFT can be understood from the point view of tie-line length through the phase compositions, and also phase densities (e.g. critical points are defined at the point of tie-line lengths becoming zero, corresponding to vanishing IFT).

Another definition of optimum is typically that the surfactant partitioning between the excess phase is 1.0. This is also not necessary. Figure 6-1 (top) illustrates how for the assumption of $C_{wo} = C_{ow} = 0$, the tie-lines joining the microemulsion and the excess phases become of equal length only for equal surfactant partitioning between the oil and water phases. For cases where the excess phases have all three components with significantly different

compositions, surfactant partitioning does not need to be equal at optimum, as shown in Fig. 6-1 (bottom), and discussed by Salager et al. (2000). Yet, the tie-line lengths (and potentially the corresponding IFTs) are equal.

In this chapter, we assume that $C_{wo} = C_{ow} = 0$, which corresponds to the assumption of immiscibility. We further assume that the surfactant partitioning into the excess phases is small. Both of these assumptions therefore allow for the optimum to be defined reasonably where $HLD_{ref} = 0$ at $K_{ow}^{s} = 1.0$. This implies that the surfactants used are high quality, in that most of the surfactant partitions into the microemulsion phase. Considering this surfactant partitioning condition at optimum, the expression for HLD is simplified to,

$$HLD = ln(K_{ow}^{s}). \tag{6-4}$$

Thus, from Eqs. 6-3 and 6-4, we can also write at equilibrium,

$$HLD = ln(K_{ow}^{s}) = ln\left(\frac{\bar{\gamma}_{sw}}{\bar{\gamma}_{so}}\right), \tag{6-5}$$

Further, for each excess phase we have,

$$\begin{aligned} ln(\bar{\gamma}_{so}C_{so}) &= ln(\bar{\gamma}_{sm}C_{sm}) \\ ln(\bar{\gamma}_{sw}C_{sw}) &= ln(\bar{\gamma}_{sm}C_{sm}). \end{aligned} \tag{6-6}$$

By combining these expressions with the definition of HLD in Eq. 6-5, we obtain,

$$K_{om}^{s} = \frac{\bar{\gamma}_{sm}}{\bar{\gamma}_{sw}} e^{HLD}$$
$$K_{wm}^{s} = \frac{\bar{\gamma}_{sm}}{\bar{\gamma}_{so}} e^{-HLD}. \qquad (6-7)$$

Equation 6-7 suggests that K-values may vary exponentially if the coefficient group in front of the exponential terms is relatively constant. Thus, we propose the following empirical form for K_{om}^{s} and K_{wm}^{s},

$$K_{om}^{s} = \Omega_{om}^{s} e^{\Omega_o HLD}$$
$$K_{wm}^{s} = \Omega_{wm}^{s} e^{-\Omega_w HLD}, \qquad (6-8)$$

where Ω_o and Ω_w are phase behavior parameters that control how the oil and water solubilization ratios change with HLD in the type III region (see Appendix to this Chapter for the derivation of Eq. 6-8). Further, Ω_{om}^{s} and Ω_{wm}^{s} are taken as dimensionless groups that determine the surfactant concentration in the corresponding excess phases.

Two additional K-values must also be estimated for the three-phase region (K_{mo}^{o} and K_{mw}^{w}). Following a similar procedure, and with $\mu_{oo} = \mu_{om}$ and $\mu_{ww} = \mu_{wm}$ at equilibrium,

$$K_{mo}^{o} = \frac{\bar{\gamma}_{oo}}{\bar{\gamma}_{om}} = \Omega_{mo}^{o}$$
$$K_{mw}^{w} = \frac{\bar{\gamma}_{ww}}{\bar{\gamma}_{wm}} = \Omega_{mw}^{w}, \qquad (6-9)$$

where $\Omega_{mo}^{o} = \bar{\gamma}_{oo}/\bar{\gamma}_{om}$ and $\Omega_{mw}^{w} = \bar{\gamma}_{ww}/\bar{\gamma}_{wm}$ are defined as the relevant dimensionless groups. In Eq. 6-9 we assume that the dimensionless groups are not constant since HLD is not present here. Trends in the activity groups Ω_{mo}^{o} and Ω_{mw}^{w} can be observed from experimental data or an existing microemulsion phase behavior model from which the compositional and HLD dependence is specified. We use the former approach, relying on the CP model.

6.2 Results and discussion

In this section, partitioning data are used to show how the parameters in the proposed empirical model for K-values vary. First, surfactant partitioning data between oil and water excess phases are given for a variety of formulation variables. Surfactant partitioning between the microemulsion and excess phases is also analyzed with respect to similar formulation variables to understand the behavior of the surfactant partition with HLD. Finally, these partitioning relations are combined with the CP phase behavior model to predict phase behavior for all compositions within the ternary diagram.

6.2.1. Surfactant partition between oil and water excess phases

We first consider several sets of experimental data for surfactant partitioning between the excess phases as a function of hydrophilic and lipophilic chain lengths, and temperature. Equations 6-3 and 6-6 are used to calculate changes in the partitioning coefficient with HLD, where the reference value of HLD is zero and the K-value is assumed to be 1.0 at optimum. The partial derivative of HLD with respect to a given formulation variable in Eq. 6-2 is constant and equal to the slope of the logarithm of surfactant partition coefficient versus the formulation variable.

6.2.1.1. Effect of hydrophilic chain length (HCL)

The partitioning between oil and water of an ethoxylated octylphenol surfactant as a function of the degree of ethoxylation for different mixtures of tetradecane and octylbenzene (C8B) corresponding to the three-phase region is shown in Fig. 6-2 (top), as presented by Graciaa et al. (2006). As the fraction of C8B in the oil increases (progressing from pure tetradecane to pure C8B), the hydrophobicity of the formulation increases due to the decrease of the *EACN* from 14 to about 8. The optimum *HCL* ranges from 8.2 for pure tetradecane to 12.6 for pure C8B. The change of HLD with *HCL* increases as the *EACN* decreases, ranging from -0.97 to -0.84. To avoid bias in the results, the K-values were calculated using a single reference state for all experiments (i.e. $HCL_{ref} = 8.2$ and $EACN_{ref} = 14$ for HLD, which corresponds to the pure tetradecane system). HLD can therefore be written as a function of only two varying parameters (i.e., all other required

parameters to determine the intensive state of the system according to the Gibbs phase rule are fixed):

$$HLD = \left(\frac{\partial HLD}{\partial HCL}\right)_{EACN}\left(HCL - HCL_{ref}\right) + \left(\frac{\partial HLD}{\partial EACN}\right)_{HCL}\left(EACN - EACN_{ref}\right). \quad (6-10)$$

In the results that follow, we assumed the change of HLD with *HCL* is approximately constant with *EACN* and equal to that of tetradecane, and the change in HLD with *EACN* is approximately constant with *HCL* and equal to that at $HCL = 2$. This assumption also makes the plots less biased. Figure 6-2 (bottom) shows the K-values when plotted as a function of HLD from Eq. 6-10, which is defined using a single reference value as explained above. Figure 6-2 (bottom) shows excellent agreement between the calculated and measured K-values when scaled by HLD. That is, the curves for each different experiment nearly collapse onto one curve.

The partitioning between oil and water of an ethoxylated nonylphenol surfactant as a function of the degree of ethoxylation, for different benzene content corresponding to the three-phase region is given in Fig. 6-3 (top), as presented by Ysambertt et al. (1997). The increase in benzene content had a significant impact on increasing the hydrophobicity of the formulation. The range of the optimum *HCL* went from 8.9 for pure n-heptane oil to 27.7 for oil with 22.7% benzene content. The change of HLD with *HCL* is clearly impacted by

benzene content, changing from -1.03 for pure n-heptane to -0.33 for oil with 22.7% benzene. For this system, both the optimum *HCL* and the change of HLD with *HCL* vary significantly with benzene content. The rescaling by HLD using Eq. 6-10 yielded unsatisfactory results. Alternatively, we define a linear correlation for the change of HLD with *HCL* as a function of *EACN*, and a quadratic correlation for the optimum *HCL* as a function of *EACN*. Using this information, we are able to calculate HLD for all systems considered following Eq. 6-11.

$$HLD = \left(\frac{\partial HLD}{\partial HCL}\right)_{EACN} \left(HCL - HCL_{ref}\right). \qquad (6-11)$$

The combined results from Eq. 6-11 are presented in Fig. 6-3 (bottom). As shown, the calculated HLD is very close to the original definition from Eq. 6-5. The result in Eq. 6-11 is analogous to that of Anton et al. (2008), Salager et al. (2014) and Delgado-Linares et al. (2016), but here we recognize the significance of the reference state and the partial derivative with HLD.

6.2.1.2. Effect of lipophilic chain length (LCL)

Similar to the previous section, it is convenient to define the lipophilic chain length (*LCL*), as the common formulation variable. Figure 6-4 (top) shows the surfactant partitioning between oil and water of fatty carboxylic acids (FA) as a function of the alkyl chain length, for different alcohol chain length (*ACL*) using the same 4% concentration corresponding to the three-phase region, as presented by Marquez et al. (2012). The optimum *LCL* for the formulation without

alcohol is -1.1, which means optimum is not obtained with FA owing to its strong lipophilicity. However, the use of 4% alcohol is sufficient to shift the formulations to a more hydrophilic state, where optimum conditions can be achieved.

For this case, the optimum *LCL* increased with increasing length of the alcohol chain length, ranging from 10.2 to 18.2. The change of HLD with *LCL* increases with decreasing alcohol chain length ranging from 0.32 to 0.51. Following a similar approach as in the previous section, we calculate HLD following Eq. 6-12, accounting for changes in *LCL* as well as *ACL* using a single reference state.

$$HLD = \left(\frac{\partial HLD}{\partial LCL}\right)_{ACL}\left(LCL - LCL_{ref}\right) + \left(\frac{\partial HLD}{\partial ACL}\right)_{LCL}\left(ACL - ACL_{ref}\right). \quad (6-12)$$

Here, $LCL_{ref} = 10.2$, which corresponds to $ACL_{ref} = 2$, the change of HLD with *LCL* is defined as that of $ACL = 2$, while the change of HLD with *ACL* is defined as that of $LCL = 8$. The results with Eq. 6-12 are excellent as shown in Fig. 6-4 (bottom), with all data nearly collapsing onto one curve.

6.2.1.3. Effect of temperature

The surfactant partitioning between oil and water excess phases of an ethoxylated octylphenol surfactant as a function of temperature, for different degrees of ethoxylation corresponding to the three-phase region is shown in Fig.

6-5 (top), as presented by Salager et al. (2000). All of the formulations presented have a strong lipophilic behavior, with very pronounced oil partitioning, which decreases with degree of ethoxylation. In addition, the change of HLD with *T* is small for all the formulations studied, but its impact increases some with degree of ethoxylation from about 0.02 to 0.06. Therefore, the optimum temperatures for these formulations range from -63K to 271K. Following a similar approach as previously presented, we calculate HLD using Eq. 6-13, which accounts for simultaneous changes in both *T* and *HCL* using a single reference state.

$$HLD = \left(\frac{\partial HLD}{\partial T}\right)_{HCL}\left(T - T_{ref}\right) + \left(\frac{\partial HLD}{\partial HCL}\right)_{T}\left(HCL - HCL_{ref}\right). \qquad (6-13)$$

For this case $T_{ref} = -63.4K$, which corresponds to $HCL_{ref} = 1$, the change of HLD with *T* is defined at $HCL = 1$, while the change of HLD with *HCL* is defined where $T = 307.5K$. The combined results are presented versus HLD in Fig. 6-5 (bottom), showing excellent agreement.

6.2.2. Surfactant partition between microemulsion and excess phases

We now examine the behavior of the surfactant partitioning coefficients between the oil and microemulsion phases and between the microemulsion and water phases as a function of HLD for different experimental data. The data is again rescaled with HLD.

Figure 6-6 (top) shows how surfactant partitioning between the oil and microemulsion phases changes with HLD using $\Omega_{om}^{s} = 0.2$ and $\Omega_{o} = 0.8$. Figure

6-6 (bottom) shows surfactant partitioning between the microemulsion and water phases with changes in HLD using $\Omega_{wm}^{s} = 0.2$ and $\Omega_{w} = 1.5$ for a petroleum sulfonate (TRS 10-410) surfactant based data from Chan and Shah (1979).

Figure 6-7 (top) shows how the surfactant partitioning between the oil and microemulsion phases changes with HLD for a very pure alkylbenzene sulfonate surfactant using parameters of $\Omega_{om}^{s} = 0.2$ and $\Omega_{o} = 0.3$, and Fig. 6-7 (bottom) shows how the surfactant partitioning between the microemulsion and water phases changes with HLD for a technical grade alkylbenzene sulfonate surfactant using $\Omega_{wm}^{s} = 0.02$ and $\Omega_{w} = 2.9$, based on the data from Salager et al. (2013A).

Figure 6-8 (top) shows how the surfactant partitioning between the oil and microemulsion phases changes with HLD for a petroleum sulfonate (TRS 10-80) surfactant with 0.74% i-pentanol concentration using parameters of $\Omega_{om}^{s} = 11.7$ and $\Omega_{o} = 0.2$. Figure 6-8 (bottom) shows how the surfactant partitioning between the water and microemulsion excess phases changes with HLD for the same surfactant system without any alcohol content using parameters of $\Omega_{wm}^{s} = 5.0$ and $\Omega_{w} = 0.09$ and the data from Wade et al. (1978).

Finally, Fig. 6-9 (top) shows how the surfactant partitioning between oil and microemulsion phases changes with HLD with $\Omega_{om}^{s} = 0.7$ and $\Omega_{o} = 1.7$, while Fig. 6-9 (bottom) shows how the surfactant partitioning between the microemulsion and water phases changes with HLD using parameters of $\Omega_{wm}^{s} = 0.6$ and $\Omega_{w} = 0.5$ and experimental data for an ethoxylated nonylphenol mixture from Salager et al. (1995).

For all systems studied in this section, both surfactant partitioning coefficients showed an excellent correlation with HLD using Eq. 6-8. Thus, the K-values from Eq. 6-8 could be used as a good estimate to determine surfactant partitioning between the microemulsion and both excess phases. The tuned Ω_o and Ω_w will be used in Sec. 6.2.3 to predict microemulsion phase behavior using the CP model.

6.2.3. Oil and water component partition between microemulsion and excess phases

In this section, we explore the behavior of oil and water partitioning between the microemulsion and excess phases as calculated by the empirical relations in Eq. 6-9. First, we present an approach where only phase behavior data is considered, and then we consider a case where both surfactant partitioning and phase behavior data are available. Further, we show how for the case considered the surfactant parameters can be used to accurately predict microemulsion phase behavior. We then combine surfactant partitioning with the CP microemulsion phase behavior model of Torrealba and Johns (2017) and show representative ternary diagrams for different HLD conditions.

Chan and Shah (1979) presented the microemulsion phase behavior for an oil composition scan for the surfactant TRS 10-410. For illustration purposes, we calculate the microemulsion composition by assuming all the surfactant is present in the microemulsion phase. Therefore, we can tune on the oil and water solubilization ratio in the type III region using the CP model with parameters of

$\Omega_o = 2.0$ and $\Omega_w = 1.2$ and an optimum solubilization ratio of 1.4. The experimental and model results are shown in Fig. 6-10.

Surfactant partitioning data was also available for the same system over the same HLD range, as is shown in Fig. 6-6. By using the surfactant partitioning data, we recalculate the oil and water partitioning between the microemulsion and excess phases. Further, by using the Ω_o and Ω_w parameters from tuning the surfactant partitioning data we successfully predict the oil and water partitioning using the model, as shown in Fig. 6-11.

By combining the parameters defined from tuning the surfactant partitioning data from Chan and Shah (1979) and using the extension of the CP phase behavior model, we are able to predict the entire compositional phase behavior for all possible HLD conditions. Figure 6-12 shows this exercise for affinity conditions in the near optimum region at $HLD = -0.5$ (top), $HLD = 0$ (middle) and $HLD = 0.5$ (bottom), and Fig. 6-13 shows affinity conditions away from optimum conditions for a type II- environment at $HLD = -2.1$ (top), and a type II+ environment at $HLD = 2.1$ (bottom). Relevant model parameters for the definition of the CP model EoS are listed in Table 6-1.

The cases with HLD away from optimum conditions show an important property for the coupled phase behavior-surfactant partitioning model, which is that for sufficient surfactant hydrophilicity (i.e. $HLD \ll 0$), the surfactant concentration in the oil excess phase tends to zero and the surfactant concentration in the water excess phase tends to a maximum value given by $C_{sw}^{max} = \Omega_{wm}^{s}/\sigma^{*}$, which defines a limiting tie-line as shown in Fig. 6-13 (top).

Similarly, for sufficient surfactant lipophilicity (i.e. $HLD \gg 0$), the surfactant concentration in the water excess phase tends to zero while the surfactant concentration in the oil excess phase tends to a maximum value given by $C_{so}^{max} = \Omega_{om}^{s}/\sigma^{*}$, defining a limiting tie-line as shown in Fig. 6-13 (bottom).

Burauer et al. (1999) studied the phase behavior of an ethylene glycol monobutyl ether (C_4E_1) surfactant, water, and n-dodecane at different temperatures. Figure 6-14 shows compositional data for 42°C (top), 52°C (middle), and 62°C (bottom) and the accompanying results using the CP EoS phase behavior model for impure excess phases. The CP EoS model is tuned to the data at 52°C and all other temperatures are predicted. The surfactant partitioning model is defined based on the data at 52°C, with $\Omega_{om}^{s} = 0.37$ and $\Omega_{wm}^{s} = 0.09$. The results show the capacity of the CP EoS model to accurately predict complex phase behavior in the presence of surfactant partitioning away from tuned conditions.

6.3 Summary

A useful approach for capturing surfactant partitioning as a function of HLD is presented and coupled with a microemulsion phase behavior model. Some key findings are:

- The HLD concept is shown to be applicable when multiple formulation variables change simultaneously, and a single reference state is used. Experimental data with different changing formulation variables collapse onto one curve as a function of HLD.

- Key dimensionless groups are identified as a function of activities, which allow for a simplified description of surfactant partitioning coefficients as a function of HLD.
- The oil and water partitioning coefficients between the microemulsion and corresponding excess phases are given as a function of HLD, which allows for the identification of dimensionless groups. These partitioning coefficients are related to the CP model of Torrealba and Johns (2017) in the cases of pure excess phases and surfactant partitioning into the excess phases.
- By combining the CP model with the surfactant partitioning model, we are able to predict the entire ternary diagram for all possible HLD conditions, removing the assumption of pure excess phases.

6.4 Appendix

The oil and water solubilization ratios in the Type III region can be expressed as (Torrealba and Johns, 2017B),

$$\sigma_o = \sigma^* e^{\Omega_o^{III} HLD}$$
$$\sigma_w = \sigma^* e^{-\Omega_w^{III} HLD}. \qquad (6-A1)$$

where Ω_o^{III} and Ω_w^{III} are parameters that control the change in solubilization ratio with HLD in the Type III region, and σ^* is the solubilization ratio at optimum conditions. We can write the surfactant concentration in the microemulsion phase in terms of the oil and water solubilization ratios as,

$$C_{sm} = \frac{1}{1 + \sigma_o + \sigma_w} = \frac{1}{1 + \sigma^*\left(e^{\Omega_o^{III} HLD} + e^{-\Omega_w^{III} HLD}\right)}. \qquad (6 - A2)$$

Based on the exponential trends in Equation 6-A1, we propose the following form for the surfactant partitioning coefficients between the excess phases and microemulsion phase,

$$\begin{aligned} K_{om}^s &= \Omega_{om}^s e^{\Omega_o^{III} HLD} \\ K_{wm}^s &= \Omega_{wm}^s e^{-\Omega_w^{III} HLD}, \end{aligned} \qquad (6 - A3)$$

where Ω_{om}^s and Ω_{wm}^s are parameters that control the surfactant concentration in the excess phases. Combining Equations $6 - A2$ and $6 - A3$, the surfactant concentration in the excess phases can be written as,

$$\begin{aligned} C_{so} &= \frac{\Omega_{om}^s e^{\Omega_o^{III} HLD}}{1 + \sigma^*\left(e^{\Omega_o^{III} HLD} + e^{-\Omega_w^{III} HLD}\right)} \\ C_{sw} &= \frac{\Omega_{wm}^s e^{-\Omega_w^{III} HLD}}{1 + \sigma^*\left(e^{\Omega_o^{III} HLD} + e^{-\Omega_w^{III} HLD}\right)}. \end{aligned} \qquad (6 - A4)$$

At $HLD = 0$, the surfactant concentration in both excess phases is given by,

$$\begin{aligned} C_{so} &= \frac{\Omega_{om}^s}{1 + 2\sigma^*} \\ C_{sw} &= \frac{\Omega_{wm}^s}{1 + 2\sigma^*}. \end{aligned} \qquad (6 - A5)$$

If partitioning data is unavailable to directly define Ω_{om}^{s} and Ω_{wm}^{s}, the model can be simplified by assuming symmetry. Further, surfactant partitioning should relate the surfactant concentration in the microemulsion phase to the critical micelle concentration at optimum (C_s^{cmc}). From Equation $6-A5$, we satisfy this condition by setting $\Omega_{om}^{s} = \Omega_{wm}^{s} = (1+2\sigma^*)C_s^{cmc}$.

As HLD approaches ∞, the surfactant concentration in both excess phases is given by,

$$C_{so} = \frac{\Omega_{om}^{s}}{\sigma^*}$$
$$C_{sw} = 0, \qquad (6-A6)$$

which corresponds to a maximum, yet finite, surfactant concentration in the oil phase and a vanishing surfactant concentration in the water phase. Similarly, as HLD approaches $-\infty$, the surfactant concentration in both excess phases is given by,

$$C_{so} = 0$$
$$C_{sw} = \frac{\Omega_{wm}^{s}}{\sigma^*}, \qquad (6-A7)$$

corresponding to a vanishing surfactant concentration in the oil phase and a maximum, yet finite, surfactant concentration in the water phase.

The model presented here removes the simplification of having a constant critical micelle concentration for all HLD and variable water-oil ratios. From Gibbs phase rule, the intensive state for a three-component, three-phase system is determined by setting two independent variables. For example, we can set pressure and temperature, which would determine HLD based on Eq. 6-2 and σ^* based on a correlation of solubilization ratio with respect to formulation variables, as discussed by Khorsandi and Johns (2016). Note that by setting both HLD and σ^*, the concentration of surfactant into the excess phases is fully determined based on Eq. 6-A4. For both Type II- and Type II+, where we have two phases, the intensive state is determined by setting three independent variables. For example, we can set pressure and temperature (which would determine both HLD and σ^*) and a tie-line parameter (e.g. σ_w° and σ_o° for the Type II- and Type II+ environments, respectively, with $\sigma_i^\circ \equiv C_i/C_s$ and C_i being the overall composition of component i). For the two-phase regions, we ignore the dependence on σ_i°, which means we assume a constant excess phase composition for a given set of HLD and σ^*. This assumption could be lifted in a future extension of the model if we have supporting experimental data.

Table 6-1. Tuned CP EoS model parameters for all cases considered.

Data set	Ω_o^{III}	Ω_w^{III}	Ω_o^{II}	Ω_w^{II}	K_o	K_w
Chan and Shah (1979)	0.8	1.5	0.8	1.5	0.3	0.3
Burauer et al. (1999)	0.9	1.4	3.0	0.014	10	0.1

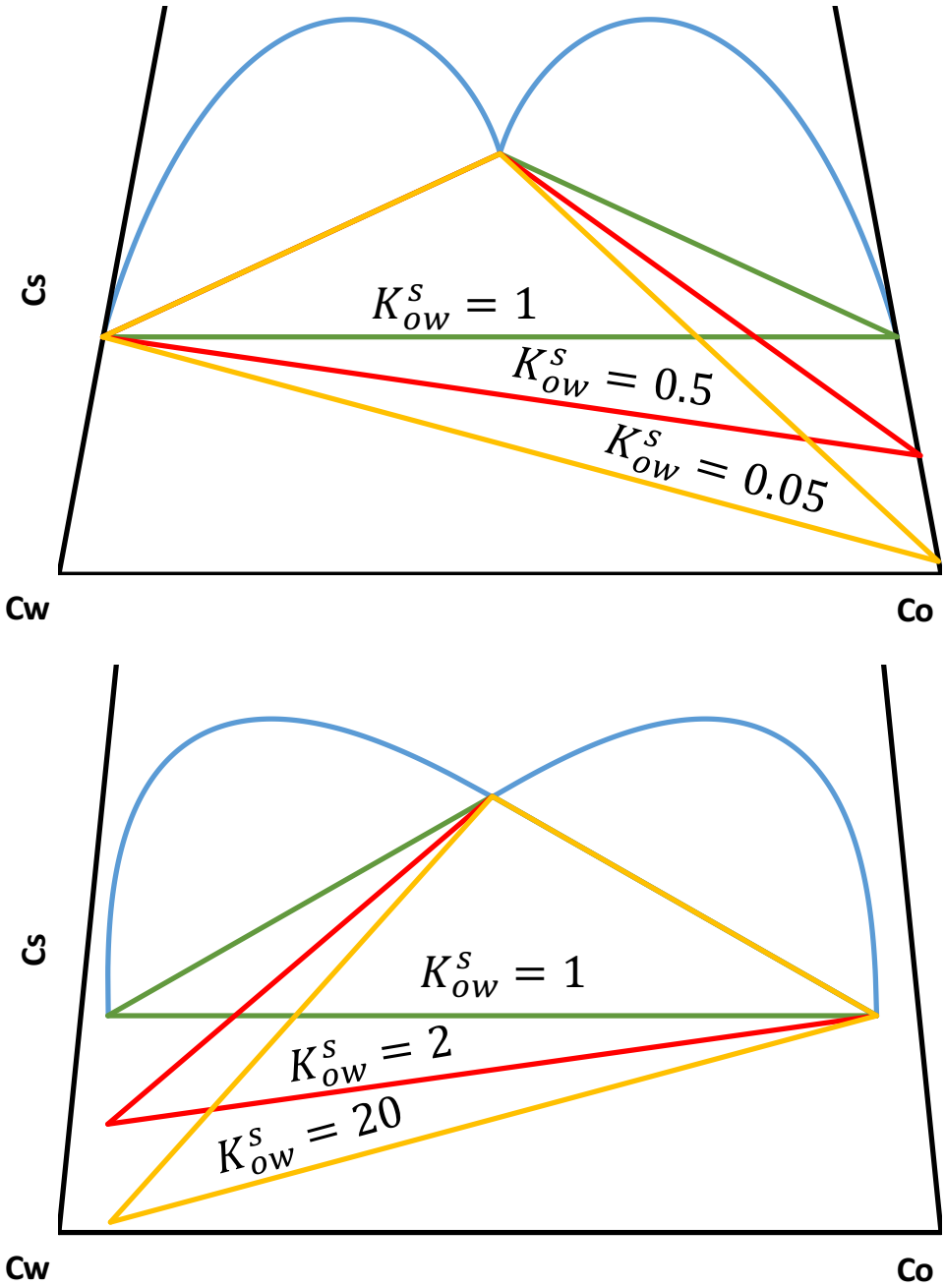

Figure 6-1. Ternary diagram (top) with three example tie-triangles (Type III environment where blue curve gives the two-phase lobes) under the assumption of $C_{wo} = C_{ow} = 0$. The classical way to express optimum corresponds to $K_{ow}^{s} = 1$, where solubilities are equal and so therefore are tie-line lengths between the microemulsion and each excess phase. This is not generally true but becomes a better approximation for pure excess phases and high-quality surfactants. Ternary diagram (bottom) showing a more general example where all three tie-triangles correspond to optimum (equal tie-line lengths), even though the water and oil solubilities are slightly different, and each tie-triangle has a different surfactant partitioning.

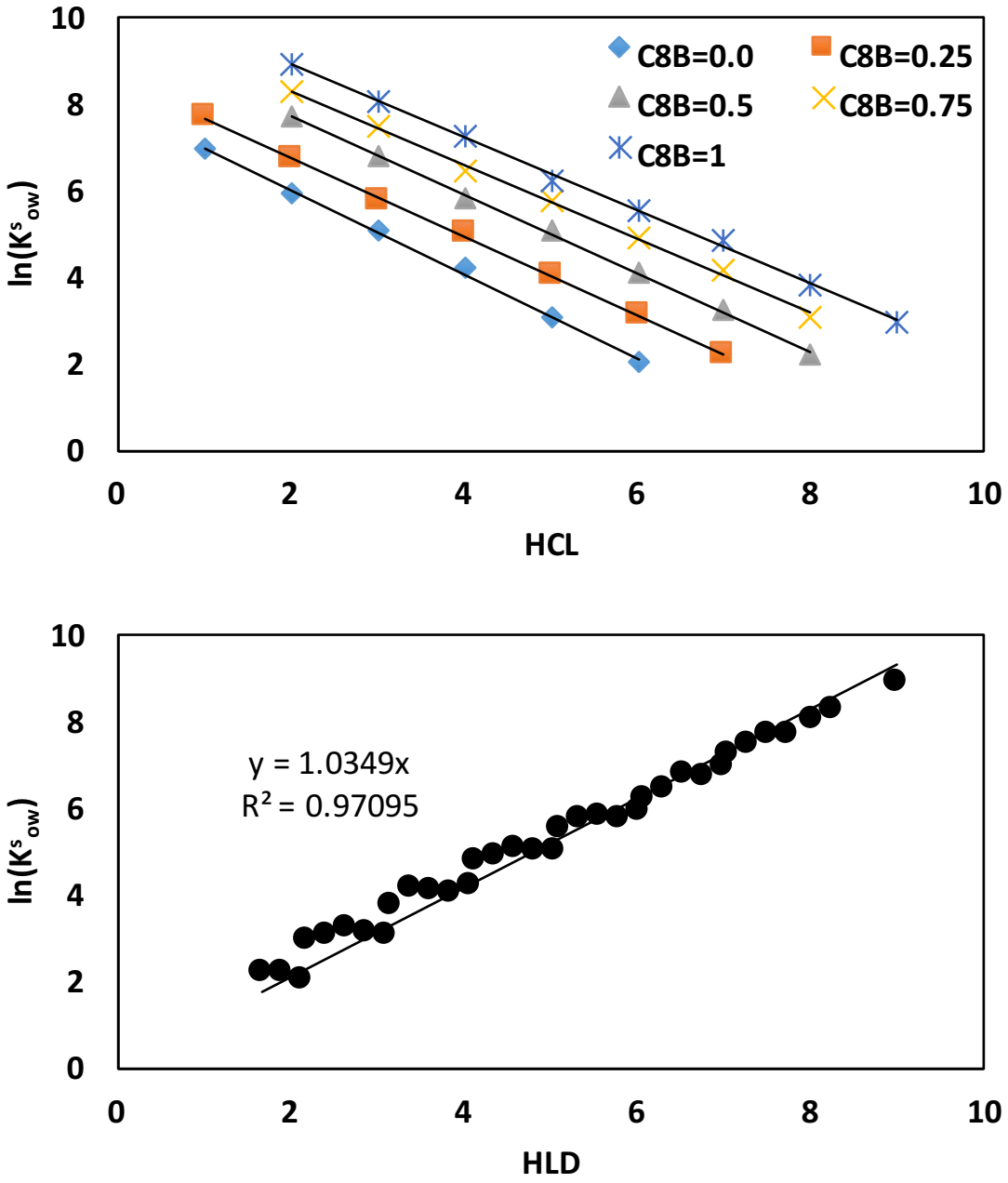

Figure 6-2. Partitioning between oil and water of an ethoxylated octylphenol surfactant as a function of *HCL*, for different mixtures of tetradecane and octylbenzene (C8B) (top), and scaled as a function of HLD (bottom); all partitioning data corresponds to the three-phase region. Data from Graciaa et al. (2006).

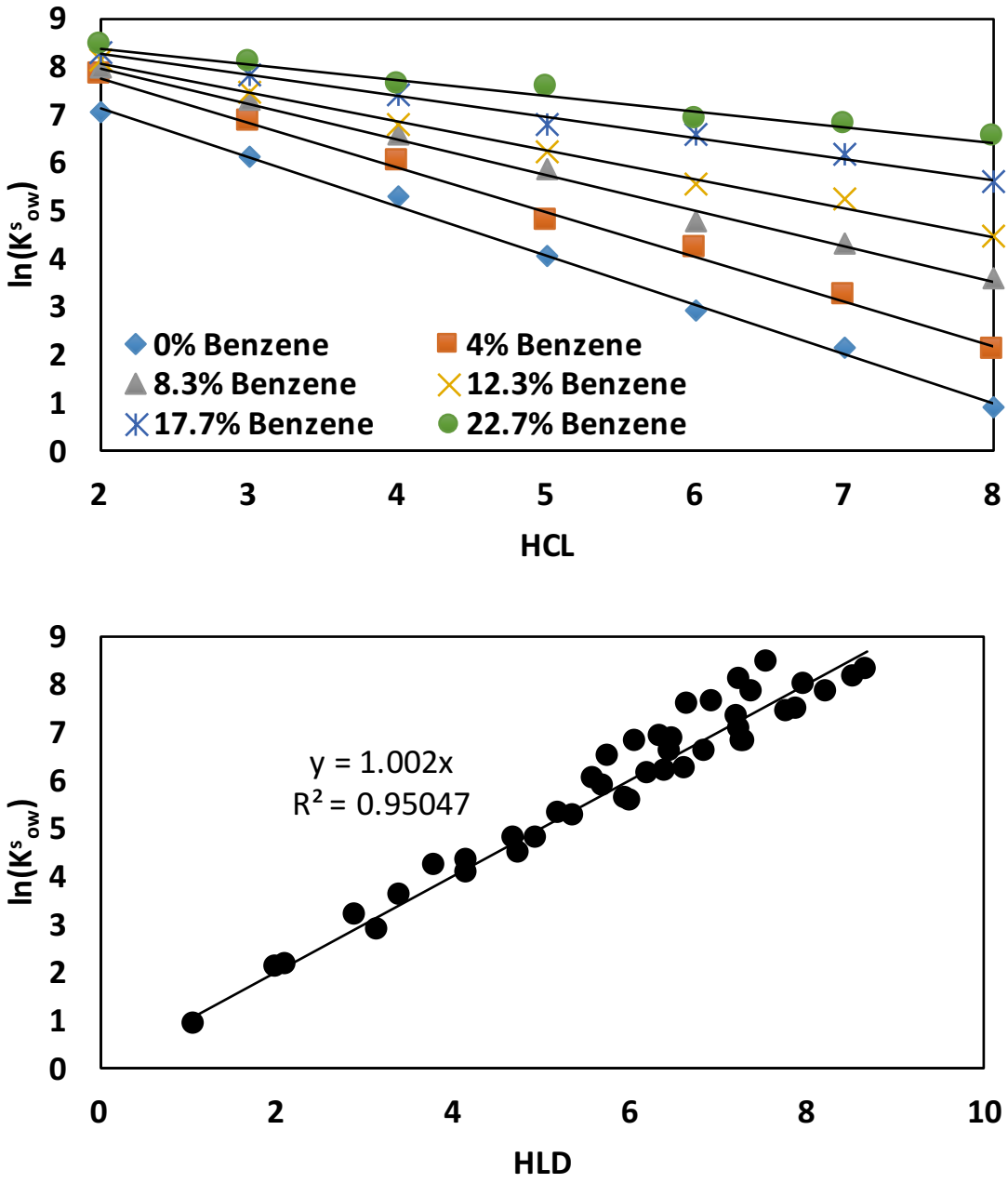

Figure 6-3. Partitioning between oil and water of an ethoxylated nonylphenol surfactant as a function *HCL*, for different benzene content (top), and scaled as a function of HLD (bottom); all partitioning data corresponds to the three-phase region. Data from Ysambertt et al. (1997).

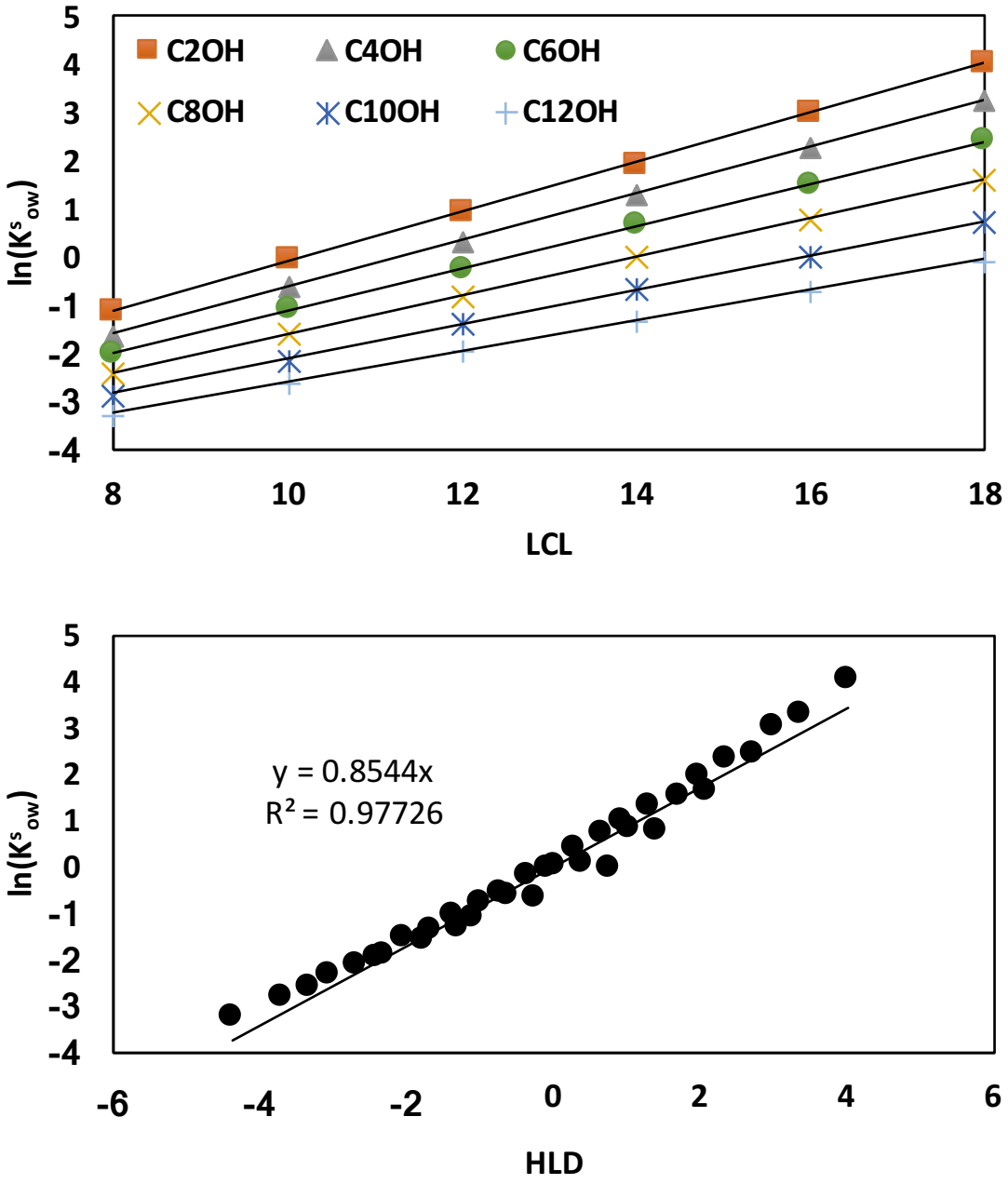

Figure 6-4. Partitioning between oil and water of fatty carboxylic acids (FA) as a function of *LCL*, for different alcohol chain length using a constant alcohol concentration of 4% (top), and scaled as a function of HLD (bottom); all partitioning data corresponds to the three-phase region. Data from Marquez et al. (2012).

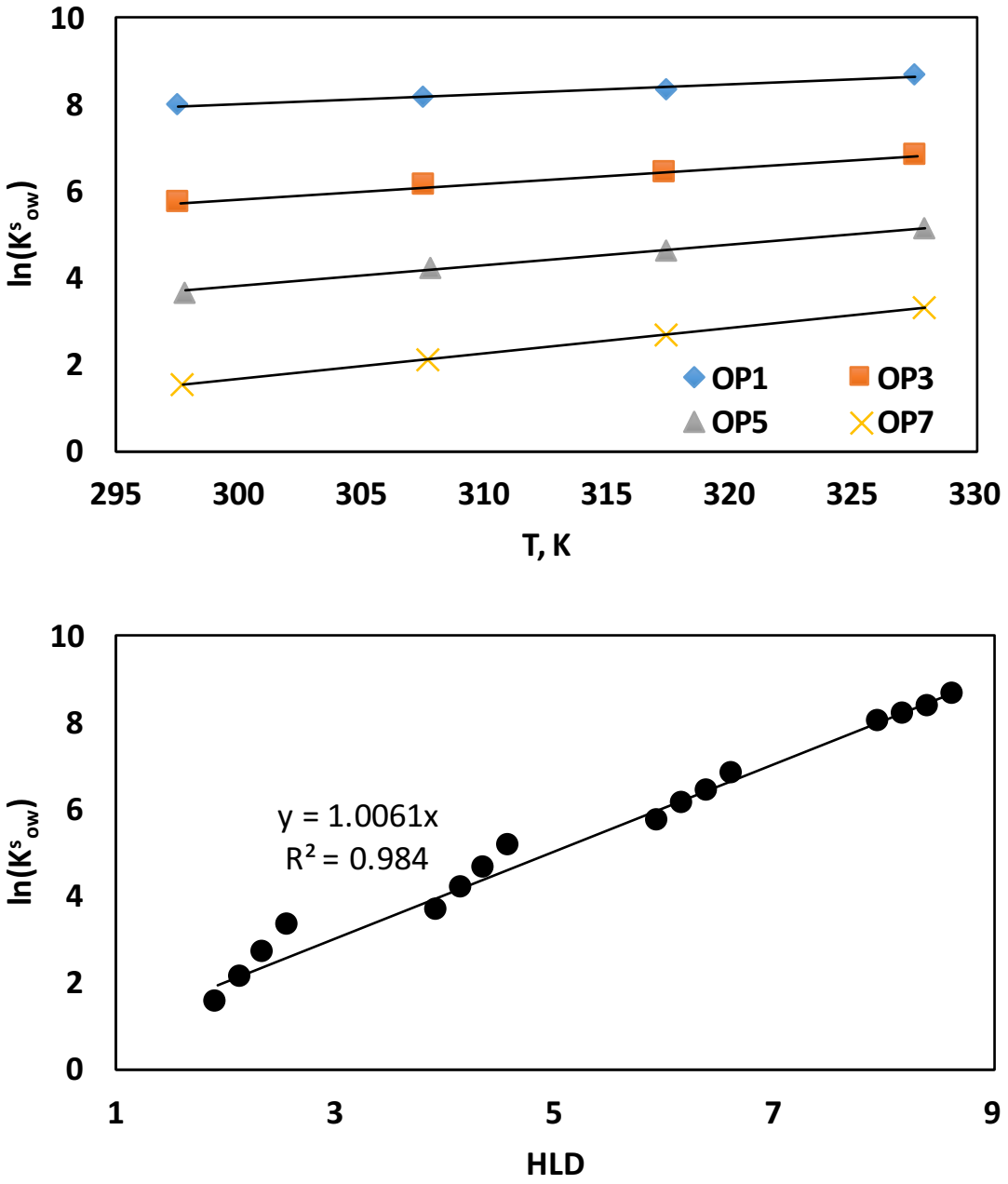

Figure 6-5. Partitioning between oil and water of different ethoxylated octylphenol surfactants as a function of temperature (top), and scaled as a function of HLD (bottom); all partitioning data corresponds to the three-phase region. Data from Salager et al. (2000).

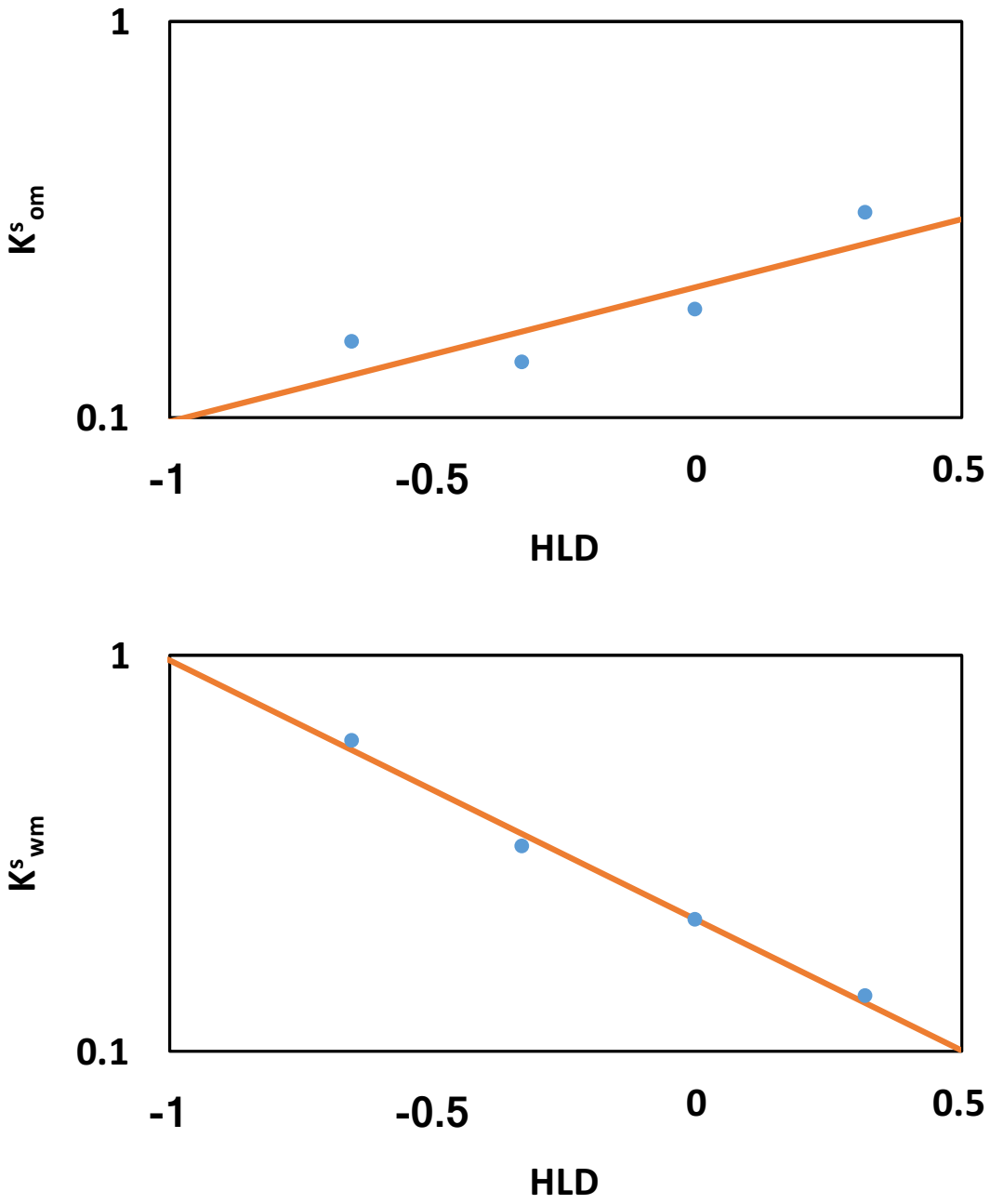

Figure 6-6. Surfactant partitioning between the oil and microemulsion phases (top) and surfactant partitioning between the microemulsion and water phases (bottom) as a function of HLD for the surfactant TRS 10-410 using data from Chan and Shah (1979).

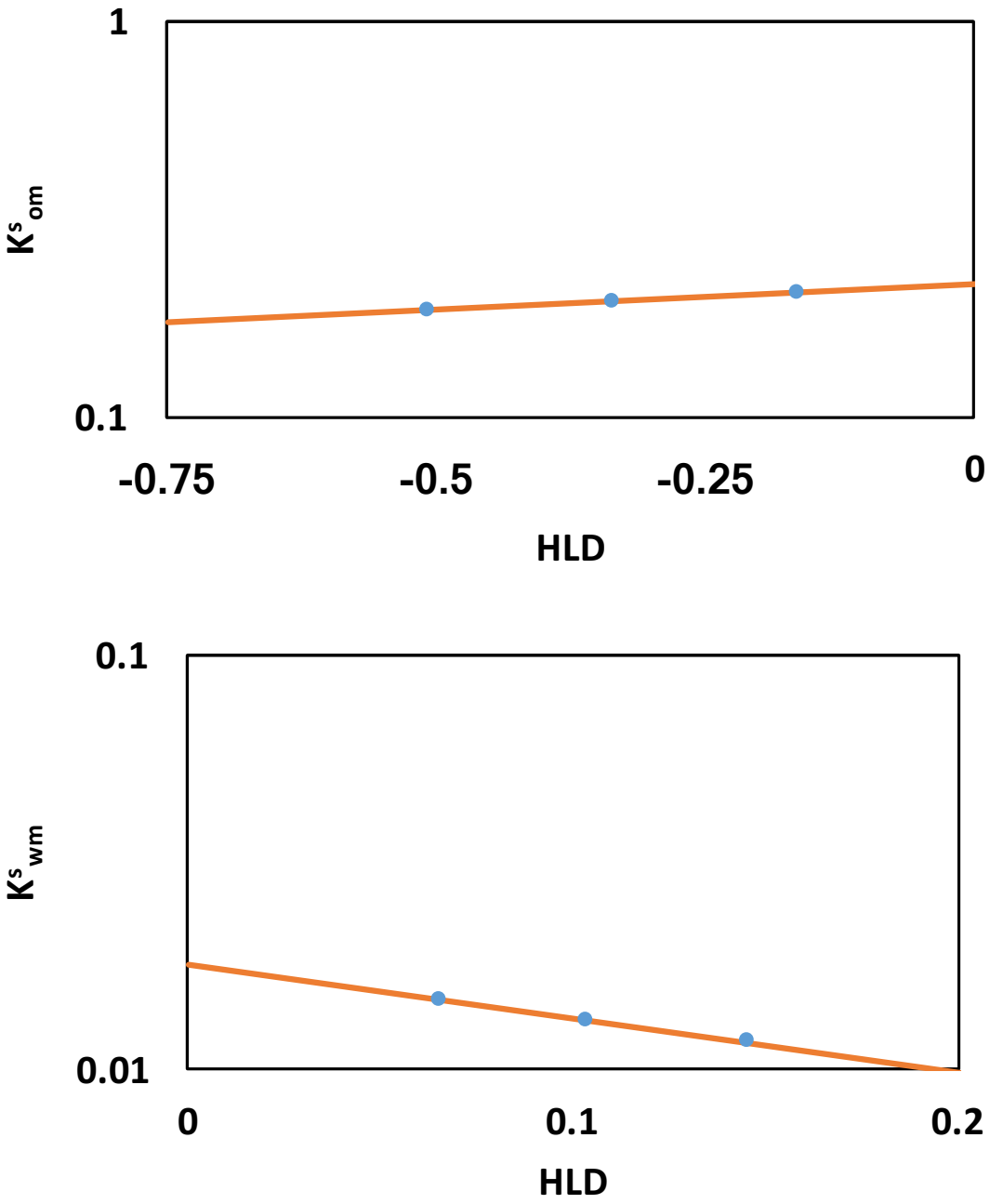

Figure 6-7. Surfactant partitioning coefficient between the oil and microemulsion phases for a pure alkylbenzene sulfonate surfactant (top) and surfactant partitioning coefficient between the microemulsion and water phases for a technical grade alkylbenzene sulfonate surfactant (bottom) as a function of HLD using data from Salager et al. (2013A).

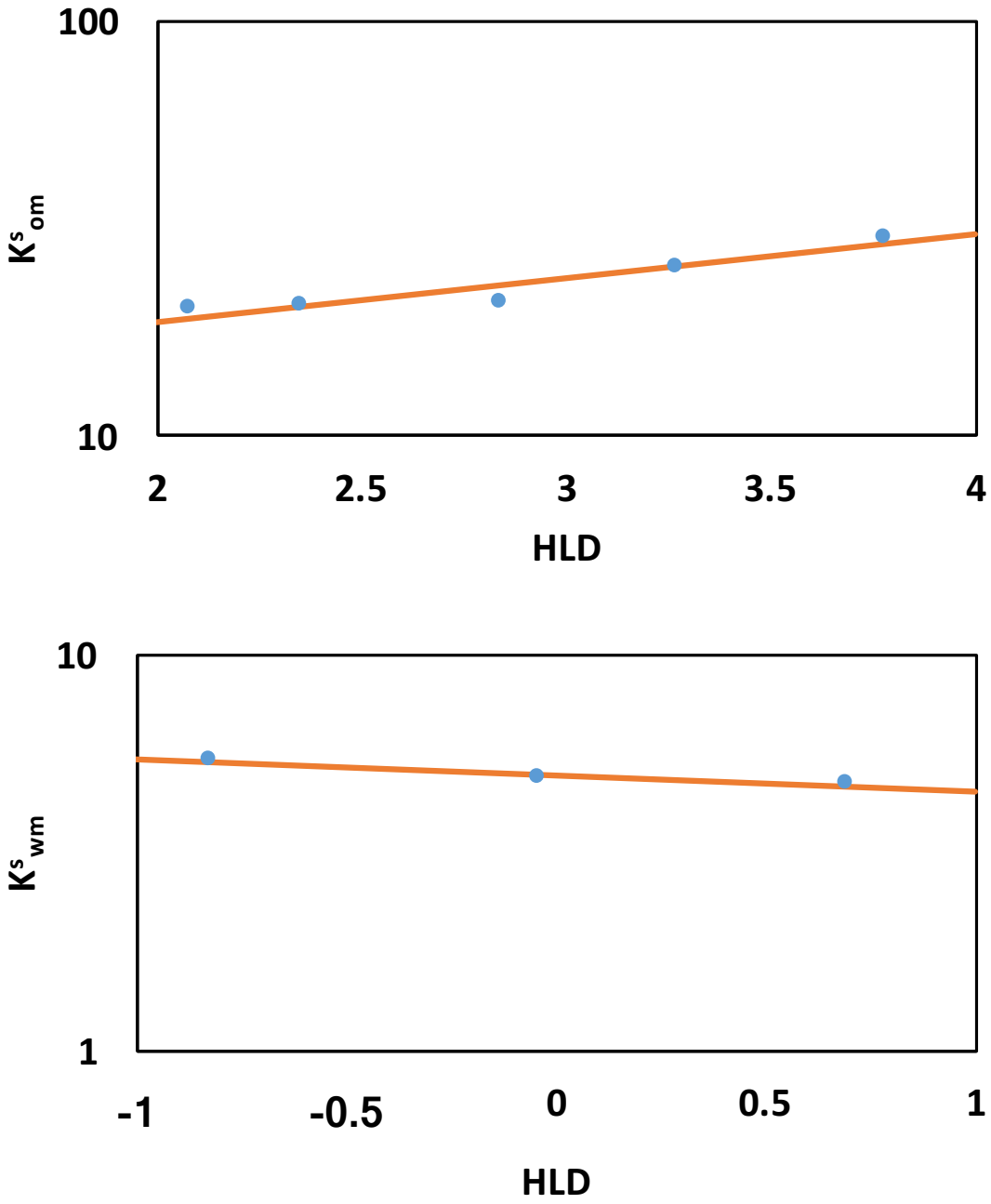

Figure 6-8. Surfactant partitioning between the oil and microemulsion phases with 0.74% i-pentanol concentration (top) and surfactant partitioning between the microemulsion and water phases without alcohol content (bottom) as a function of HLD for the surfactant TRS 10-80 using data from Wade et al. (1978).

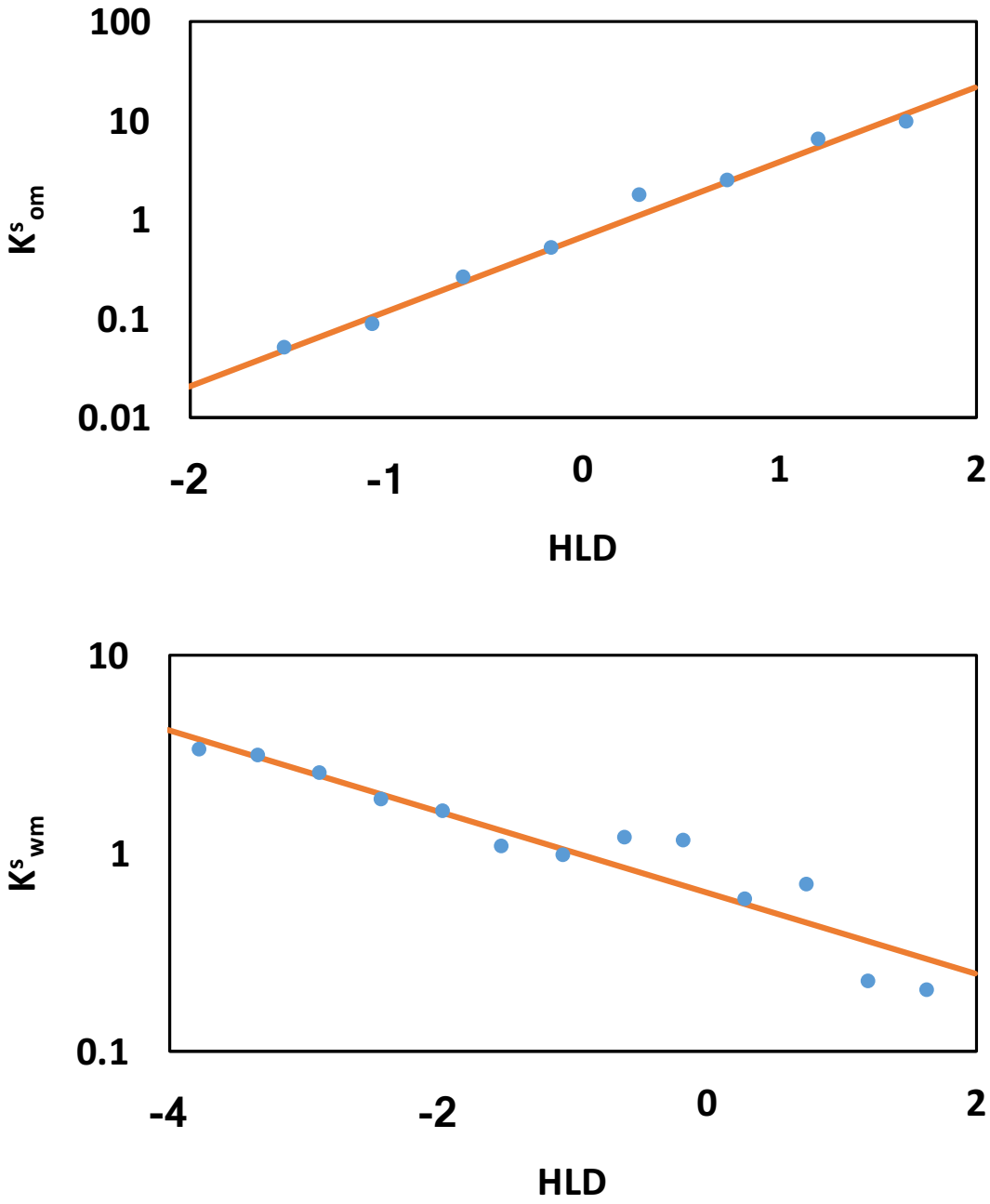

Figure 6-9. Surfactant partitioning between the oil and microemulsion phases (top) and surfactant partitioning between the microemulsion and water phases (bottom) as a function of HLD for an ethoxylated nonylphenol surfactant using data from Salager et al. (1995).

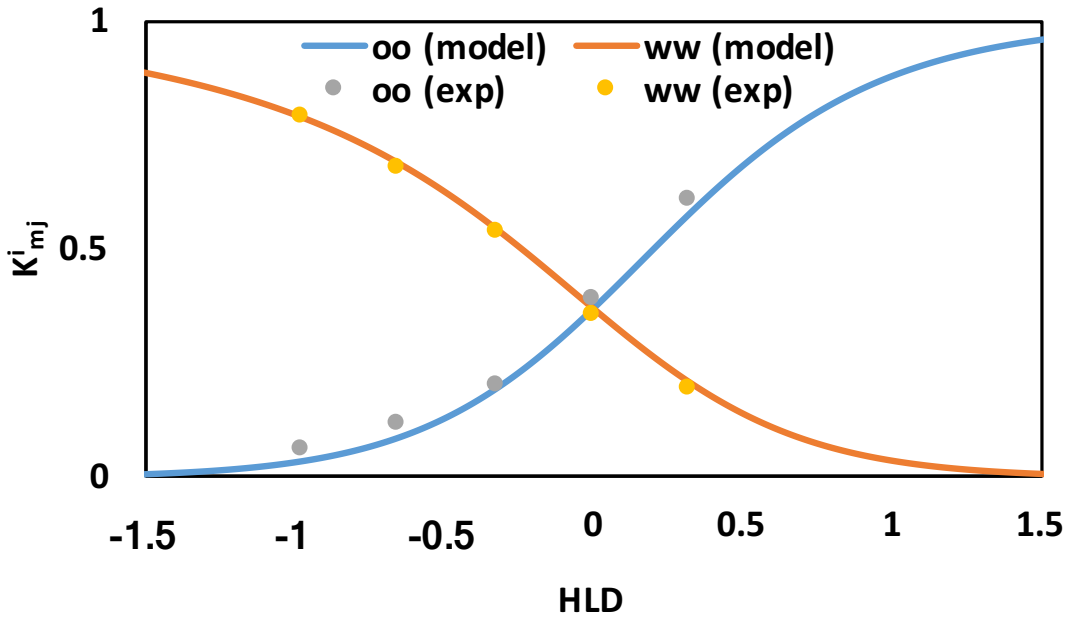

Figure 6-10. Three-phase oil and water partitioning experimental data, and the corresponding model results assuming pure excess phases. Data from Chan and Shah (1979).

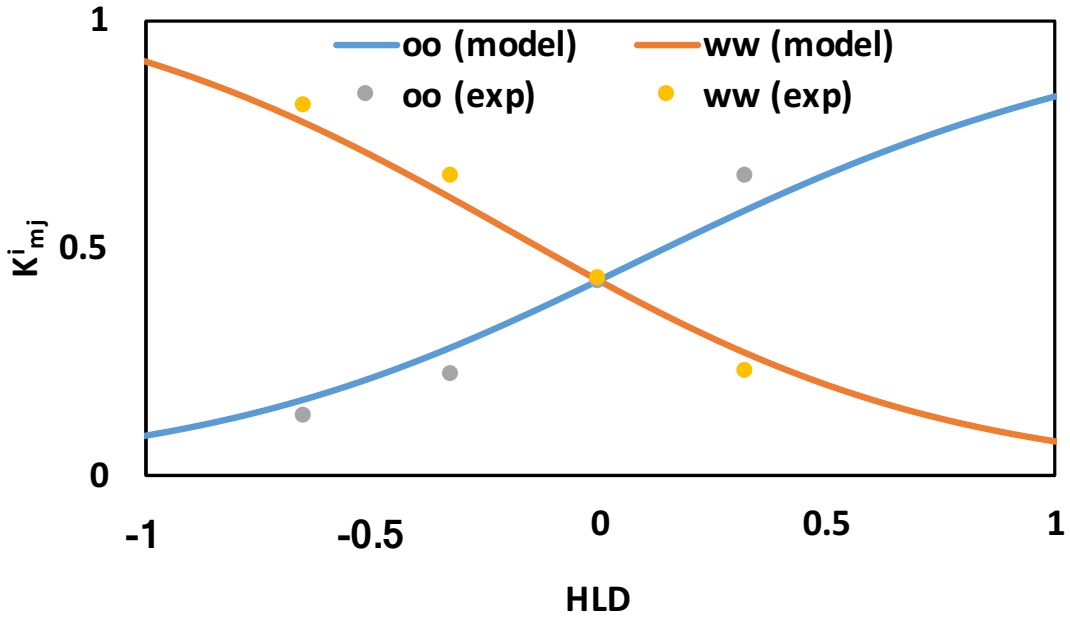

Figure 6-11. Three-phase oil and water partitioning experimental data, and the corresponding model predictions allowing for surfactant partitioning into the excess phases. Data from Chan and Shah (1979).

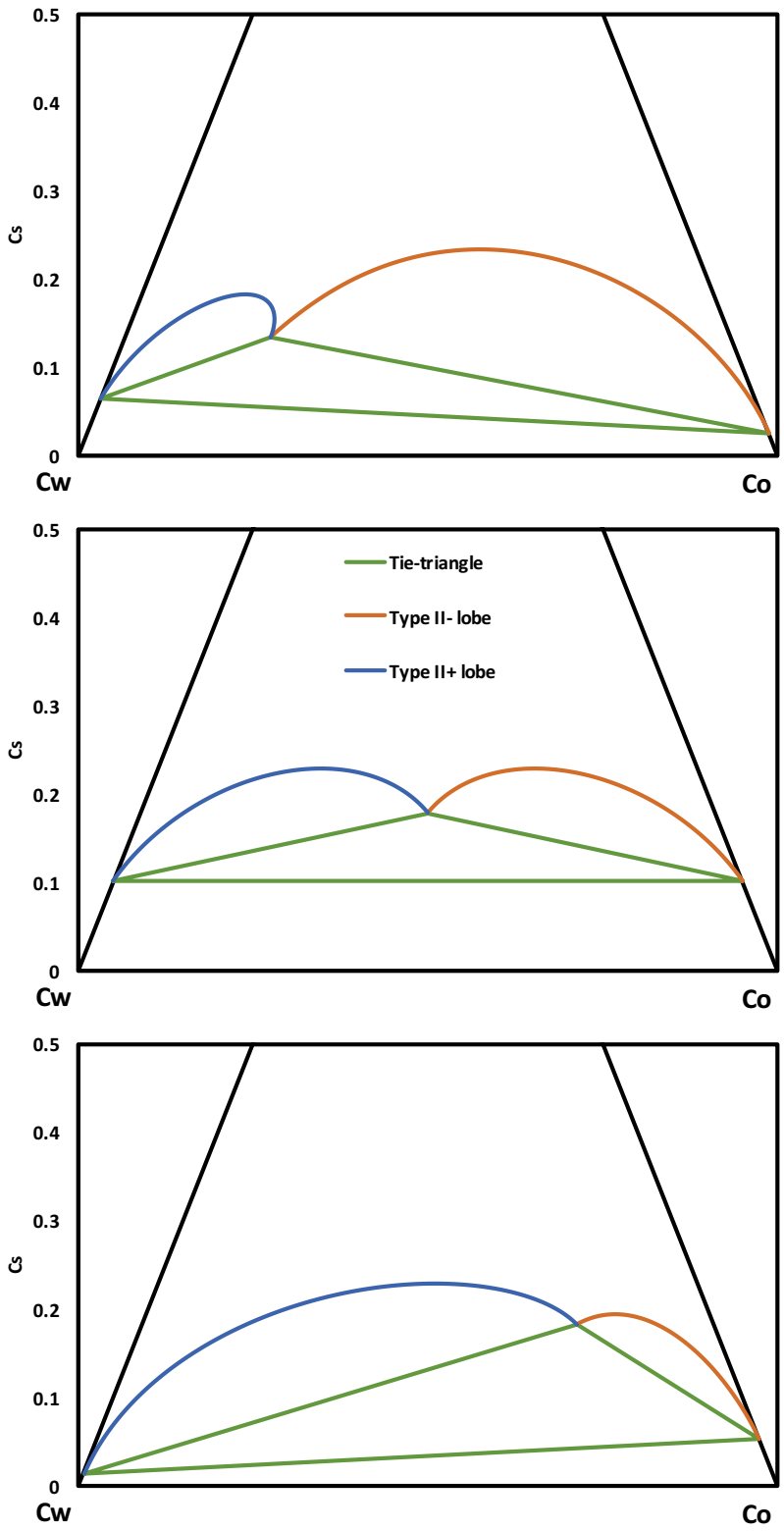

Figure 6-12. Model results showing the partitioning of surfactant into the excess phases for different HLD conditions in the Type III environment (i.e. $HLD = -0.5$, top; $HLD = 0$, middle; and $HLD = 0.5$, bottom). Model parameters are defined using the data from Chan and Shah (1979).

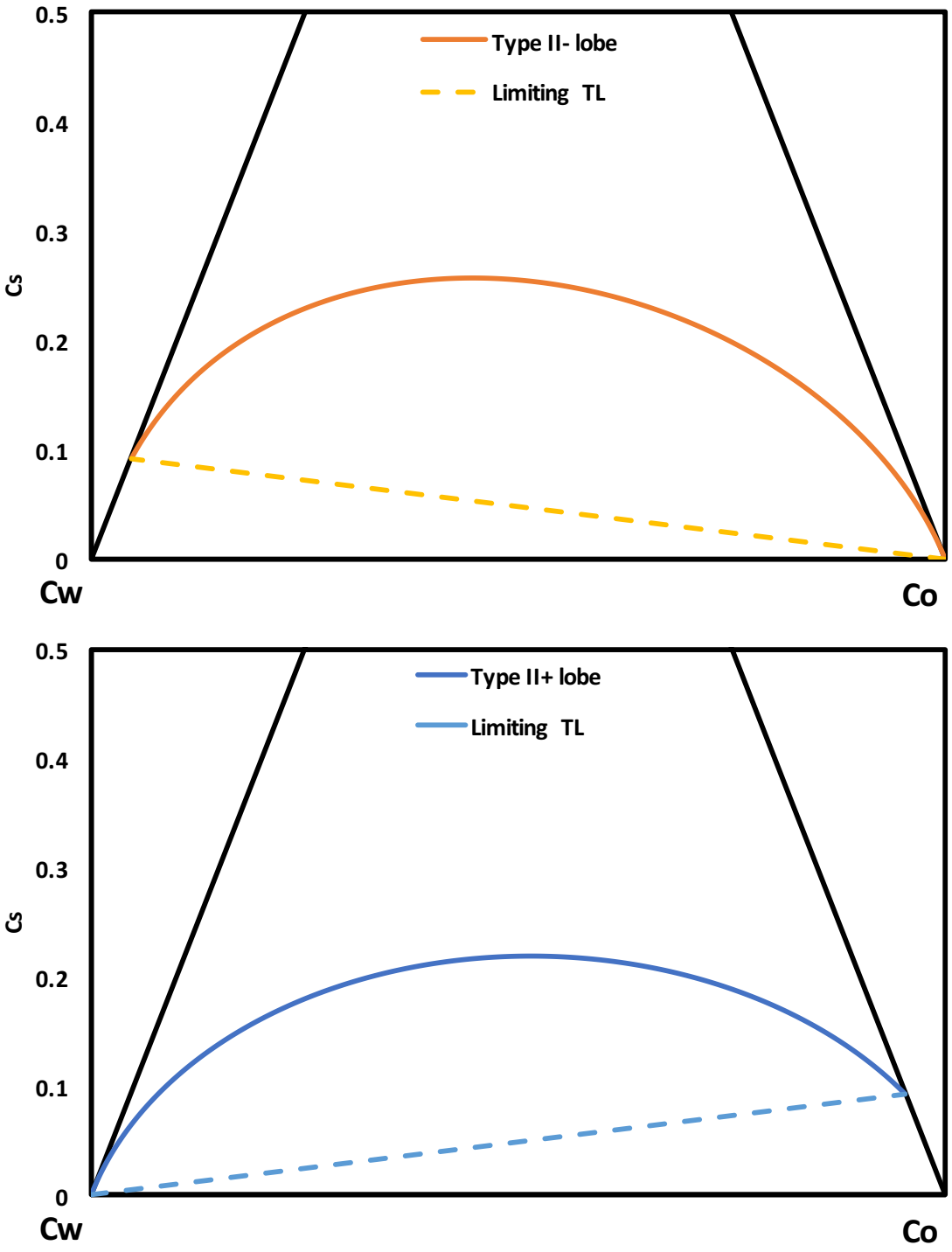

Figure 6-13. Model results showing the partitioning of surfactant into the excess phases for a Type II- environment with $HLD = -2.1$ (top), and a Type II+ environment with $HLD = 2.1$ (bottom. Model parameters are defined using the data from Chan and Shah (1979).

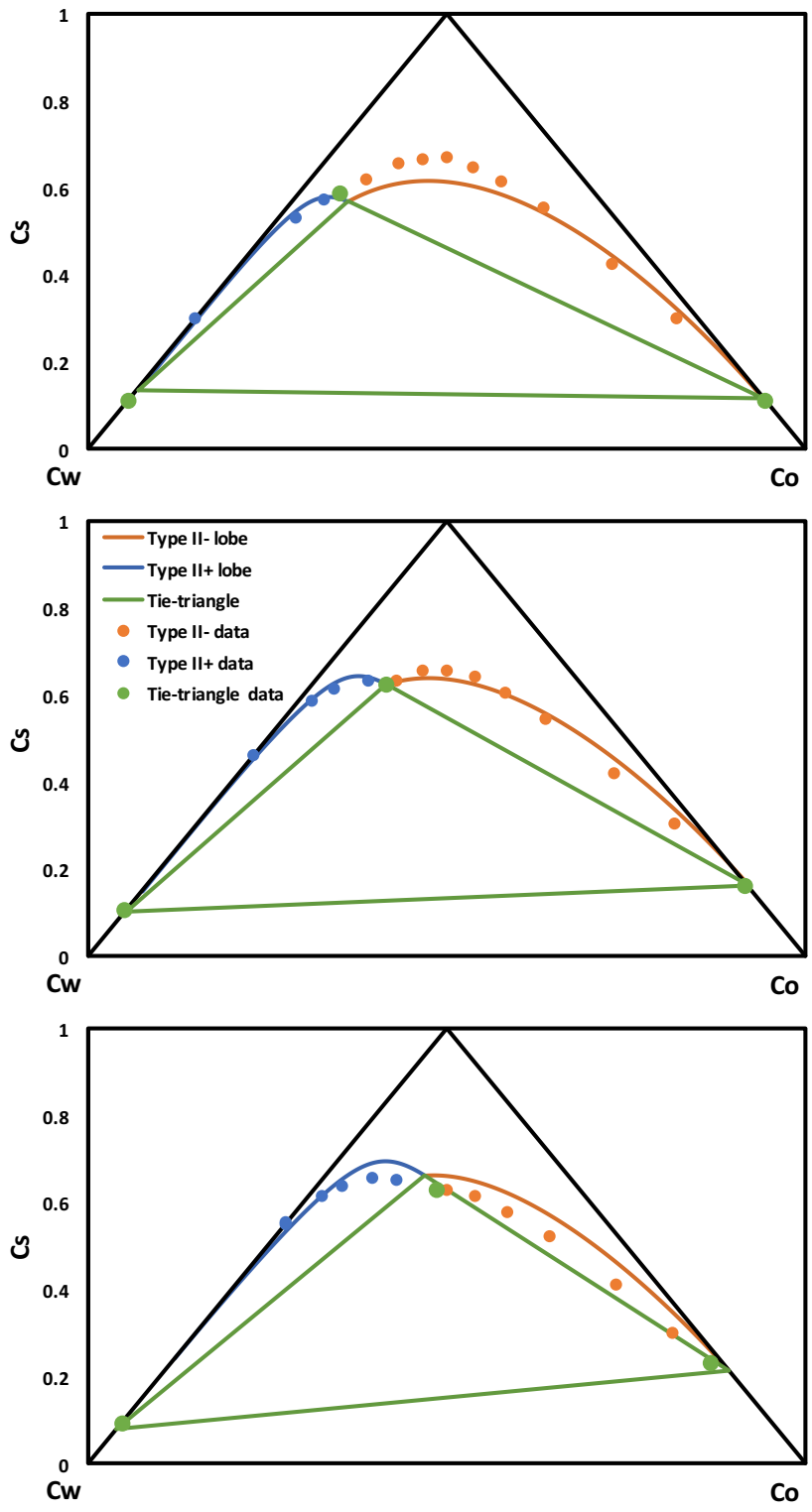

Figure 6-14. Ternary experimental data, and CP EoS model (with impure excess phases) tuned results for a composition scan using dodecane at 52°C (middle) and predictions for 42°C (top) and 62°C (bottom). Experimental data from Burauer et al. (1999).

Part IV

Concluding Remarks

Chapter 7

Conclusions and Future Research

In this chapter, we highlight important results and conclusions from this dissertation, and propose possible areas of future research and natural extensions to this research.

7.1 Conclusions

In this dissertation, we improved the understanding of surfactant-oil-brine systems by using concepts from thermodynamics and interfacial physics.

In Chapter 3, we presented a robust curvature-based microemulsion phase behavior model, which is coupled with interfacial tensions to allow for a more accurate modeling of fluid interactions. Some specific conclusions are:

- We developed a novel approach to consider variable curvatures in the context of microemulsion phase behavior. This approach allows us to describe spherical, cylindrical and bicontinuous micellar geometries based on the general framework of using prolate spheroids.
- The model is successful in qualitatively and quantitatively capturing physical behavior from typical microemulsion experiments. Some examples include an $\mathcal{H}$-scan for a fixed overall composition, and a composition-scan for fixed $\mathcal{H}$.

- The model relies on a robust interpolation procedure for the principal curvatures in composition space, based on the principal curvatures from the invariant and critical points.
- The three-phase oil and water solubilization ratios developed from this approach are consistent with those developed by Torrealba and Johns (2017A) from an interfacial tension model, which were based on a principal curvature definition.
- The model is tied with Huh's correlation to present a coupled approach to accurately capture phase behavior and interfacial tensions.
- The model removes all assumptions and limitations in Khorsandi and Johns (2016) model as identified by Torrealba and Johns (2017B).

In Chapter 4, we introduced a consistent model that allows to capture and predict relevant interfacial tensions of microemulsion systems for all Winsor types and overall compositions. This model is coupled with Huh's equation, which allowed us to define a coupled interfacial tension-phase behavior model. The main conclusions are:

- The model is developed considering micellar curvatures for the definition of interfacial tensions, making the phase behavior estimation physically representative.
- The presented approach allows for a consistent definition of all relevant interfacial tension in microemulsion systems for all HLD and composition conditions, and offers accurate predictions of the corresponding phase behavior.

- The interfacial tension between oil and water is tied to HLD by using film bending energy arguments and empirical relations for microscopic curvatures. This oil-water interfacial tension is found to be quadratic with HLD. Similarly, the characteristic length scale is tied to HLD following empirical expressions for the characteristic length scale and principal curvatures; the characteristic length scale is found to scale with the inverse of HLD. Comparison to experimental data show excellent results.
- Models for the oil-microemulsion and microemulsion-water interfacial tensions are developed based on phase transition boundary conditions, which show accurate results when compared to experimental data. These models are extended to account for compositional changes.
- Using Huh's equation, the interfacial tension is linked to phase behavior in order to present a coupled model for all microemulsion phase environments.
- The oil-water interfacial tension, characteristic length scale and solubilization ratio are tied at optimum condition under the assumption of bicontinuous micellar arrangement, which allows for increased predictability of the coupled interfacial tension-phase behavior model.

In Chapter 5, a new phase behavior EoS model was introduced based on an empirical formulation suggested by changes in chemical potentials (CP) with HLD. The CP EoS model relies on the HLD measure for surfactant affinity quantification, which captures a broad range of formulation state variables. Some specific conclusions are the following:

- The CP EoS phase behavior model satisfactorily tunes experimental data (including crude oil) for an HLD-scan and ternary diagram data. Tuning honors phase boundaries between the type III and type II regions, while accurately capturing experimental phase volume fractions.
- The new model eliminates the need for the *NAC* equations, does not assume a constant correlation length in the three-phase region, or that micelles are spherical in shape.
- The CP EoS model was extended to incorporate surfactant partitioning into the excess phases, which allows for a more complete description of the phase behavior of surfactant-oil-brine systems.

In Chapter 6, a useful approach for capturing surfactant partitioning as a function of HLD is presented and coupled with a microemulsion phase behavior model. Some key findings are:

- The HLD concept is shown to be applicable when multiple formulation variables change simultaneously, and a single reference state is used. Experimental data with different changing formulation variables collapse onto one curve as a function of HLD.
- Key dimensionless groups are identified as a function of activities, which allow for a simplified description of surfactant partitioning coefficients as a function of HLD.
- The oil and water partitioning coefficients between the microemulsion and corresponding excess phases are given as a function of HLD, which allows for the identification of dimensionless groups. These partitioning

coefficients are related to the CP model of Torrealba and Johns (2017) in the cases of pure excess phases and surfactant partitioning into the excess phases.

7.2 Summary of predictive capabilities

In this section, the predictive capabilities of different contributions from this dissertation are emphasized. Some specific examples are:

- The curvature model introduced in Chapter 3 is shown to have accurate predictive capabilities in the Type III region for a variety of pressure and temperature scans using the proposed methodology.
- The interfacial tension model introduced in Chapter 4 allows for oil-water interfacial tensions predictions at optimum and away from optimum condition for a wide range of cases, which can minimize the number of experiments needed for a given system and allow for accurate estimations away from experimental conditions.
- The CP model introduced in Chapter 5 was shown to have three-phase predictive capabilities. For the cases considered, the CP EoS model offered improved tuning and predictions than the HLD-*NAC* EoS model.
- The surfactant partitioning model introduced in Chapter 6 is combined with the CP model, which allows for accurate predictions of ternary diagrams in the presence of surfactant partitioning.

7.3 Future research

Given the complex interaction of amphiphilic compounds with both oil and water, there are many areas of open research that are of natural interest for petroleum engineering applications. These areas include the following:

- Impact of polymer on microemulsion phase behavior: most enhanced oil recovery field implementations would combine surfactant with polymer in the injection stream. Austad and Taugbol (1995) reported changes in microemulsion phase behavior by the addition of two commonly used polymers in petroleum applications (namely, xanthan gum and partially hydrolyzed polyacrylamide). Some possible questions include the change of optimum solubilization and interfacial tension with polymer molecular weight and polymer concentration.
- Impact of polymer on microemulsion rheology: Lapasin et al. (2001) studied the impact on microemulsion viscosity of adding varying concentrations of polymer for oil in water microemulsions (Type II-environment). Possible questions include to study the impact on rheology of adding a fixed concentration of polymer to a surfactant-oil-brine system for varying surfactant affinity conditions (e.g. a salinity scan).
- Impact of polymer on surfactant-rock interactions: most adsorption isotherms for both surfactant and polymer are measured independently, and are only a function of the individual component concentration. This fails to account for the fact that the surfactant and polymer may compete for the rock surface sites available for adsorption. Possible questions

include how to capture preferential adsorption as a function of surfactant and polymer concentrations, molecular properties, and rock minerology.

- Impact of preferential amphiphilic partitioning or adsorption on oil recovery from the point of view of reservoir simulation: the coupled interfacial tension-phase behavior model was extended to understand how variable alcohol content impacts relevant microemulsion properties. However, it is of interest to tie these improvements with physical sources of amphiphilic losses (e.g. partitioning, adsorption) in a reservoir simulator in order to quantify the impact on oil recovery from accounting for amphiphilic compounds moving at different speeds as opposed to the assumption that these chemicals move at the same speed.
- Compositionally-dependent microemulsion relative permeability curves: enhanced oil recovery performance forecasts are mostly generated using reservoir simulations, which account for both fluid flow and phase behavior mechanisms. Fluid flow is principally a function of the mobility of the different phases, which depends on both viscosity and relative permeability. For surfactant-oil-brine systems, there is limited understanding of the impact of microemulsion composition on relative permeability curves.
- Optimum solubilization correlations with formulation variables for improved phase behavior predictability: phase behavior characterization studies are typically conducted by changing a single formulation variable (e.g. salinity, temperature, pressure). However, reservoir-scale displacement processes

involve simultaneous changes in multiple formulation variables. Therefore, phase behavior models should be characterized ensuring the accurate capture of phase behavior under such conditions. As described in this dissertation, one possible way forward is to correlate model parameters (e.g. optimum solubilization, $\mathcal{H}_U$, and $\mathcal{H}_L$) with formulation variables. Future research could include more comprehensive characterization of these correlations, especially when more than two formulation variables are changed.

Bibliography

Acosta, E., Szekeres, E., Sabatini, D.A., Harwell, J.H. (2003). Net-Average Curvature Model for Solubilization and Supersolubilization in Surfactant Microemulsions. Langmuir. 19 (1), 186–195.

Acosta, E.J. (2008). The HLD-NAC equation of state for microemulsions formulated with nonionic alcohol ethoxylate and alkylphenol ethoxylate surfactants. Colloids and Surfaces A: Physicochemical and Engineering Aspects. 320: 193-204.

Acosta, E.J., Kiran, S.K., Hammond, C.E. (2012). The HLD-NAC Model for Extended Surfactant Microemulsions. Journal of Surfactants and Detergents. 15:495-504.

Austad, T., Strand, S. (1996). Chemical Flooding of Oil Reservoirs 4. Effects of Temperature and Pressure on the Middle Phase Solubilization Parameters Close to Optimum Flood Conditions. Colloids and Surfaces A: Physicochemical and Engineering Aspects. 108 (1996), 243-252.

Austad, T., and Taugbol, K. (1995). Chemical flooding of oil reservoirs 1. Low tension polymer flood using a polymer gradient in the three-phase region. Colloids and Surfaces A: Physicochemical and Engineering Aspects. 101 (1), 87-97.

Anton, R. E., Anderez, J. M., Bracho, C., Vejar, F., Salager, J. L. (2008). Practical Surfactant Mixing Rules Based on the Attainment of Microemulsion-Oil-Water Three-Phase Behavior Systems. Interfacial Processes and Molecular Aggregation of Surfactants. R. Narayanan. Berlin, Springer-Verlag Berlin. 218, 83-113.

Aveyard, R., Binks, B.P., Clark, S., Fletcher, P.D.I. (1990). Cloud Points, Solubilisation and Interfacial Tensions in Systems Containing Nonionic Surfactants. Journal of Chemical Technology and Biotechnology 48(2): 161-171.

Bellocq, A.M., Bourbon, D., Lemanceau, B. (1981). Three-dimensional phase diagrams and interfacial tensions of the water—dodecane—pentanol—sodium octylbenzene sulfonate system. Journal of Colloid and Interface Science 79(2): 419-431.

Bellocq, A.M., Bourbon, D., Lemanceau, B., Fourche, G. (1982). Thermodynamic, interfacial, and structural properties of polyphasic microemulsion systems. Journal of Colloid and Interface Science 89(2): 427-440.

Ben Ghoulam, M., Moatadid, N., Graciaa, A., Lachaise, J. (2002). Effects of Oxyethylene Chain Length and Temperature on Partitioning of Homogeneous Polyoxyethylene Nonionic Surfactants Between Water and Isooctane. Langmuir. 18 (11), 4367-4371.

Bennett, K.E., Phelps, C.H.K., Davis, T.E., Scriven, L.E. (1981). Microemulsion Phase Behavior-Observations, Thermodynamic Essentials, Mathematical Simulation. SPE Journal. 21 (06), 747-762.

Berghaus, M., Paulus, M., Salmen, P., Al-Ayoubi, S., Tolan, M., Winter, R. (2016). Near-Surface and Bulk Behavior of Bicontinuous Microemulsions under High-Pressure Conditions. The Journal of Physical Chemistry B. 120(29): 7148-7153.

Borkovec, M. (1989). From micelles to microemulsion droplets: Size distributions, shape fluctuations, and interfacial tensions. The Journal of Chemical Physics 91(10): 6268-6281.

Bourrel, M., Salager, J.L, Schechter, R.S., Wade, W.H. (1980). A Correlation for Phase Behavior of Nonionic Surfactants. Journal of Colloid and Interface Science. 75 (2), 451-461.

Bourrel, M., Schechter, R.S. (2010). Microemulsions and Related Systems: Formulation, Solvency, and Physical Properties. Paris, France: Editions Technip.

Bravo, B., Sanchez, J., Caceres, A., Chavez, G., Ysambertt, F., Marquez, N., Jaimes, M., Briceno, M. I., Salager, J. L. (2008). Partitioning of Fatty Acids in Oil/Water Systems Analyzed by HPLC. Journal of Surfactants and Detergents. 11 (1), 13-19.

Brooks, B. W. and H. N. Richmond (1994). The Application of a Mixed Nonionic Surfactant Theory to Transitional Emulsion Phase Inversion .2. The Relationship Between Surfactant Partitioning and Transitional Inversion - A Thermodynamic Treatment. Journal of Colloid and Interface Science. 162 (1), 67-74.

Burauer, S., Sachert, T., Sottmann, T., Strey, R. (1999). On microemulsion phase behavior and the monomeric solubility of surfactant. Physical Chemistry Chemical Physics. 1: 4299-4306.

Butler, E. C. and K. F. Hayes (1998). Micellar Solubilization of Nonaqueous Phase Liquid Contaminants by Nonionic Surfactant Mixtures: Effects of Sorption, Partitioning and Mixing. Water Research. 32 (5), 1345-1354.

Cazabat, A.M., Langevin, D., Meunier, J., Pouchelon, A. (1982). Critical Behavior in Microemulsions. Advances in Colloid and Interface Science 16(1): 175-199.

Chan, K. S. and D. O. Shah (1979). The Effect Of Surfactant Partitioning On The Phase Behavior And Phase Inversion Of The Middle Phase Microemulsions. SPE of AIME International Symposium on Oilfield and Geothermal Chemistry. Houston, Texas.

Chandra, P., Safran, S.A. (1991). Structure Factor for Microemulsions with Finite Spontaneous Curvature. Langmuir. 7 (9), 1849-1854.

Chen, F., Holten-Andersen, J., Tyle, H. (1993). New Developments of the UNIFAC Model for Environmental Application. Chemosphere. 26 (7): 1325-1354.

Cheng, H. Y., Kontogeorgis, G. M., Stenby, E. H. (2005). Correlation and Prediction of Environmental Properties of Alcohol Ethoxylate Surfactants Using the UNIFAC Method. Industrial & Engineering Chemistry Research. 44 (18), 7255-7261.

Crook, E. H., Fordyce, D. B., Trebbi, G. F. (1965). Molecular Weight Distribution of Nonionic Surfactants .2. Partition Coefficients of Normal Distribution and Homogeneous P,T-Octylphenoxyethanols (3PES). Journal of Colloid Science. 20 (3), 191-288.

Davis, H.T. (1994). Factors determining emulsion type: hydrophile-lipophile balance and beyond. Colloids and Surfaces A: Physicochemical and Engineering Aspects. 91: 9-24.

Davis, T.H., and Scriven, L.E. (1980). The Origins of Low Interfacial Tensions for Enhanced Oil Recovery. Paper presented at the SPE Annual Technical Conference and Exhibition held in Dallas, Texas.

De Gennes, P.G., and Taupin, C. (1982). Microemulsions and the Flexibility of Oil/Water Interfaces. The Journal of Physical Chemistry. 86 (13), 2294–304.

Debye, P., Anderson Jr., H.R., Brumberger, H. (1957). Scattering by an Inhomogeneous Solid. II. The Correlation Function and Its Application. Journal of Applied Physics. 28(06): 679-683.

Delgado-Linares, J. G., Pereira, J. C., Rondon, M., Bullon, J., Salager, J. L. (2016). Breaking of Water-in-Crude Oil Emulsions. 6. Estimating the Demulsifier Performance at Optimum Formulation from Both the Required Dose and the Attained Instability. Energy Fuels. 30 (7), 5483-5491.

Eastoe, J. (2003). Surfactant Chemistry. Lectures given at the China Research Institute for Daily Chemical Industry (RIDCI).

Fountain, J. C., Starr, R. C., Middleton, T., Beikirch, M., Taylor, C., Hodge, D. (1996). A Controlled Field Test of Surfactant-Enhanced Aquifer Remediation. Ground Water. 34(5): 910-916.

Fredenslund, A., Jones, R.L., Prausnitz, J.M. (1975). Group-Contribution Estimation of Activity Coefficients in Nonideal Liquid Mixtures. AIChE Journal. 21(6): 1086-1099.

Ghosh, S., and Johns, R.T. (2014). A New $HLD - NAC$ Based EOS Approach to Predict Surfactant-Oil-Brine Phase Behavior for Live Oil at Reservoir Pressure and Temperature. SPE Annual Technical Conference and Exhibition. Amsterdam, The Netherlands.

Ghosh, S., and Johns, R.T. (2016A). An Equation-of-State Model to Predict Surfactant/Oil/Brine-Phase Behavior. SPE Journal. 21 (04), 106-125.

Ghosh, S., and Johns, R.T. (2016B). Dimensionless Equation of State to Predict Microemulsion Phase Behavior. Langmuir. 32 (35), 8969-8979.

Graciaa, A., Anderez, J., Bracho, C., Lachaise, J., Salager, J. L., Tolosa, L., Ysambertt, F. (2006). The Selective Partitioning of the Oligomers of Polyethoxylated Surfactant Mixtures Between Interface and Oil and Water Bulk Phases. Advances in Colloid and Interface Science. 123, 63-73.

Guest, D., Auvray, L., Langevin, D. (1985). Persistence length measurements in middle phase microemulsions. Journal de Physique Lettres. 46 (22), 1055-1063.

Hand, D.B. (1929). Dineric Distribution: I. The Distribution of a Consolute Liquid Between Two Immiscible Liquids. Physics and Chem. 34, 1961–2000.

Healy, R.N., Reed, R.L. (1974). Physicochemical Aspects of Microemulsion Flooding. SPE Journal. 14(05), 491-501.

Healy, R.N., Reed, R.L. (1977). Some Physicochemical Aspects of Microemulsion Flooding: A Review. In D.O. Shah and R.S. Schechter (Eds.), Improved Oil Recovery by Surfactant Flooding (383-437). New York, NY: Academic Press, Inc.

Helfrich, W. (1973). Elastic Properties of Lipid Bilayers: Theory and Possible Experiments. Z. Naturforsch 28(11): 693-703.

Huh, C. (1979). Interfacial Tensions and Solubilizing Ability of a Microemulsion Phase That Coexists with Oil and Brine. Journal of Colloid and Interface Science. 71 (2), 408-426.

Huh, C. (1983). Equilibrium of a Microemulsion That Coexists with Oil or Brine. SPE Journal 23(5): 829-847.

Jin, L., Budhathoki, M., Jamili, A., Li, Z., Luo, H., Ben Shiau, B.J., Delshad, M., Harwell, J.H. (2017). Predicting microemulsion phase behavior using physics based HLD-NAC equation of state for surfactant flooding. Journal of Petroleum Science and Engineering. 151:213-223.

Jouffroy, J., Levinson, P., de Gennes, P.G. (1982). Phase Equilibria Involving Microemulsions (Remarks on the Talmon-Prager Model). J. Physique. 43, 1241-1248.

Kahl, H., Quitzch, K., Stenby, E.H. (1997). Phase equilibria of microemulsion forming system n-decyl- β -D-glucopyranoside/water/n-octane/1-butanol. Fluid Phase Equilibria. 139 (1-2): 295-309.

Kahlweit, M., Strey, R., Busse, G. (1991). Effect of Alcohols on the Phase Behavior of Microemulsions. The Journal of Physical Chemistry. 95(13): 5344-5352.

Kamei, D.T., King, J.A., Wang, D.I.C., Blankschtein, D. (2001). Understanding Viral Partitioning in Two-Phase Aqueous Nonionic Micellar Systems: 2. Effect of Entrained Micelle-Poor Domains. Biotechnology and Bioengineering. 78(2): 203-216.

Kaur, G., Chiappisi, L., Prevost, S., Schweins, R., Gradzielski, M., Mehta, S.K. (2012). Probing the Microstructure of Nonionic Microemulsions with Ethyl Oleate by Viscosity, ROESY, DLS, SANS, and Cyclic Voltammetry. Langmuir. 28: 10640-10652.

Kheyfets, B., Galimzyanov, T., Drozdova, A., Mukhin, S. (2016). Analytical calculation of the lipid bilayer beinding modulus. Physical Review E. 94(04): 042415-1-042415-11.

Khorsandi, S., and Johns, R.T. (2016). Robust Flash Calculation Algorithm for Microemulsion Phase Behavior. Journal of Surfactants and Detergents. 19, 1273-1287.

Khorsandi, S., and Johns, R.T. (2017). Robust Flash Calculation Algorithm for Microemulsion Phase Behavior. International Application No. PCT/2017/048727.

Kiran, S.K., Acosta, E.J. (2015). HLD-NAC and the Formation and Stability of Emulsions Near the Phase Inversion Point. Industrial & Engineering Chemistry Research. 54(25):6467-6479.

Koukounis, C., Wade, W.H., Schecter, R.S. (1983). Phase Partitioning of Anionic and Nonionic Surfactant Mixtures. SPE Journal. 23 (02), 301-310.

Kronberg, B., Holmberg, K., Lindman, B. (2014). Surface Chemistry of Surfactants and Polymers. West Sussex, UK, John Wiley & Sons.

Kunieda, H., Shinoda, K. (1982). Correlation between Critical Solution Phenomena and Ultralow Interfacial in a Surfactant/Water/Oil System. Bulletin of the Chemical Society of Japan. 55 (6), 1777-1781.

Kunz, W., Testard, F., Zemb, T. (2009). Correspondence between Curvature, Packing Parameter, and Hydrophilic-Lipophilic Deviation Scales around the Phase-Inversion Temperature. Langmuir. 25 (1), 112-115.

Lake, L.W., Johns, R.T., Rossen, W.R., Pope, G.A. (2014). Fundamentals of Enhanced Oil Recovery. Richardson, TX, Society of Petroleum Engineers.

Lapasin, R., Grassi, M., Coceani, N. (2001). Effects of polymer addition on the rheology of o/w microemulsions. Rheology Acta. 40 (2), 185-192.

Leitao, H, Somoza, A. M., Telo da Gama, M. M. (1996). Scaling of the interfacial tension of microemulsions: A phenomenological description. Journal of Chemical Physics. 105 (7), 2875-2883.

Lee, C.H., Lin, W.C., Wang, J. (2001). All-optical measurements of the bending rigidity of lipid-vesicle membranes across structural phase transitions. Physical Review E. 64(02): 020901-1-020901-4.

Lekkerkerker, H. N. W., Kegel, W. K., Overbeek, J. Th. G. (1996). Phase Behavior of Ionic Microemulsions. Phys. Chem. 10 (3), 206-217.

Marquez, N., Bravo, B., Chavez, G., Ysambertt, F., Salager, J. L. (2012). Partitioning of Fatty Carboxylic Acids and Ethoxylated Nonionic Surfactants in Microemulsion-Oil-Water Systems. Topics in the Colloidal Aggregation and Interfacial Phenomena. M. Garcia-Sucre, A. Loszan, A. J. Castellanos-Suarez and J. Toro-Mendoza. Kerala, India, Research Signpost.

Marquez, N., Bravo, B., Ysambertt, F., Chavez, G., Subero, N., Salager, J. L. (2003). Analysis of Polyethoxylated Surfactants in Microemulsion-Oil-Water Systems III. Fractionation and Partitioning of Polyethoxylated Alcohol Surfactants. Analytica Chimica Acta. 477 (2), 293-303.

Marquez, N., Graciaa, A., Lachaise, J., Salager, J. L. (2002). Partitioning of Ethoxylated Alkylphenol Surfactants in Microemulsion-Oil-Water Systems: Influence of Physicochemical Formulation Variables. Langmuir. 18 (16), 6021-6024.

May, E.R., Narang, A., Kopelevich, D.I. (2007). Role of molecular tilt in thermal fluctuations of lipid membranes. Physical Review E. 76(02): 021913-1-021913-6.

Nelson, P.H. (2009). Pore-throat sizes in sandstones, tight sandstones, and shales. AAPG Bulletin. 93(03): 329-340.

Nouraei, M., Acosta, E.J. (2017). Predicting solubilization features of ternary phase diagrams of fully dilutable lecithin linker microemulsions. Journal of Colloid and Interface Science. 495:178-190.

Phan, T. T., Attaphong, C., Sabatini, D. A. (2011). Effect of Extended Surfactant Structure on Interfacial Tension and Microemulsion Formation with Triglycerides. Journal of the American Oil Chemists' Society. 88 (8), 1223-1228.

Pope, G.A., and Nelson, R.C. (1978). A Chemical Flooding Compositional Simulator. SPE Journal. 18 (05), 339-354.

Pouchelon, A., Meunier, J., Langevin, D., Chatenay, D. (1980). Low Interfacial Tensions in Three-Phase Systems Obtained with Oil-Water Surfactant Mixtures. Chemical Physics Letters. 76 (2), 277-281.

Ravera, F., Ferrari, M., Liggieri, L. (2000). Adsorption and Partitioning of Surfactants in Liquid-Liquid Systems. Advances in Colloid and Interface Science. 88 (1-2), 129-177.

Robbins, M.L. (1977). Theory for the Phase Behavior of Microemulsion. In K.L., Mittal (Ed.), Micellization, Solubilization, and Microemulsions: Volume 2, 713-754. Boston, MA: Springer US.

Rosen, M., J., and Kunjappu, J. T. (2012). Surfactants and Interfacial Phenomena. Hoboken, NJ, John Wiley & Sons.

Roshanfekr, M. (2010). Effect of Pressure and Methane on Microemulsion Phase Behavior and Its Impact on Surfactant-Polymer Flood Oil Recovery (Doctoral dissertation).

Roshanfekr, M. and R. T. Johns (2011). Prediction of Optimum Salinity and Solubilization Ratio for Microemulsion Phase Behavior with Live Crude at Reservoir Pressure. Fluid Phase Equilibria. 304(1-2): 52-60.

Rossen, W.R., Brown, R.G., Davis, H.T., Prager, S., Scriven, L.E. (1982). Thermodynamic Modeling of Pseudoternary Phase Behavior. SPE Journal. 22 (06), 945-961.

Safran, S.A., Roux, D., Cates, M.E., Andelman, D. (1986). Origin of Middle-Phase Microemulsions. Physical Review Letters. 57 (04), 491-494.

Salager, J. L. (1988). Phase Transformation and Emulsion Inversion on the Basis of Catastrophe Theory. Encyclopedia of Emulsion Technology. 3: 55.

Salager, J.L., Anton, R.E., Arandia, M.A., Forgiarini, A.M. (2017). How to Attain Ultralow Interfacial Tension and Three-Phase Behavior with Surfactant Formulation for Enhanced Oil Recovery: A Review. Part 4. Robustness of the Optimum Formulation Zone Through the Insensibility to Some Variables and the Occurrence of Complex Artifacts. Journal of Surfactants and Detergents 20 (5), 987-1018.

Salager, J. L., Anton, R. E., Sabatini, D. A., Harwell, J. H., Acosta, E. J., Tolosa, L. I. (2005). Enhancing Solubilization in Microemulsions - State of the Art and Current Trends. Journal of Surfactants and Detergents. 8 (1), 3-21.

Salager, J. L., Forgiarini, A. M., Bullon, J. (2013A). How to Attain Ultralow Interfacial Tension and Three-Phase Behavior with Surfactant Formulation for Enhanced Oil Recovery: A Review. Part 1. Optimum Formulation for Simple Surfactant-Oil-Water Ternary Systems. Journal of Surfactants and Detergents. 16 (4), 449-472.

Salager, J. L., Forgiarini, A. M., Marquez, L., Manchego, L., Bullon, J. (2013B). How to Attain Ultralow Interfacial Tension and Three-Phase Behavior with Surfactant Formulation for Enhanced Oil Recovery: A Review. Part 2. Performance Improvement Trends from Winsor's Premise to Currently Proposed Inter- and Intra-Molecular Mixtures. Journal of Surfactants and Detergents 16 (5), 631-663.

Salager, J.L., Forgiarini, A., Bullon, J. (2016). Predicting the Interfacial Tension Change at Optimum Formulation for Enhanced Oil Recovery. Inform 26 (7), 14–18.

Salager, J. L., Manchego, L, Marquez, L., Bullon, J., Forgiarini, A. (2014). Trends to Attain a Lower Interfacial Tension in a Revisited Pure Alkyl Polyethyleneglycol Surfactant-Alkane-Water Ternary System. Basic Concepts and Straightforward Guidelines for Improving Performance in Enhanced Oil Recovery Formulations. Journal of Surfactants and Detergents 17 (2), 199-213.

Salager, J. L., Marquez, N., Anton, R. E., Graciaa, A., Lachaise, J. (1995). Retrograde Transition in the Phase-Behavior of Surfactant Oil-Water Systems Produced by an Alcohol Scan. Langmuir. 11 (1), 37-41.

Salager, J. L., Marquez, N., Graciaa, A., Lachaise, J. (2000). Partitioning of Ethoxylated Octylphenol Surfactants in Microemulsion-Oil-Water Systems: Influence of Temperature and Relation Between Partitioning Coefficient and Physicochemical Formulation. Langmuir. 16 (13), 5534-5539.

Salager, J. L., Morgan, J. C., Schechter, R. S., Wade, W. H., Vasquez, E. (1979). Optimum Formulation of Surfactant-Water-Oil Systems for Minimum Interfacial-Tension or Phase-Behavior. Society of Petroleum Engineers Journal. 19(2): 107-115.

Salter, S.J. (1977). The Influence of Type and Amount of Alcohol on Surfactant-Oil-Brine Phase Behavior and Properties. Fifty Second Annual Fall Technical Conference and Exhibition of the Society of Petroleum Engineers of AIME. Denver, Colorado.

Schulman, J.H., and Montagne, J.B. (1961). Formation of Microemulsions by Amino Alkyl Alcohols. Annals of the New York Academy of Sciences. 92, 357-365.

Scriven, L.E. (1976). Equilibrium bicontinuous structure. Nature. 263(5573): 123-125.

Sheng, J. (2010). Modern Chemical Enhanced Oil Recovery. Burlington, MA, Gulf Professional Publishing.

Sottmann, T., Lade, M., Stolz, M., Schomacker, R. (2002). Phase Behavior of Nonionic Microemulsions Prepared from Technical-Grade Surfactants. Tenside Surfactants Detergents. 39 (1), 20-28.

Sottmann, T, Strey, R. (1997). Ultralow interfacial tensions in water—n-alkane—surfactant systems. Journal of Chemical Physics. 106 (20), 8606-8615.

Sottmann, T, Strey, R., Chen, S.H. (1997). A small-angle neutron scattering study of nonionic surfactant molecules at the water-oil interface: Area per molecule, microemulsion domain size, and rigidity. Journal of Chemical Physics. 106 (15), 6483-6491.

Strey, R. (1993). On the Stability Range of Microemulsions: From the Tricritical Point to the Lamellar Phase in Water/Formamide-Octane-C_iE_j Systems. Berichte der Bunsengesellschaft für physikalische Chemie. 97(05): 742-750.

Strey, R. (1994). Microemulsion Microstructure and Interfacial Curvature. Colloid & Polymer Science. 272 (8), 1005-1019.

Strey, R. (1996). Phase behavior and interfacial curvature in water-oil-surfactant systems. Current Opinion in Colloid & Interface Science. 1 (3), 402-410.

Talmon, Y., and Prager S. (1977). Statistical Mechanics of Microemulsions. Nature. 267, 333-335.

Talmon, Y., and Prager S. (1978). Statistical Thermodynamics of Phase Equilibria in Microemulsions. J. Chem. Phys. 69 (7), 2984-2991.

Tanford, C. (1972). Micelle Shape and Size. The Journal of Physical Chemistry. 76(21): 3020-3024.

Torrealba, V.A., Johns, R.T. (2016). Partition Coefficient Relations in Surfactant-Oil-Brine Systems for Improved Description of Microemulsion Phase Behavior. Paper presented at the SPE EOR Conference at Oil and Gas West Asia held in Muscat, Oman.

Torrealba, V.A. and Johns, R.T. (2017A). Coupled Interfacial Tension and Phase Behavior Model Based on Microscopic Curvatures. Under review.

Torrealba, V.A., Johns, R.T. (2017B). Microemulsion Phase Behavior Model Using Empirical Trends in Chemical Potentials. SPE International Conference on Oilfield Chemistry. Montgomery, Texas.

Troncoso, A. B. and E. Acosta (2015). The UNIFAC Model and the Partition of Alkyl and Alkylphenol Ethoxylate Surfactants in the Excess Phases of Middle Phase Microemulsions. Fluid Phase Equilibria. 397, 117-125.

Wade, W. H., Morgan, J. C., Schechter, R. S., Jacobson, J. K., Salager, J. L. (1978). Interfacial-Tension and Phase Behavior of Surfactant Systems. Society of Petroleum Engineers Journal. 18 (4), 242-252.

Wennerstrom, H., Balogh, J., Olsson, U. (2006). Interfacial tensions in microemulsions. Colloids and Surfaces A: Physicochemical and Engineering Aspects 291(1-3): 69-77.

Widom, B. (1975). Antonoff's Rule and the Structure of Interfaces near Tricritical Points. Physical Review Letters. 34 (16), 999-1002.

Winsor, P. A. (1954). Solvent Properties of Amphiphilic Compounds. London, UK, Butterworth.

Winsor, P. A. (1968). Binary and Multicomponent Solutions of Amphiphilic Compounds. Solubilization and the Formation, Structure, and Theoretical Significance of Liquid Crystalline Solutions. Chemical Reviews. 68 (1), 1-40.

Xiren, M., Shutang, Q. (1988). Experimental Study of Abnormal Phase Behavior of Microemulsion with Daqing Oil. SPE International Meeting on Petroleum Engineering. Tianjin, China.

Ysambertt, F., Anton, R., Salager, J. L. (1997). Retrograde Transition in the Phase Behaviour of Surfactant-Oil-Water Systems Produced by an Oil Equivalent Alkane Carbon Number Scan. Colloids and Surfaces A: Physicochemical and Engineering Aspects. 125 (2-3), 131-136.

Vita

Victor Torrealba is originally from Valencia, Venezuela. He holds a Bachelor of Science (Honors) in Petroleum and Natural Gas Engineering, a Master of Science in Energy and Mineral Engineering (Petroleum and Natural Gas Engineering option), and earned a Doctor of Philosophy degree in Energy and Mineral Engineering (Petroleum and Natural Gas Engineering option) all from The Pennsylvania State University. His research interests include physics of surfactant-oil-water systems, thermodynamics, phase behavior, enhanced oil recovery techniques, pore-scale displacement processes and imaging techniques for porous media applications.